Order Number 9507296

Magnetic reconnection in the presence of sheared plasma flow

La Belle-Hamer, Annette Louise, Ph.D.

University of Alaska Fairbanks, 1994

U·M·I
300 N. Zeeb Rd.
Ann Arbor, MI 48106

MAGNETIC RECONNECTION IN THE PRESENCE OF SHEARED PLASMA FLOW

A

THESIS

Presented to the Faculty of the University of Alaska

in Partial Fulfillment of the Requirements

for the Degree of

DOCTOR OF PHILOSOPHY

By

Annette L. La Belle-Hamer. B.A., M.S.

Fairbanks, Alaska

May 1994

MAGNETIC RECONNECTION IN THE PRESENCE OF

SHEARED PLASMA FLOW

by

Annette L. La Belle-Hamer, M.S.

RECOMMENDED:

L. C. Lee, Chairman, Advisory Committee

Head, Physics Department

APPROVED:

Dean, College of Natural Sciences

Dean of the Graduate School

April 27, 1994

Date

Abstract

Classical models of magnetic reconnection consist of a small diffusion region bounded by two slow shocks, across which the plasma is accelerated. Most space plasma current sheets separate two different plasmas, violating symmetry conditions across the current sheet. One form of asymmetry is a sheared plasma flow. In this thesis, I investigate the magnetic reconnection process in the presence of a shear flow across the current sheet using two-dimensional magnetohydrodynamic (MHD) simulations. The results show that only for sheared flow below the average Alfvén velocity of the inflow regions can steady state magnetic reconnection occur. A detailed examination of the Rankine-Hugoniot jump conditions reveals that the two slow shocks of earlier models are replaced by a strong intermediate shock and a weaker slow shock in the presence of shear flow.

Both symmetric and asymmetric density profiles are examined. Depending upon the direction of the flow in the adjacent inflow region, the effects from the sheared flow and the effects from the density asymmetry will compete with or enhance each other. The results are applied to the dayside and flank regions of the magnetosphere. For tailward flow in the flanks, the two asymmetries compete making the magnetic field transition layer broad with the high speed flow contained within the transition region. For the dayside region, the magnetic field transition region is thin and the accelerated flow is earthward of the sharp current layer (magnetopause). These results are consistent with the data.

A velocity shear in the invariant direction was examined under otherwise symmetric conditions. With the magnetic field initially only in the $x-y$ plane, B_z, and consequently field-aligned current, is generated by the initial v_z. The field-aligned current depends on the velocity profiles in all directions. For a velocity sheared in both the z and the y direction, the results show a very localized region of large field-aligned currents.

Table of Contents

List of Figures

List of Tables

Acknowledgements

It is difficult to know where to start. A phase of my life, that has lasted six years, is coming to a close. At this time, I feel a strong desire to express my appreciation to those who have helped me along the way. Dr. Lou-Chuang Lee has supported me, more than just monetarily, for my entire graduate program, and for that, I am truly grateful. Through thick and thin, if he lost his belief in me I never knew about it. He is a great scientist and a fantastic teacher and I am honored to be associated with him. To my other committee members–Drs. Syun-Ichi Akasofu, Joe Hawkins, John Morack, and Mr. Dan Swift–goes appreciation for the time spent reading the document. I would like to give a special word of thanks to Dan Swift for the time and assistance he gave my thesis that was above and beyond the call of duty.

Once upon a time, many years ago, Dr. Akasofu hired a young undergrad to digitize magnetometer data part-time while going to school. My first taste of magnetospheric research was due to my time spent at the Institute in those young, formative years. I would like to say thank you for his time, effort, and continued interest in my career.

This thesis would not be complete without expressing gratitude to Dr. Antonius Otto. Antonius is a clear-thinking individual with a firm grasp on basic physics. I am grateful for the time and effort he has expended towards my enlightenment and I hope it will not be in vain. I am grateful, as well, for his friendship for me and my family.

On the topic of friends and colleagues, there are many I would like to mention. Graduate school is an experience that bonds the participants (similar to slavery except we don't, in general, sing). The graduate students at the GI support one another as only fellow travellers can. I cherish the friends I have made here. Drs. and/or soon to be Drs. Jim Conner, Dirk Lummerzheim, Joe Minow, Kathy Hanks,

Pat Moore, Don Hampton, Curt Szuberla, John Williams, Ding Da-Qing, Don Rice (okay, so he is not a grad), Yu Lin, Gerard Fasel, Tom Immel, Peter Delamere, Ming Yan, Zhiwei Ma, Gwang-son Choe, Hengjin Cai, and their respective spouses (listed in random order), just to name a few, have been important to the maintainence of my sanity. My dear friends the Burrs and the Pittas, being outside of the university setting, have given me a stable base in reality.

The support staff of the GI has not only supported me in my professional endeavors but has also given me a feeling of personal support. I cannot thank them enough for leading me through (by the nose, at times) the labyrinth of paperwork and other such necessities of daily life at the GI. From the ranks of the support staff come some dear friends–specifically, Kate Barr, Kathy Berry, Deb Coccia, and, okay, the ENTIRE business office! The library staff, lead by Judy Triplehorn, has gone out of their way to give all researchers the aid they need, regardless of rank, which I appreciate greatly. The staff at the CRC (especially Celia Rohwer and Dave 'the unix guy' Covey) has answered so many of my distress calls that I only have to say 'Hi' in my oh-my-god-what-happened-to-my-computer voice and they know immediately to whom they are talking.

Last but not least, my family has been a constant source of energy and inspiration, enabling me to keep going when times got tough. And, they did get tough. My husband, Brendan, is a rock. Thank you for being there, Bren, and pushing me back into the ring, repeatedly, when I thought it was time to throw in the towel. My two kids, Tully and Hannah, helped me to continue working towards my degree–their shining faces never doubted me. The love and support I received from my family was invaluable during my graduate program. My parents, parents-in-law, siblings, and siblings-in-law also provided me with attaboys and you-can-do-it's when necessary.

Considering all the emotional support I have received over the years, I guess it would have been pretty embarrassing to quit. To quote the beloved M.C. Hammer, I am 'too legit to quit'. I am grateful for the love, friendship, and support that I have received commensurate with my Ph.D.

In parting, I would like to quote a street sign seen somewhere in Vermont that, to me, is applicable to life in general, but certainly to life in academia.

"Choose your rut carefully, you will be in it for the next 40 miles"

CHAPTER 1

Introduction

There are many regions in space in which it may be possible for magnetic reconnection to occur. In the process of magnetic reconnection, energy stored in the magnetic fields is rapidly converted into kinetic energy of the plasma. For large scale magnetic structures, the energy released can be substantial [Priest and Forbes, 1986]. For this reason, the process of magnetic reconnection is believed to be of primary importance in the dynamics of space plasmas.

The focus of this thesis is on regions in space plasmas in which magnetic reconnection takes place in the presence of a sheared plasma flow. Specifically, the dayside and flank regions of the magnetosphere configurations are examined. Each of these cases has a unique configuration worthy of individual attention. Figure 1.1 shows an overview of the Earth's magnetopause. The velocity shear across the magnetopause increases with increasing distance away from the subsolar point.

One aspect of the presence of sheared plasma flow is the development of the Kelvin-Helmholtz (KH) instability. In an inviscid fluid, the presence of a velocity shear makes the fluid susceptible to the KH instability no matter how small the difference in velocities [*Chandrasekhar*, 1961]. The development of the KH can be affected, under certain conditions, by the presence of magnetic fields [*La Belle-Hamer et al.*, 1988; *La Belle-Hamer*, 1988 and references therein]. A current sheet, on the other hand, with a finite resistivity present is susceptible to the tearing mode instability [*Furth et al.*, 1963]. The development of the tearing mode instability can initiate magnetic reconnection. *La Belle-Hamer et al.* [1988] and *La Belle-Hamer* [1988] investigated the relationship between the developing KH instability and the tearing mode instability in an incompressible plasma. The development of the KH instability modulates the current sheet, creating a spatial variation in the thickness

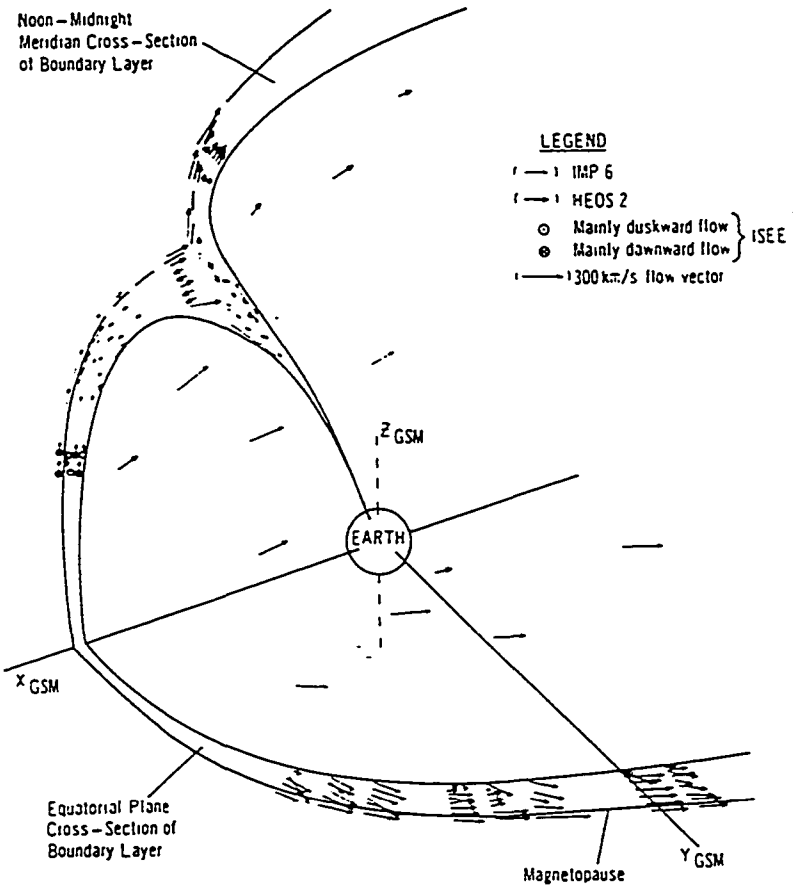

Figure 1.1. Overview of the Earth's magnetosphere showing satellite measurements of the velocity shear across the magnetopause. Along the flanks, the velocity increases with increasing distance from the subsolar region.

of the current sheet. Since the growth rate of the tearing instability depends upon the thickness of the current sheet, this modulation affects the growth rate. Regions of thinned current sheet tear at an enhanced rate.

La Belle-Hamer [1988] explored situations in which the KH instability developed and examined the effects this development would have on magnetic reconnection. In this thesis, magnetic reconnection is triggered and the effects that a sheared plasma flow, without the development of the KH instability, have on the magnetic reconnection process are examined. Second, all the simulations in *La Belle-Hamer's* work were incompressible. The question remains, then, how does the presence of sheared plasma flow affect the development of magnetic reconnection in a compressible plasma? This thesis, using compressible MHD code, will investigate this question.

1.1 Observations

The solar wind impinging upon the magnetosphere creates a velocity shear across the magnetopause current sheet. The direction and magnitude of the velocity shear relative to the current sheet plane is dependent upon location along the magnetopause. The solar wind plasma tends to flow parallel to the magnetopause and the velocity increases with increasing distance from the subsolar point.

The primary motivation for this study was provided by *Gosling et al.'s* [1986] observations of the mid-latitude flank magnetopause. Figure 1.2 shows the satellite position relative to the Earth. Note that the observations are not in either the equatorial nor the meridonal plane. They are in the near-tail region ($-10R_E < x < 0R_E$, GSM coordinates), which is located tailward of the terminator but near the Earth. An R_E is defined as one Earth radius. The observations are taken at mid-latitude, hereafter referred to as the flank in this thesis. The characteristics of these observations are in stark contrast with the dayside magnetopause observations.

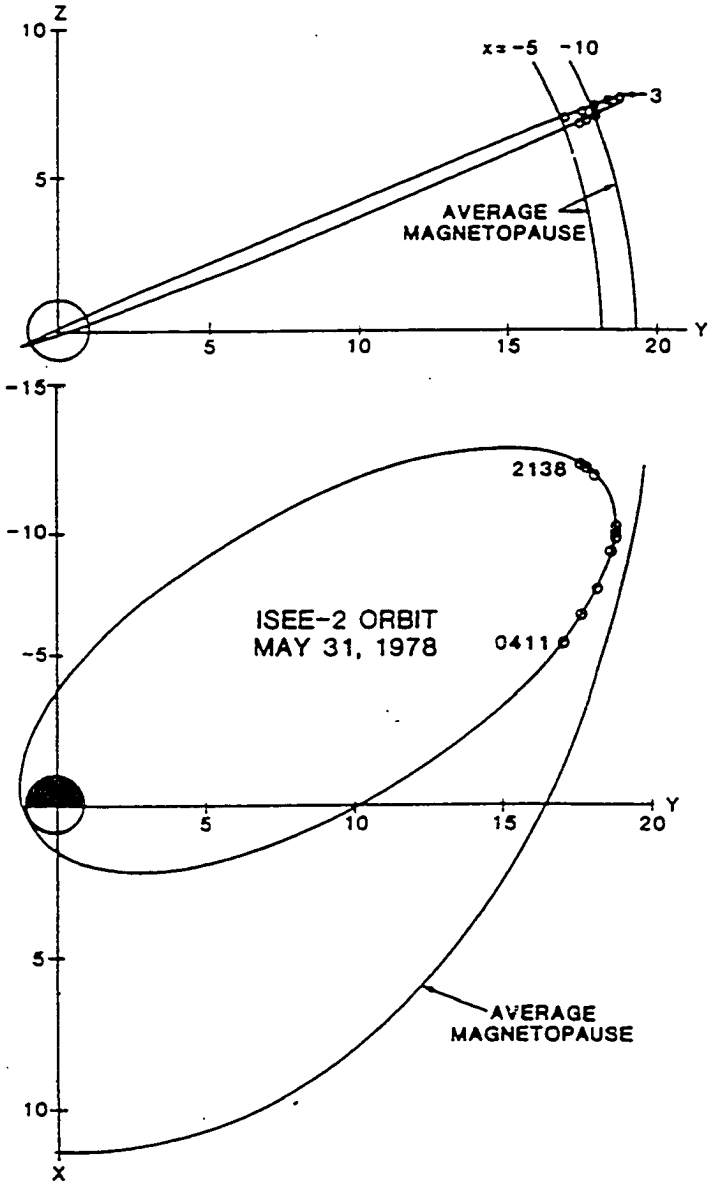

Figure 1.2. Gosling et al. [1986] satellite coordinates for the observations of the Earth's flank shown with respect to GSM coordinate system.

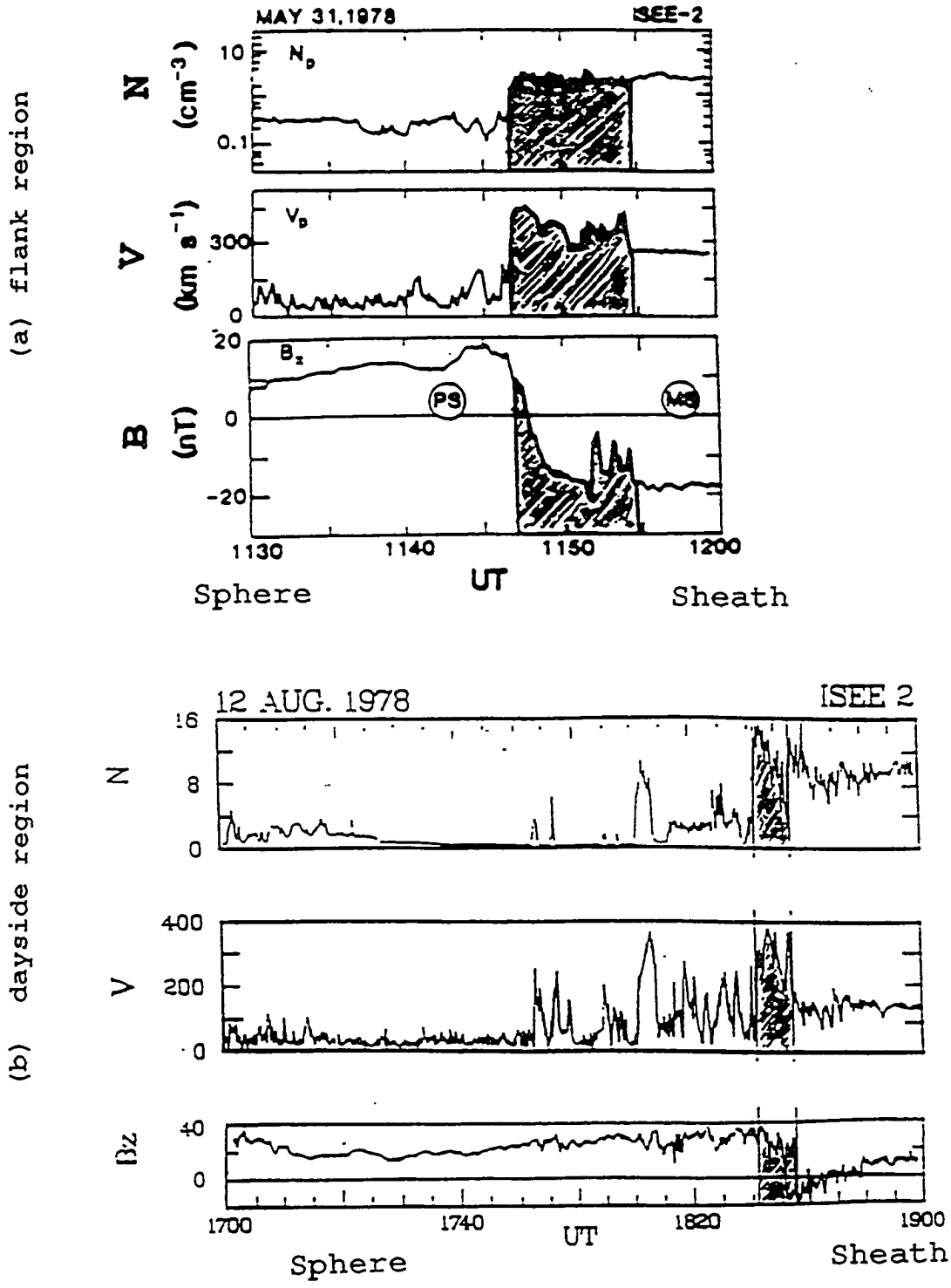

Figure 1.3. Satellite observations of (a) the flank region of the magnetosphere (from *Gosling et al.*, [1986]) and (b) the dayside region of the magnetosphere (from *Gosling et al.*, [1990a,b]).

Figure 1.3 shows the magnetic field, plasma density and velocity observed in both the (a) flank and (b) dayside regions of the magnetosphere. In the flanks (see Figure 1.3a), accelerated flows were observed on the duskside, and to a lesser extent on the dawnside, of the near-tail magnetopause, where accelerated flows are defined as regions which exhibit flow velocities larger than the magnetosheath flow velocities. Properties of the accelerated flows are different, in many respects, from those at the dayside magnetopause. The accelerated flows reported by *Gosling et al.* [1986] are: (1) confined to a region where the magnetic field changes from the magnetosheath to the magnetospheric orientation; (2) correlated to large components of the interplanetary magnetic field (IMF) antiparallel to the nearby geomagnetic field (3) typically highest on the magnetospheric side of the current sheet. When they are present, the transition from the magnetosheath to the magnetospheric magnetic field orientation is contained in a relatively wide region and no boundary layer is observed earthward of the transition region. The plasma density in the accelerated flow region maintains nearly magnetosheath values and the ion and electron temperatures are intermediate between magnetospheric and magnetosheath values. They occur intermittently with individual flow events as long as ten minutes. The accelerated flows exhibit structure within the current sheet and are associated with disturbances propagating tailward. These observations have been interpreted as possible signatures of magnetic reconnection in the flank region of the magnetopause.

In the dayside region, the velocity is parallel to the magnetic fields in the meridonal plane, while the velocity is perpendicular to the magnetic fields in the equatorial plane. The geomagnetic field and a southward interplanetary magnetic field (IMF) are antiparallel across the magnetopause. This configuration lends itself to the possibility of magnetic reconnection at the dayside magnetopause [Dungey, 1961]. The velocity shear across the magnetopause in the subsolar region is very

small. The velocity increases with increasing distance from the subsolar point, but the shear still remains considerably smaller in the dayside region than in the near-tail region.

Figure 1.3b shows observations which exhibit typical characteristics of crossings of the dayside magnetopause. The magnetic field discontinuity is sharp and thin in comparison with the flank observations in Figure 1.3a. In addition, the acceleration region, which is shaded, is Earthward of the magnetic field transition region. These are the main differences in the observations from the dayside region versus the flank region. It is the purpose here to examine the properties of magnetic reconnection in the flank regions of the magnetosphere and to compare the results to the dayside observations.

1.2 Magnetic Reconnection

Magnetic reconnection has been the subject of many analytical and numerical studies. The process is important for the conversion of magnetic energy to kinetic energy in many plasma configurations [*Parker,* 1957; *Dungey,* 1964]. Magnetic reconnection has been used to explain various observations including the flux erosion which occurs with a southward IMF [e.g., *Rijbeek and Cowley,* 1984] and flux transfer events (FTEs) [*Russell and Elphic,* 1979]. The structure and dynamics of magnetic reconnection depend greatly on the initial and boundary conditions, as well as on the assumed dissipation [e.g., *Priest and Forbes,* 1986; *Yan et al.,* 1992]. *Yan et al.* [1992] showed that for a localized resistivity enhancement, Petschek reconnection can be obtained but no steady state configuration can be obtained for a uniform resistivity. Petschek-like magnetic reconnection configuration is shown in Figure 1.4.

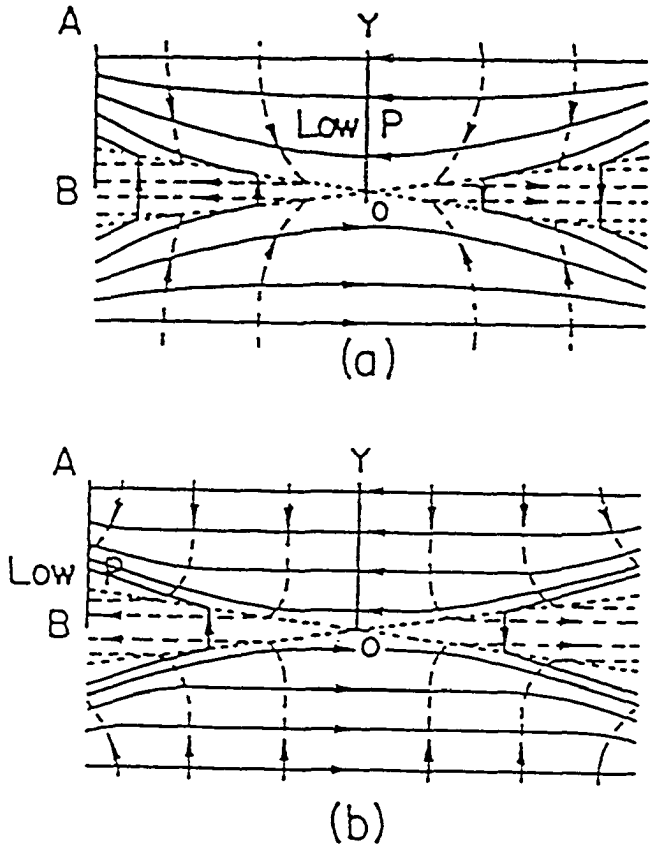

Figure 1.4. Schematic sketch of (a) Petschek's and (b) Sonnerup's magnetic reconnection configuration. The solid lines are the magnetic field lines and the dashed lines are the streamlines in both (a) and (b). In Petschek's model, the inflow regions have converging flow while Sonnerup's model has divergent flow in the inflow regions.

The basic process of magnetic reconnection can be explained as follows. The simplified Ohm's law can be written as

$$\mathbf{E} + \mathbf{v} \times \mathbf{B} = \eta \mathbf{j} \tag{1.1}$$

where $\mathbf{E}$ is the electric field, $\mathbf{v}$ the flow velocity, $\mathbf{B}$ the magnetic field, η the scalar resistivity, and $\mathbf{j}$ the current density. Faraday's law,

$$\nabla \times \mathbf{E} + \frac{1}{c}\frac{\partial \mathbf{B}}{\partial t} = 0 \tag{1.2}$$

in its differential form and Ampére's law

$$\nabla \times \mathbf{B} = \frac{4\pi}{c}\mathbf{j} \tag{1.3}$$

combined with equation 1.2 yields the induction equation

$$\frac{\partial \mathbf{B}}{\partial t} = \nabla \times (\mathbf{v} \times \mathbf{B}) + \frac{1}{\mu_o \sigma}\nabla^2 \mathbf{B} \tag{1.4}$$

The induction equation determines how $\mathbf{B}$ varies in time. The first term describes convection of the field with the plasma flow and the second term describes the diffusion of the magnetic field through the plasma. The dynamics of the plasma depends on which term dominates.

If diffusion across field lines is negligible, the magnetic field is said to be frozen in the plasma. In essence, this means that if two plasma elements are intially located on the same field line, they will remain on the same field line despite the field line's motion. It is equally valid to say that the magnetic field moves with the plasma or the plasma moves in magnetic flux tubes.

If the diffusion across field lines is not small, then the second term on the right hand side of the induction equation is no longer negligible. Two plasma elements which initially share a field line may no longer share a field line after diffusion takes place. The magnetic field diffuses through the plasma in such a way as to decrease

the field gradients. In the case with a localized enhancement of the resistivity, the magnetic field topology is allowed to change.

The relative magnitude of the two terms in the induction equation is related to the magnetic Reynolds number, R_m, and is given by

$$R_m \equiv \mu_o \sigma v_A L \sim \frac{|\nabla \times (\mathbf{v} \times \mathbf{B})|}{\frac{1}{\mu_o \sigma} \nabla^2 \mathbf{B}}$$

where v_A is the Alfvén speed in the flow and L is the characteristic length of the system. For R_m large, convection dominates and the plasma behaves as frozen-in as described above. For R_m small, diffusion dominates and the coupling between the fluid motion and the magnetic field motion is weak.

Many studies of magnetic reconnection focus on the stationary reconnection process. The Sweet-Parker magnetic reconnection model [*Sweet, 1958; Parker, 1957*] contains a current sheet across which the plasma properties are symmetric. The reconnection rate in their model depends primarily on the resistivity and is too small to account for a fast conversion of magnetic to kinetic energy. *Petschek* [1964] suggested a revision of the model in which resistivity is important only in a small diffusion region of limited length relative to the system. This diffusion region is bounded by an inflow region and an outflow region, which are separated by slow shocks. The plasma is accelerated by the slow shocks and the conversion of energy is more efficient. Many different models of magnetic reconnection that have been developed by various authors consist of a small diffusion region, which is bounded by two pairs of slow shocks.

If R_m is calculated using the system size applicable to the space plasmas I am interested in, then L would be on the order of an Earth radius, $\sim 6 \times 10^3$ km. For a v_A of approximately 400 kms^{-1} and a collisional frequency of about 3 days, R_m would be approximately 10^{11}. Therefore, for large scale plasmas, convection will

dominate. However, using *Petschek's* model, the diffusion region for the magnetic reconnection process has a much smaller scale size. Over this smaller scale, the diffusion process may dominate and the magnetic field lines 'break' and reconnect in such a way to decrease the current density.

1.3 The Scope of This Work

In this thesis, the non-linear development of magnetic reconnection in the presence of sheared plasma flow will be examined using a compressible magnetohydrodynamic (MHD) simulation code. A complete analytical solution is not possible to this highly non-linear problem. In the absence of an analytical solution, the evolution of the plasma and the magnetic fields embedded in it are examined. How the fields and other characteristics of the plasmas evolve in time gives insight into the physical processes. The simulations focus on the dynamics of the plasma and magnetic fields involved. The results are then applied to the flank and dayside regions of the magnetosphere.

Three velocity profiles will be examined and discussed. First, anti-parallel flow in which the velocity is parallel to the magnetic field on both sides of the current sheet will be examined. This velocity shear profile will be examined both with and without density asymmetry. The asymmetric density configuration can be applied to both the dayside and flank regions of the magnetopause depending upon the relative flow shear. Second, the stationary frame will be examined in which the plasma flow is zero in the magnetosphere and non-zero in the magnetosheath. This configuration examines magnetic reconnection in a frame in which the resistive region is stationary with respect to the magnetosphere. Since the velocity of the reconnection region is unknown, both the stationary frame simulations and the moving frame simulations give information about the nature of the magnetic reconnection in the presence of sheared plasma flow. And, third, the case with a

component of the flow velocity perpendicular to the magnetic field shear will be examined. This configuration has applications on both the dayside and the flank region of the magnetopause.

1.4 References

Chandrasekhar, S., Hydrodynamic and hydromagnetic stability, *Oxford University Press,* Amen House, London, E. C. 4, 1961. Dungey, J. W., Interplanetary magnetic field and the aurral zones, *Phys. Rev. Lett.*, 6, 47, 1961.

Furth, H. P., J. Killeen, and M. N. Rosenbluth, Finite-resistivity instabilities of a sheet pinch, *Phys. Fluids*, 6, 459, 1963.

Gosling, J. T., M. F. Thomsen, S. J. Bame, and C. T. Russell, Accelerated plasma flows at the near-tail magnetopause, *J. Geophys. Res.*, 91, 3029, 1986.

Gosling, J. T., M. F. Thomsen, S. J. Bame, T. G. Onsager, and C. T. Russell, The electron edge of the low latitude boundary layer during accelerated flow events, *Geophys. Res. Lett., 17*, 1833, 1990a.

Gosling, J. T., M. F. Thomsen, S. J. Bame, R. C. Elphic, and C. T. Russell, Plasma Flow reversals at the dayside magnetopause and the origin of asymmetric polar cap convection, *J. Geophys. Res.*, 95,8073, 1990b.

La Belle-Hamer, A. L., Z. F. Fu, and L. C. Lee, A mechanism for patchy reconnection at the dayside magnetopause, *Geophys. Res. Lett.*, 15, 152, 1988.

La Belle-Hamer, A. L., The Kelvin-Helmholtz and tearing instabilities in relation to magnetic reconnection at the Earth's dayside magnetopause, *Master's Thesis*, University of Alaska, Fairbanks, 1988.

Parker, E. N., Sweet's mechanism for merging magnetic fields in conducting fluids, *J. Geophys. Res., 62*, 509, 1957.

Petschek, H. E., Magnetic field annihilation, in AAS-NANA Symposium on the Physics of Solar Flares, *NASA Spec. Publ., SP-50*, 425, 1964.

Priest, E. R., and T. G. Forbes, New models for fast steady state magnetic reconnection, *J. Geophys. Res., 91*, 5579, 1986.

Rijnbeek, R. P., and S. W. H. Cowley, Magnetopause flux erosion events are flux transfer events, *Nature*, 309, a135, 1984.

Russell, C. T., and R. C. Elphic, ISEE observations of flux transfer events at the dayside magnetopause, *Geophys. Res. Lett., 6*, 33, 1979.

Sweet, P. A., The neutral point theory of solar flares, in *Electromagnetic Phenomena in Cosmical Physics*, ed. by B. Lehnert, p. 123, Cambridge University Press, London, 1958.

Yan, M., L. C. Lee and E. R. Priest, Fast magnetic reconnection with small separatrix angles, *J. Geophys. Res., 97*, 8277, 1992.

CHAPTER 2
Symmetric Inflow Conditions

This chapter has been published in Physics of Fluids B, 1, 706, 1994.

2.1 Introduction

Magnetic reconnection has been the subject of many analytical and numerical studies. The process is important for the conversion of magnetic energy to kinetic energy in many plasma configurations.[1,2] The structure and dynamics of magnetic reconnection depend greatly on the initial and boundary conditions, as well as on the assumed dissipation.[3]

Many studies of magnetic reconnection focus on the stationary reconnection process. The Sweet-Parker magnetic reconnection model [4,2] contains a current sheet across which the plasma properties are symmetric. The reconnection rate in their model depends primarily on the resistivity and is too small to account for a fast conversion of magnetic to kinetic energy. Petschek [5] suggested a revision of the model in which resistivity is important only in a small diffusion region of limited length relative to the system. This diffusion region is bounded by an inflow region and an outflow region, which are separated by slow shocks. The plasma is accelerated by the slow shocks and the conversion of energy is more efficient.

Various incompressible two dimensional models of magnetic reconnection have been developed and studied both theoretically and numerically [6,7]. More general boundary conditions were adapted to unify the incompressible models [8] and studied by corresponding simulations [3,9]. In the above papers, the reconnection geometry includes two slow shocks, similar to earlier theoretical work.

It has long been postulated that violation of any of the three basic assumptions in Petschek's [5] model will lead to the formation of intermediate waves in the neutral sheet [10]. Namely, the assumptions in the compressible model used by Petschek

are: (i) all plasma parameters are symmetric across the neutral sheet; (ii) the magnetic fields on the two sides of the neutral sheet are strictly anti-parallel (iii) the magnitude of the external magnetic field is independent of distance from the neutral line. Various violations of the above assumptions, in an attempt to approach a more realistic scenario, have been studied by many authors.[10,11,12,13,14,15]

It should be noted that, based on conventional ideal magnetohydrodynamic (MHD) theories, the intermediate shocks had been considered unstable or nonevolutionary [16,17,18]. In Petschek and Thorne's [10] work rotational discontinuities, not intermediate shocks, are present. Wu [19] found in a resistive MHD simulation that rotational discontinuity is unstable and disintegrates into several wave modes due to the diffusion of the transverse magnetic field in the discontinuity. Recent simulation work by Wu, based on dissipative MHD equations, showed that the intermediate shocks can be formed [20,21]. In particular, Wu suggested that intermediate shocks, not rotational discontinuities, may be involved in many physical situations such as at the Earth's magnetopause during magnetic reconnection processes [19].

Asymmetric conditions across the current layer can create an outflow region significantly different than the two slow shocks of the Petschek model. Shi and Lee [15] examined the influence of asymmetric magnetic field and density on the shock structure which are typical for the dayside magnetopause. The asymmetry in the inflow regions leads to the development of an intermediate shock on the side with the highest density and a slow shock on the side with the lowest density. Lin et al. [22] also found the presence of intermediate shocks in the magnetic reconnection layer for the asymmetric cases.

In addition to asymmetries in the magnetic field and plasma density, the solar wind impinging upon the magnetosphere creates a velocity shear across the magnetopause. The magnitude and direction of the velocity shear are dependent upon the

position along the magnetopause. Gosling et al. [23] reported observations of accelerated plasma flows at the near-tail dusk side magnetopause at moderate latitudes. The accelerated flows are confined to a region where the magnetic field rotates between the magnetosheath and magnetospheric field and they are correlated with largely antiparallel interplanetary magnetic field (IMF). These observations have been interpreted as signatures of magnetic reconnection in the flank region of the magnetopause.

Few studies of magnetic reconnection have included a sheared plasma flow. Mitchell and Kan [12] extended the reconnection model by Sonnerup [6] for a two-dimensional incompressible plasma to include plasma flow parallel to the magnetic field in the inflow regions. The geometry of the inflow and outflow regions can be greatly altered by the addition of this flow velocity. They concluded that solutions exist as long as the difference between the magnitude of $\mathbf{B} \cdot \mathbf{V}$ in the two inflow regions does not exceed a critical magnitude, which depends on the inflow quantities. We will address the existence of a critical velocity in our simulations.

La Belle-Hamer et al. [24] studied the dayside magnetopause region with a sheared plasma flow across the neutral sheet. However the shock structure of the neutral sheet was not examined. Heyn et al. [25] studied the structure of the reconnection region and Biernat et al. [26] applied this analysis to the Earth's magnetopause. However, in their ideal MHD formulation, intermediate shocks are not present.

In this thesis, we are interested in an asymmetry in the flow pattern generated by sheared plasma flow across the current sheet, and the effect that flow will have on the reconnection region. The focus is on the evolution of the MHD discontinuities in the presence of plasma flowing in opposite directions on either side of the current layer. For this analysis we will use a two-dimensional, compressible MHD simulation. In order to highlight the main physics, we will confine our discussions

to the cases with all the plasma properties symmetric across the current sheet. In addition, the magnetic field and tangential velocity are antiparallel across the current layer in all the cases herein. This implicitly assumes a frame of reference at rest with respect to the X line. In order to decrease the effect of the boundary conditions, the system size is large in comparison to the current layer thickness. In the vicinity of the reconnection region, an approximately steady-state configuration develops. The size of the stationary region increases with time. We will study the structure of this steady-state region. This is the first report of the formation of intermediate shocks due to the presence of sheared plasma flow.

2.2 Numerical Code and Initial Conditions

The numerical simulation in this study uses a two-dimensional compressible MHD code which is discussed in Otto et al. [27]. The time advancement is achieved by the leap frog method with second order accuracy in time and space. The compressible MHD equations used can be written as:

$$\frac{\partial \rho}{\partial t} = -\nabla \cdot (\rho \mathbf{v}) \tag{2.1}$$

$$\frac{\partial \rho \mathbf{v}}{\partial t} = -\nabla \cdot [\rho \mathbf{v}\mathbf{v} + (p + \frac{B^2}{2\mu_o})\bar{\bar{\mathbf{I}}} - \frac{\mathbf{B}\mathbf{B}}{\mu_o}] \tag{2.2}$$

$$\frac{\partial \mathbf{B}}{\partial t} = \nabla \times [\mathbf{v} \times \mathbf{B} - \eta \mathbf{j}] \tag{2.3}$$

$$\frac{\partial \varepsilon}{\partial t} = -\nabla \cdot \mathbf{S} \tag{2.4}$$

where

$$\varepsilon = \frac{\rho v^2}{2} + \frac{B^2}{2\mu_o} + \frac{p}{\gamma - 1} \quad \text{and} \tag{2.5}$$

$$\mathbf{S} = (\varepsilon + p + \frac{B^2}{2\mu_o})\mathbf{v} - (\mathbf{B} \cdot \mathbf{v})\frac{\mathbf{B}}{\mu_o} + \frac{\eta}{\mu_o}\mathbf{j} \times \mathbf{B} \tag{2.6}$$

and ρ is the mass density, $\mathbf{v}$ is the bulk flow velocity, p is the plasma pressure. $\mathbf{B}$ is the magnetic field, $\mathbf{j}$ is the current density and η is the magnetic resistivity.

The three basic quantities used for the normalization are the asymptotic magnetic field (B_0), the density (ρ_0) at $x = \pm\infty$, and the initial current sheet half thickness (a). All other quantities are normalized in terms of these three. Therefore, the velocity is normalized by the Alfvén velocity $V_{Ao} = B_o/\sqrt{\rho_o \mu_o}$, pressure by the magnetic pressure $B_o^2/2\mu_o$, current by B_o/a, resistivity by a^2/τ_d, where τ_d is the diffusion time. Time is measured in units of Alfvén transit time, $t_A = a/V_{Ao}$.

The initial current sheet is located in the $x = 0$ plane. The initial magnetic field and velocity are specified as

$$\mathbf{B} = \tanh(x)\hat{\mathbf{y}} \tag{2.7}$$

$$\mathbf{v} = v_o \tanh(x)\hat{\mathbf{y}} \tag{2.8}$$

In each of the cases presented below, the resistivity initiates the onset of magnetic reconnection. The resistivity is given by

$$\eta = \eta_o(1.0 - \exp^{-\frac{t}{15}})\mathrm{sech}^2\left(\frac{x}{l_x}\right)\mathrm{sech}^2\left(\frac{y}{l_y}\right) \tag{2.9}$$

where η_o is a constant. The resistivity is constant after an initial ramp time and is localized in space. In the cases presented here, $l_x = l_y = 3$ and $\eta_o = 0.05$.

The simulation domain is a rectangular box in the $x - y$ plane, extending in the x direction from -20 to 20 and in the y direction from 0 to 100. The grid is non-uniform, with a higher resolution in the current sheet than at the boundaries with 201 gridpoints in the x direction and 403 gridpoints in the y direction. The resolution in the x-direction is 0.05 and in the y direction is 0.2, unless otherwise stated. The derivative of each physical quantity with respect to the boundary normal direction is set to zero at $y = 100$ and at $x = \pm 20$. These are referred to as free boundary conditions. Consistent with the initial conditions, the point of symmetry is imposed at $(x, y) = (0, 0)$, i.e., all properties obey either $f(x, y) = f(-x, -y)$ or $g(x, y) = -g(-x, -y)$. Discontinuities tend to develop

on the grid scale due to the very low numerical dissipation of the the leap frog method used in the simulations. We used a background resistivity of 0.001 in order to smooth the large gradients on the grid scale.

2.3 Results

We have simulated many cases to examine the effects of a sheared plasma flow ($v_o \neq 0$) on magnetic reconnection. Without sheared flow, two slow shocks are present. For shear flow with a velocity above the Alfvén velocity of the inflow region ($v_o > 1$), we found that the current density and the electric field at the X line drops to zero. The existence of this critical velocity is consistent with previous analytical results of Mitchell and Kan[12] using an incompressible plasma. In the presence of sheared flow with $0 < v_o < 1$, an intermediate shock and a slow shock border the outflow region. It is our purpose here to examine the shock structure for these reconnecting cases. We will consider in detail the cases with $v_o = 0$ and $v_o = 0.6$.

2.3.1 Case 1: The zero initial velocity case

In order to provide a reference for the simulation results with sheared plasma flow, we will first illustrate the reconnection geometry obtained with zero initial shear velocity. Figure 2.1 shows the magnetic field, velocity, the z-component of the current density, and the electric field for the case with zero shear at $t = 160t_A$. In order to enhance the features, the region shown is not the entire simulation box. The resistivity is centered at $(x, y) = (0, 0)$.

The magnetic field contours show distinct regions of the reconnection geometry. Two regions with very low velocity and large, uniform magnetic field extend from near the $x = \pm 10$ boundary in toward the center. We will refer to these regions as the inflow regions, in keeping with convention. These regions are separated by a region where the field is weak and nearly perpendicular to the strong field in the

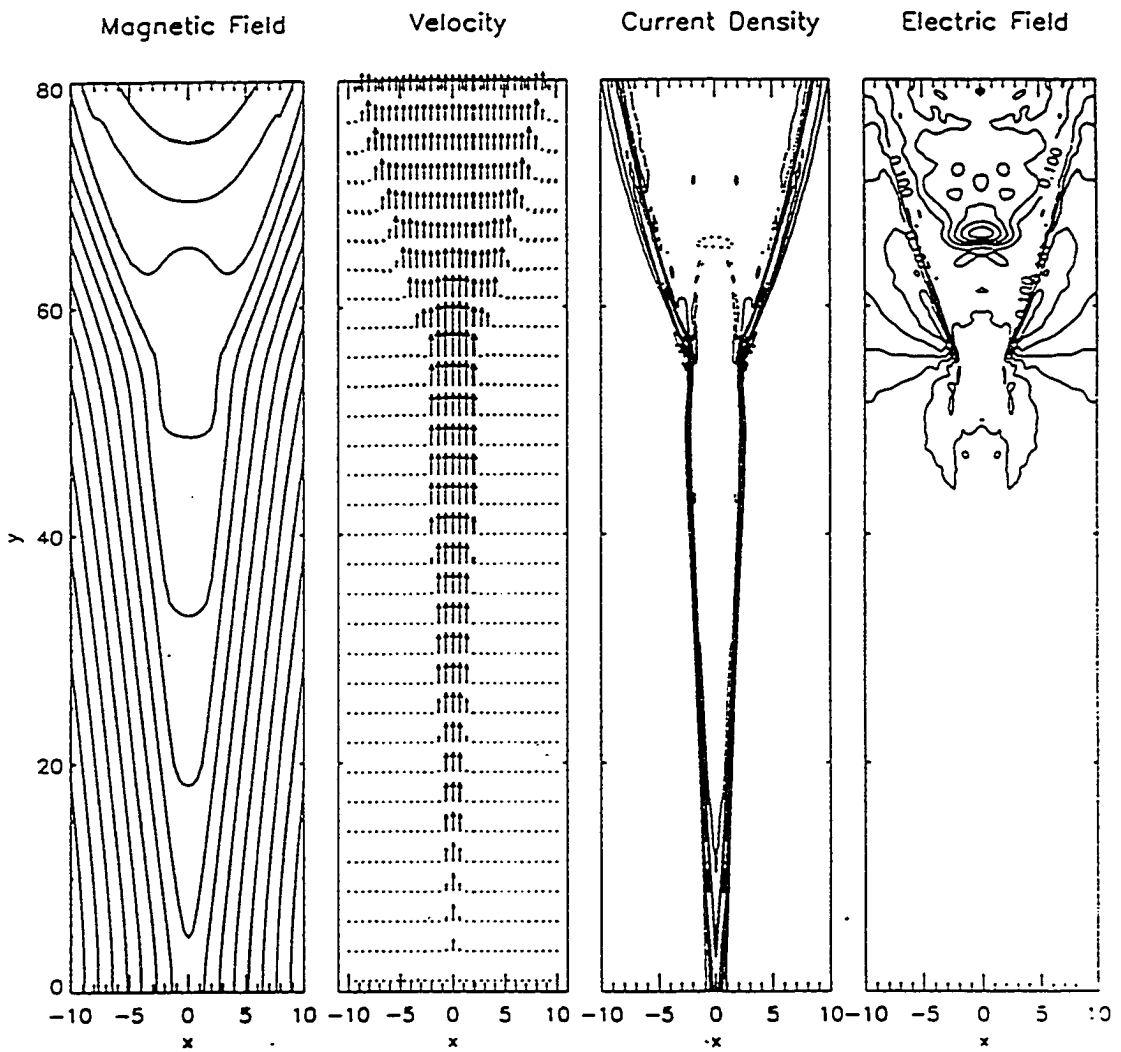

Figure 2.1. Contours of constant vector potential (magnetic field lines), velocity vectors, and contours of z components of the current density (j_z) and electric field (E_z) at $160t_A$ with zero initial velocity (case 1).

inflow region. This region of weak field extends like a wedge from the origin to about $y = 50$ and will be referred to as the outflow region. The plot also shows a fourth region of rather weak magnetic field at the leading edge of the outflow region. In this region the plasma has not been fully accelerated by the reconnection process and the configuration is not in a steady state. Here, the separatrix angle increases significantly caused by the slower outflow speed and the accumulation of magnetic flux.

The nonzero B_x component in the outflow region connects magnetic flux from one side of the inflow region to the other, thereby illustrating that magnetic reconnection proceeds.

The velocity in the outflow region is directed along the y axis and the plasma has been accelerated. The current density contours illustrate the presence of two thin current layers which are symmetric with respect to $x = 0$ for $y < 50$. These current layers bound the outflow region. The convection region is seen to be in steady state by examining the electric field contours. Since $\frac{\partial \mathbf{B}}{\partial t} = -\nabla \times \mathbf{E}$, the locally constant region of the electric field contours implies a good approximation of a steady state. In the region $y > 50$, the electric field varies spatially and this is the non-steady state region. Later we will identify the thin structures which separate the inflow and outflow regions as slow shocks. The four plots in Figure 2.1 thus present a summary of a Petschek-like reconnection process.

Figure 2.2 contains a horizontal slice through the simulation box at $y = 25a$ and $t = 160t_A$. The top panel shows B_y (solid line) and B_x (dotted line). The second panel contains j_z. The third panel contains the y components of the Alfvén velocity V_{Ay} (solid line) and the plasma velocity V_y (dashed line). The final panel contains the plasma pressure (solid line) and the density (dotted line). The top two panels show clearly two symmetric thin current structures with a width of 0.25, assuming a sech^2 profile. The velocity is seen to be accelerated in the region between the

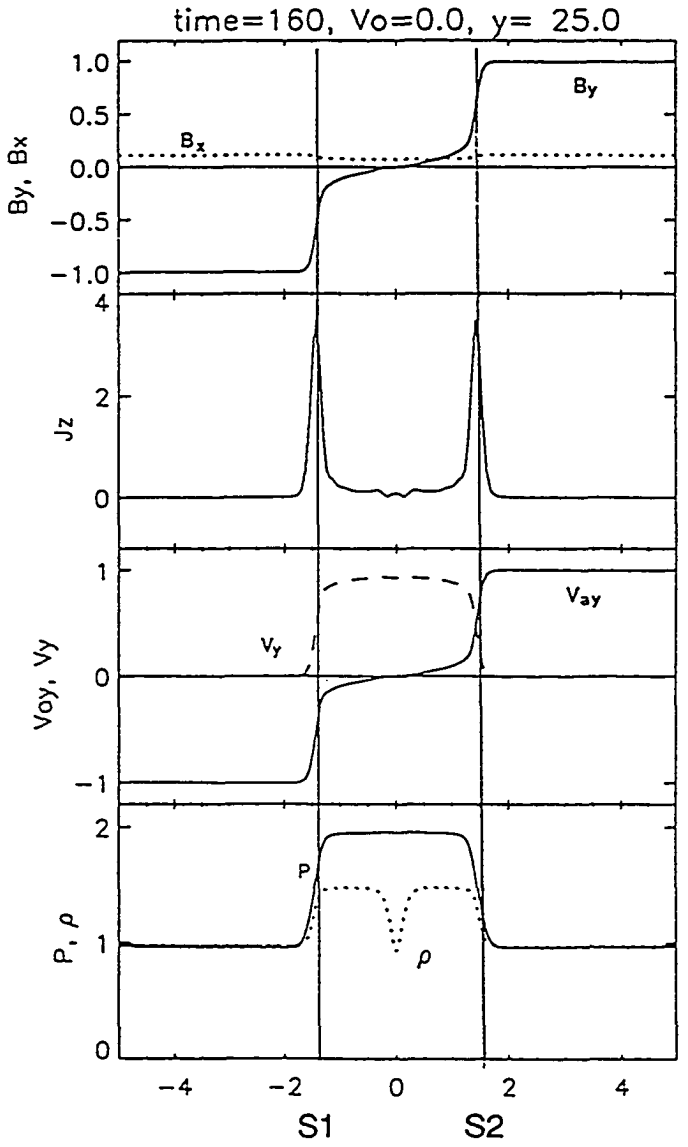

Figure 2.2. Horizontal slice of the plasma parameters at $y = 25$ and $t = 160t_A$. From top to bottom, magnetic field (B_x dotted, B_y solid line), z component of the current density, velocity (V_{ay} solid, V_y dashed), pressure (solid) and density (dotted) for the case with zero initial velocity (case 1).

two current discontinuities. The pressure increases, the density increases, and the magnetic field magnitude decreases across the two discontinuities with the outflow region being downstream of both structures. The last panel shows a dip in the density at about $x = 0$. We interpret this as two contact discontinuities associated with the finite width of the initial current sheet but do not regard them to be of any importance for further discussion in this paper.

2.3.2 Case 2: The sheared plasma flow case

In the following cases, there exists an initial plasma flow tangential to the current sheet. The flow velocity is described by equation 2.8. Observations in the flank region indicate that a velocity shear exists between the magnetosheath and the magnetosphere, with a large magnetosheath plasma velocity and a small magnetospheric velocity [23]. Our simulation is carried out in the frame with an antiparallel velocity profile in which the magnetosheath and the magnetosphere velocity magnitudes are equal.

Figure 2.3 shows the magnetic field, velocity, contours of the z component of current density j_z and electric field E_z at time $t = 160t_A$ for the case with an initial velocity $v_o = 0.6$. The plots illustrate clearly the entirely different structure of the reconnection geometry in the presence of shear flow across the current layer. It is obvious that the symmetry with respect to the y axis, which was present in the zero initial shear case, is destroyed. The magnetic field changes direction sharply on the negative x side and the entire outflow region is tilted with respect to y. As in the zero initial shear case, however, the nonzero B_x component in the outflow region connects magnetic flux from one side of the inflow region to the other, indicating that magnetic reconnection proceeds.

The current density contours show a thin well-defined current layer structure in the negative x quadrant. A comparison with Figure 2.1 shows that the current

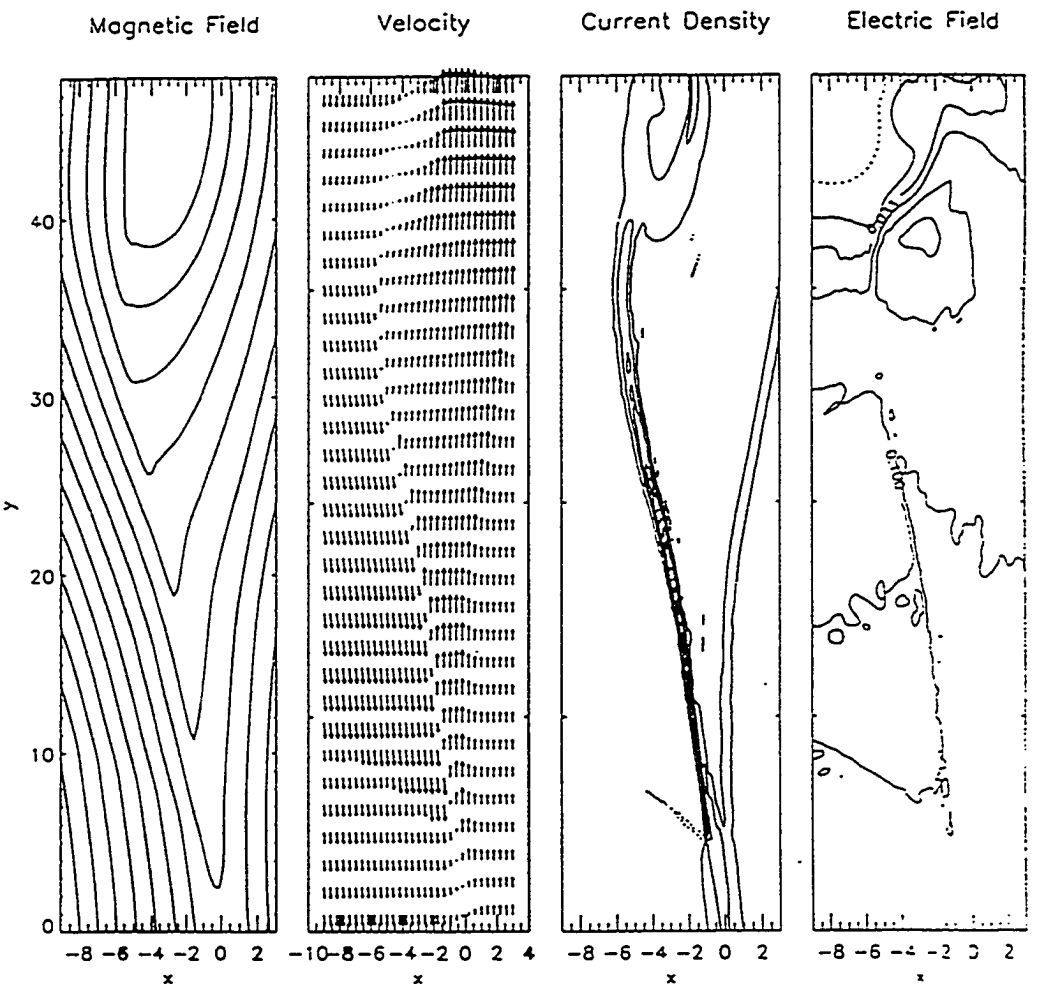

Figure 2.3. Contours of constant vector potential (magnetic field lines), velocity vectors, and contours of constant current density (J_z) and electric field (E) at $160t_A$ for initial velocity of $v_o = 0.6$ (case 2).

layers formed in the outflow region are not symmetric as in the zero velocity case. The current layer at negative (positive) x will be denoted I1 (S2). This choice of names will be made clearer in the next section. I1 has a much larger angle and S2 has a much smaller angle with respect to the y axis than the purely symmetric case. These current layers bound the outflow region as in the zero velocity case.

The velocity in the outflow region is also not symmetric about the y axis; however it is still directed along y. Again, acceleration takes place at the current layers I1 and S2, which extend from the reconnection site. Across the current layer I1, the velocity has changed both magnitude and direction. Across S2, the magnitude of the velocity has increased in the outflow region. Thus, the acceleration of the plasma in the outflow region can be seen to be greater across I1 than across S2. The accelerated flow is, then, located between these two shock structures.

In order to examine the shock structures in detail, Figure 2.4 shows a slice of the different parameters at $y = 10$ and $t = 160t_A$ as a function of x. It can be seen that the y component of the magnetic field, or the tangential component, changes sign across I1. This suggests an intermediate shock[19,28] and thus the naming convention. The vast majority of the current in the outflow region is contained in I1, with some across S2. The thickness of the two current structures is different from the zero velocity case in which the current layers were each 0.25 in thickness and about 4 in magnitude, assuming a sech^2 profile. In this case, I1 has a thickness of approximately 0.15 and S2 is thicker with a thickness of about 0.8. The magnitudes are also quite different with a maximum for I1 about 8 and for S2 about 0.5. The separation between I1 and S1 increases with increasing y. Again, there are the contact discontinuities in between I1 and S2 in which only the density is affected.

Figure 2.4 illustrates that the inflow region to the left of I1 has additional structure. In the region marked by A, density and pressure are lower and magnetic

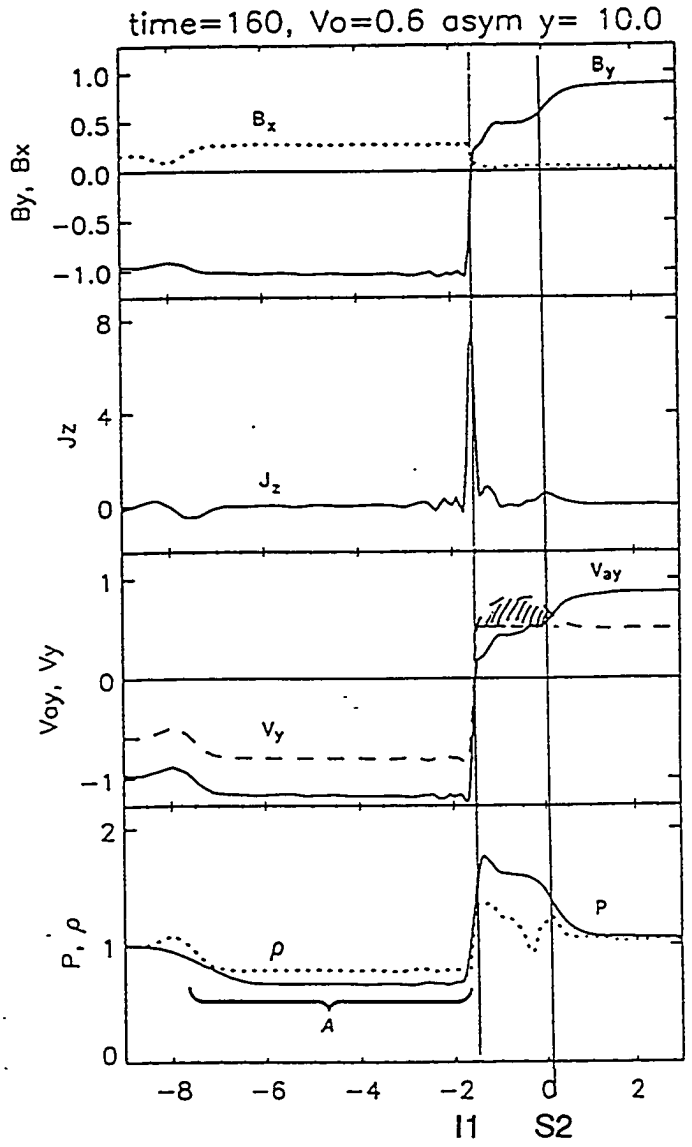

Figure 2.4. Horizontal slice of the plasma parameters at $y = 10$ and $t = t_A$ for case 2. From top to bottom, magnetic field (B_x dotted, B_y solid line), z component of the current density, velocity (V_{ay} solid, V_y dashed), pressure (solid) and density (dotted).

field and plasma velocity are larger than the region to the left of A. A plausible explanation for the larger velocity and lower density is relatively large plasma transport across I1. This transport rarefies the plasma left of I1 and momentum conservation may require an increase in the flow speed. However, the dominant structures are I1 and S2.

We will examine the Rankine-Hugoniot conditions relating the upstream and downstream conditions for the shock structures for both cases in the next section.

2.4 The Rankine-Hugoniot jump conditions

For the current layers discussed earlier in this paper, it is useful to examine the Rankine-Hugoniot relations. Each type of MHD discontinuity satisfies specific jump conditions [9]. Jump conditions relate the upstream and downstream conditions without describing the structure within the discontinuity. We are primarily concerned with MHD slow and intermediate shocks. Jump conditions are different for each type of MHD shock and are indicated by square brackets such that $[F] = F_2 - F_1$, where subscript 1 is used to indicate upstream and subscript 2 to indicate downstream for various quantities (F) [28,29]. For slow shocks, in which $C_{s1} < v_{n1} < C_{I1}$ and $v_{n2} > C_{s1}$, the tangential magnetic field does not change direction and $[\rho] > 0$, $[P] > 0$, $[|B|] < 0$, $[v_n] < 0$. The letter C denotes the wave speed and the subscript s denotes the slow mode, I the intermediate mode, and n the direction normal to the discontinuity. For intermediate shocks, in which $v_{n1} \geq C_{I1}$ and $v_{n2} < C_{I2}$, the tangential magnetic field changes direction and $[\rho] > 0$, $[P] > 0$, $[|B|] \neq 0$, $[v_n] < 0$. Note that $C_{I1} = V_{An1}$ and $C_{I2} = V_{An2}$, where V_{An} denotes the normal Alfvén speed.

In order to calculate the jump conditions locally in our simulation, we need to transform into the appropriate frame. Since we know that the normal component

of the magnetic field and the mass flux density are continuous across the discontinuities, we first rotate into the frame where these conditions are well satisfied. The angle of rotation (α) is the angle between the shock and the y axis. Once rotated, points are chosen upstream and downstream of the shock and the jump conditions are calculated. As stated above, the outflow region is defined as downstream for all the discontinuities. The results for three different current layers are presented in Table 1.

The first two rows serve to identify the current layer described by the respective column. y and α indicate at which y values the properties are obtained and the angle of the discontinuity with respect to the y axis, respectively. The values for $[B_n]$, $[\rho v_n]$, $[B_n]/B_{n1}$ can be used to estimate the error in the jump conditions which follow. The error ranges between about 1-5%. For rotational discontinuities, the Walen relation, or $[V_{At}] = [V_t]$, is valid. Since density changes from upstream to downstream across shocks, in general, the Walen relation does not strictly hold. However, if the density change is not large, the Walen relation is approximately satisfied. Therefore, the values for $[V_{At}]$ and $[V_t]$ were also included.

The properties of the shock for the zero velocity case were calculated using the negative x side only since the shock structures are symmetric. For the $v_o = 0.0$ case, $C_{s1} < V_{n1} \leq C_{I1}$ and $V_{n2} < C_{s2} < C_{I2}$. The tangential magnetic field does not change sign across the shock. The normal velocity decreases across the shock and satisfies the slow shock inequalities, as seen in Table 1. In addition, the jump conditions listed above for the slow shock are satisfied. Thus, for the case with zero initial velocity shear, the shocks are classified as slow shocks.

For case 2, with an initial velocity $v_o = 0.6$, two current layers are examined. The first is I1, located in the negative x quadrant. The normal velocity is greater than the normal Alfvén velocity upstream of I1, $V_{n1} > V_{An1}$, and less than the normal Alfvén velocity downstream of I1, $C_{s2} < V_{n2} < V_{An2}$. The tangential magnetic

field changes sign across I1. The jump conditions listec under intermediate shocks above are satisfied. In addition, the $[V_{At}] \sim [V_t]$ condition is well satisfied. These characteristics support the intermediate shock classification.

It is interesting to compare the characteristics of S2 in this case with S1 in case 1 ($v_o = 0.0$). Since the downstream region is defined as the outflow region, the upstream of S2 is to the right in Figure 2.4. From upstream to downstream, the density increases, the magnetic field magnitude decreases and the tangential component of the magnetic field does not change sign. This suggests a weak slow shock. However, the conditions for a slow shock are not all satisfied: $V_{n1} < C_{s1}$ and $V_{n2} < C_{s2}$. However, the difference between the normal velocities and the slow mode velocities is on the order of the error caused by finite resolution and the deviations from an ideal steady state. This current layer is fairly wide compared to the previously analysed structure and may not be a well defined discontinuity within the resolution of this simulation.

2.5 Discussion and Summary

We have examined magnetic reconnection in the presence of sheared plasma flow. This is the first report of the formation of intermediate shocks due to the presence of sheared plasma flow. In this study, the plasma properties and magnetic field strength are symmetric across the neutral sheet. The presence of a velocity shear, however, introduces an asymmetry in the structure of the outflow layer.

By violating the symmetric conditions of Petschek's model, we have changed the shock structure in the neutral sheet. In the symmetric zero velocity case in Figure 2.1, the plasma is rapidly accelerated at two strong current layers to a uniform velocity along the neutral sheet. The tangential component of the magnetic field drops to essentially zero. The jump conditions and upstream and downstream parameters identify these layers as two slow shocks.

For shear flow above the critical velocity, which is the Alfvén velocity of the inflow regions, reconnection is switched off. With the velocity shear below the critical velocity, the plasma on the side with the velocity flowing in the negative y direction requires a larger change in the tangential magnetic field in order to be accelerated to the same velocity along the initial current sheet. The plasma on the other side, with the velocity initially flowing in the positive y direction, requires a much smaller tangential magnetic field change. The symmetry is destroyed and the tangential magnetic field changes sign across I1, as seen in the simulations. Up and down stream properties strongly indicate this structure is an intermediate shock.

Figure 2.5 shows a schematic for both the purely symmetric case (a) and the case with sheared flow present (b). As sketched in Figure 2.5a, for the purely symmetric case only slow shocks are formed. Our results indicate that the addition of the sheared plasma flow causes the formation of an intermediate shock and a slow shock pair (Figure 2.5b). The sheared plasma flow, where $v_o \neq 0$, introduces an asymmetry which creates an asymmetric outflow region, bounded by an intermediate shock and a slow shock rather than the two slow shocks of Petschek's model. The formation of intermediate shocks in the presence of sheared flow was also confirmed in the framework of one-dimensional hybrid simulations by Lin and Lee [30].

These results may be of large importance for the observations of different magnetopause and boundary layer structures at the dayside and the flank region of the Earth's magnetopause. A boundary layer of enhanced flow velocity is generally observed on the magnetospheric side of the magnetopause (i.e., the major current layer) at the dayside magnetosphere [31,32,33,34]. This can be significantly different at the flank magnetopause where enhanced tailward flow is observed to be confined to the current transition region [23]. The point symmetry with respect to the

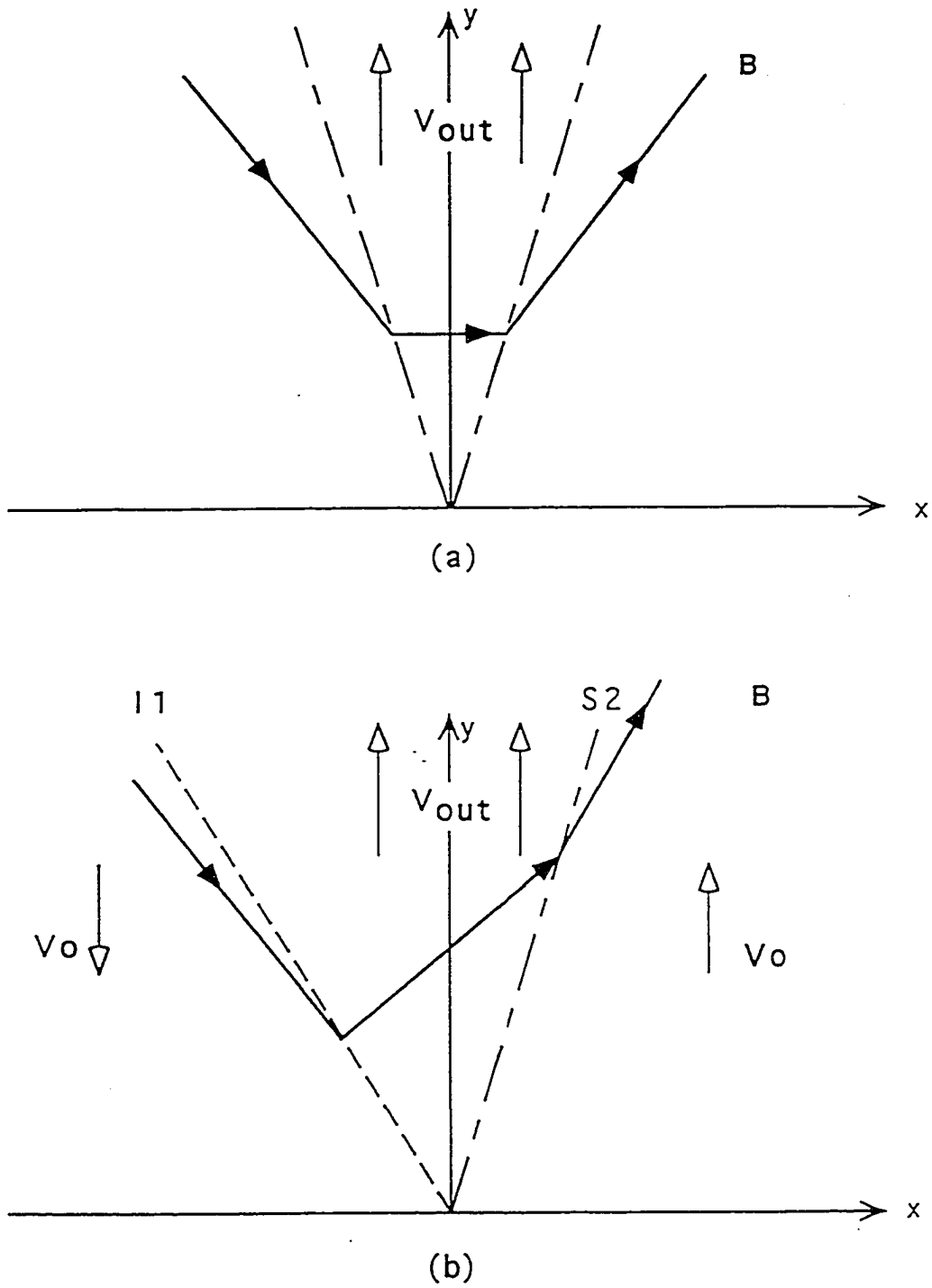

Figure 2.5. Schematic drawing of the neutral sheet shows (a) in the symmetric case the slow shocks on either side and (b) the development of the shock structure into a slow and intermediate shock on the side with the plasma moving towards the reconnection region.

origin in observed in Figures 3 and 5 implies that the presence of the strong shear flow, present in the flank region of the magnetosphere, may be responsible for this difference.

We caution, however, that the real system may be considerably more complicated than the cases considered here due to the presence of asymmetric density. For a strongly asymmetric density with no plasma shear present the intermediate shock forms on the magnetosheath side[15,19]. Asymmetries in both the plasma density and the shear flow may introduce competitive effects for the structure of the current layers in the outflow regions, especially for the tailward accelerated flow. These competitive effects are examined when the velocity shear is accompanied by a strong density gradient by La Belle-Hamer et al.[35]. The main result presented here is that the presence of a sheared plasma flow in the magnetic reconnection process will create an asymmetric outflow region and lead to the formation of an intermediate shock.

2.6 Acknowledgments

The authors appreciate informative discussions with Y. Lin and T. Eastman concerning this topic. This work is supported by National Aeronautics and Space Administration (NASA) Grant No. NAG 5-1504 and National Science Foundation Grant No. ATM91-11509.

Table 1. . Jump Conditions

Table 1. Jump Conditions

shock	case 1	case 2	case 2
	S1	I1	S2
y	25	10	10
α	2.5°	8.7°	0.0°
$[B_n]$	-0.0001	-0.0013	-0.0037
$[\rho v_n]$	-0.0034	0.003	-0.0006
$[B_n]/B_{n1}$	-0.0018	-0.011	-0.087
$[V_{At}]$	0.97	1.57	0.32
$[V_t]$	0.94	1.55	0.25
$[\lvert B_t \rvert]$	-0.95	-0.50	-0.30
$[\rho]$	0.50	0.45	0.15
$[p]$	1.00	0.96	0.44
$[v_n]$	-0.03	-0.054	0.003
V_{An1}	0.07	0.13	0.04
V_{An2}	0.06	0.10	0.03
V_{n1}	0.07	0.15	0.02
V_{n2}	0.04	0.10	0.02
C_{s1}	0.05	0.07	0.03
C_{s2}	0.06	0.09	0.03

Table Caption:

Table 1. The jump conditions calculated from the simulations and the upstream and downstream properties for the current layers for Case 1 (zero initial velocity) and Case 2 (v_o=0.6).

1. Dungey, J. W., , *Phys. Rev. Lett.*, 6, 47 (1961).
2. Parker, E. N., *J. Geophys. Res., 62*, 509 (1957).
3. Yan, M., L. C. Lee and E. R. Priest, *J. Geophys. Res., 97*, 8277 (1992).
4. Sweet, P. A., *Electromagnetic Phenomena in Cosmical Physics*, ed. by B. Lehnert, p. 123, Cambridge University Press, London (1958).
5. Petschek, H. E., in *AAS-NASA Symposium on the Physics of Solar Flares*, edited by W. N. Hess (National Aeronautics and Space Agency, Washington, DC, 1964), p. 425.
6. Sonnerup, B. U. Ö., *J. Plasma Phys., 4*, 161 (1970).
7. Yeh, T., and W. I. Axford, *J. Plasma Phys., 4*, 207 (1970).
8. Priest, E. R., and T. G. Forbes, *J. Geophys. Res., 91*, 5579 (1986).
9. Lee, L. C., and M. Yan, *Phys. of Fluids, B*, 4, 3808 (1992).
10. Petschek, H. E., and R. M. Thorne, *Astrophys. J.*, 147, 1157 (1967).
11. Levy, R. H., H. E. Petschek and G. L. Siscoe, *AIAA J., 2*, 2065 (1964).
12. Mitchell, H. G., and J. R. Kan, *J. Plasma Physics*, 20, 31 (1978).
13. Sato, T., and T. Hayashi, *Phys. Fluids, 22*, 1189 (1979).
14. Scholer, M., *J. Geophys. Res., 94*, 15, 099 (1989).
15. Shi, Y. and L. C. Lee, *Planet. Space. Sci., 38*, 437 (1990).
16. Germain, P., *Rev. Mod. Phys.*, 32, 951 (1960).
17. Jeffery, A., and T. Taniuti, *Non-linear Wave Propagation*, Academic, Orlando, Fla. (1964).
18. Kantrowitz, A. R. and H. E. Petschek, *Plasma Physics in Theory and applications*, ed. W. B. Kunkel, pp. 148-206, MacGraw-Hill, New York (1966).
19. Wu, C. C., *J. Geophys. Res.*, 93, 3969 (1988).
20. Wu, C. C., *Geophys. Res. Lett.*, 14, 668 (1987).
21. Wu, C. C., *J. Geophys. Res.*, 95, 8149 (1990).
22. Lin, Y., L. C. Lee and C. F. Kennel, *Geophys. Res. Lett., 19*, 229 (1992).
23. Gosling, J. T., M. F. Thomsen, S. J. Bame, and C. T. Russell, *J. Geophys. Res.*, 91, 3029 (1986).
24. La Belle-Hamer, A. L., Z. F. Fu, and L. C. Lee, *Geophys. Res. Lett.*, 15, 152 (1988).
25. Heyn, M. F., H. K. Biernat, R. P. Rijbeek, and V. S. Semenov, *J. Plasma Physics*, 40, 235 (1988).

26. Biernat, H. K., M. F. Heyn, and R. P. Rijnbeek, *J. Geophys. Res.*, 94, 287 (1989).
27. Otto, A., K. Schindler, and J. Birn, *J. Geophys. Res.*, 95, 15,023 (1990).
28. Landau, L. D., and E. M. Lifshitz, *Electrodynamics of Continuous Media*, pp213-238, Pergamon Press (1960).
29. Lin, Y. and L. C. Lee, *Space Sci. Rev.*, Structure of reconnection layers in the magnetosphere (1993).
30. Lin, Y. and L. C. Lee, *Geophys. Res. Lett.*, Structure of flank reconnection layer in the presence of shear flows, to be submitted (1993).
31. Eastman, T. E., and L. A. Frank, *J. Geophys. Res.*, 87, 2187 (1982).
32. Sonnerup, B. U. O., G. Paschmann, I. Papamastorakis, N. Sckopke, G. Haerendel, S. J. Bame, J. R. Asbridge, J. T. Gosling and C. T. Russell, *J. Geophys., Res., 86*, 10049 (1981).
33. Gosling, J. T., M. F. Thomsen, S. J. Bame, T. G. Onsager, and C. T. Russell, *Geophys. Res. Lett., 17*, 1833 (1990a).
34. Gosling, J. T., M. F. Thomsen, S. J. Bame, R. C. Elphic, and C. T. Russell, *Geophys. Res. Lett., 17*, 2245 (1990b).
35. La Belle-Hamer, A. L., A. Otto, and L. C. Lee, *J. Geosphys. Res.*, Magnetic reconnection in the presence of sheared flow: Application to the Earth's magnetopause (1993).

CHAPTER 3
Asymmetric Inflow Conditions

3.1 Introduction

Magnetic reconnection in various regions of the Earth's magnetopause has been examined by many authors using both theoretical and simulation studies [*Dungey*, 1961; *Mitchell and Kan*, 1978; *Fu and Lee*, 1985; *LaBelle-Hamer et al.*, 1988; *Otto et al.*, 1990; *Shi et al.*, 1991]. These studies have shown that onset conditions, the dynamical evolution, and geometrical properties depend strongly on the local plasma conditions and magnetic field geometry. Of particular importance for the reconnection process seems to be the presence of a sheared flow across the magnetopause [*La Belle-Hamer et al.*, 1994].

The primary motivation for this study was provided by *Gosling et al.'s* [1986] observations of the mid-latitude flank magnetopause. The characteristics they reported are in stark contrast with the dayside observations. Accelerated flows were observed on the dusk side, and to a much lesser extent on the dawn side, of the near-tail magnetopause. Properties of these accelerated flows are, in many respects, different from those at the dayside magnetopause. The main characteristics of the accelerated flows reported by *Gosling et al.* [1986] include: (1) they are confined to a region where the field changes from the magnetosheath (MSH) to the magnetospheric (MSP) field orientation, (2) they are correlated to antiparallel interplanetary magnetic field (IMF), (3) they occur intermittently with individual flow events as long as ten minutes, (4) they are typically highest on the magnetospheric side of the current sheet, (5) the ion and electron temperatures are intermediate between magnetospheric and magnetosheath values, and (6) no boundary layer is observed, that is, no magnetosheath-like plasma earthward of the magnetic field transition region. These observations have been interpreted as possible signatures

of magnetic reconnection in the flank region of the magnetopause. In addition, *Gosling et al.* [1991] reported high latitude observations of accelerated flow regions with similar properties. The high latitude observations contain regions with earthward flow.

At the dayside magnetopause, the observations indicate that the magnetopause is on the sunward, or magnetosheath, side of the accelerated high speed flow which contains a layer of magnetosheath-like plasma [*Sonnerup et al.,* 1981; *Eastman et al.,* 1985; *Paschmann et al.,* 1986; *Gosling et al.,* 1991]. The key differences between the flank observations and the dayside observations are the location of the accelerated flow region relative to the magnetic field turning region and the width of the magnetic field transition region. At the dayside, the magnetic field rotates sharply from MSH orientation to MSP orientation, while the field transition region is very broad in the flank region.

It is the purpose here to examine the properties of magnetic reconnection in the flank regions of the magnetosphere in the presence of a sheared plasma flow and plasma density asymmetry. The results are compared with those cases without shear flow, which are more typical for the subsolar dayside magnetopause. I will compare typical properties in the simulations with the corresponding observations in the flank region and at the dayside magnetopause.

A sketch of the coordinate system used in the study and the relationship to the observations of *Gosling et al.* [1986] is shown in Figure 3.1. A local coordinate system is introduced, in which the geomagnetic field is in the negative y direction, x is perpendicular to the magnetopause, and z completes the right hand coordinate system. At the location of *Gosling et al.*'s observations, the dusk side geomagnetic field is primarily in the negative y direction in simulation coordinates with a small z component and the IMF is essentially antiparallel to the nearby geomagnetic field. If the IMF is nearly antiparallel to the geomagnetic field, then the field may be

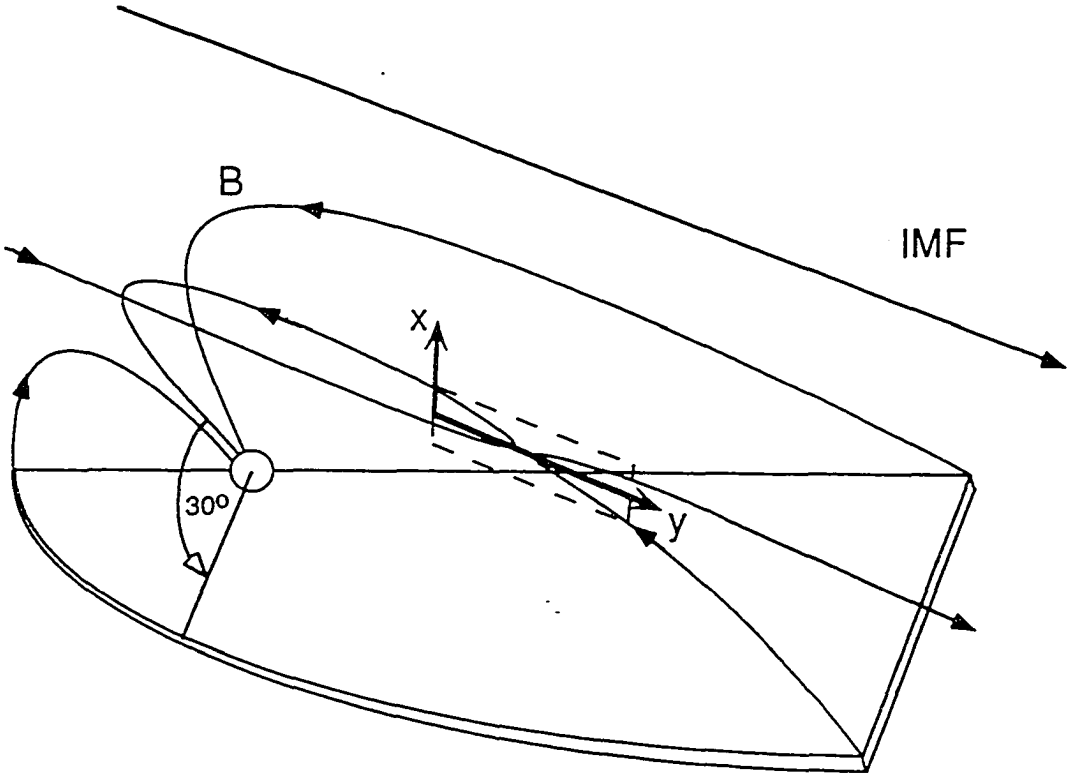

Figure 3.1. Sketch of the coordinate system used in the simulation and the relationship to the observations of Gosling et al. [1986].

susceptible to the development of the tearing instability and magnetic reconnection in that region.

Plasma flow in the flank magnetosheath will convect the reconnected field lines tailward. Based on our simulations, magnetic reconnection ceases for sufficiently large values of the shear velocity. Therefore, the existence of a critical shear velocity separating reconnecting and nonreconnecting solutions is expected and sought. A plausible physical mechanism will be presented to explain the switch off of the magnetic reconnection process for shear flow above the critical velocity.

In addition to a critical velocity, we expect the shear flow to affect the structure of the reconnection region and other properties based on the theoretical work with incompressible plasma done by *Sonnerup* [1970] and *Mitchell and Kan* [1978] and our recent work with compressible plasma [*La Belle-Hamer et al.*, 1994]. In Chapter 2, we examined steady state magnetic reconnection in a sheared plasma with symmetric plasma density and magnetic field strength and found that an intermediate shock and a slow shock replace the slow shock pair bordering the outflow region. Addition of an asymmetric density, which is studied in the present work, can alter both the shock structure and reconnection properties.

A two-dimensional (2-d) compressible magnetohydrodynamic (MHD) computer simulation will be used to explore magnetic reconnection under conditions comparable to the near-tail flank and the dayside regions of the magnetosphere. Specifically, the dependence of magnetic reconnection on the relative velocity shear across the magnetopause will be explored in detail. There are two basic reconnection geometries: (1) the reconnection region is swept tailward with the magnetosheath plasma and (2) the reconnection region is stationary with respect to the magnetosphere. In this paper, we will focus on the first geometry. The simulation takes place in the rest frame of the reconnection region, assuming the velocity of the reconnection region is half the solar wind velocity.

In the following section, the numerical method used in our simulations will be presented. In section 3, the main characteristics of the steady state region of the simulation are described and discussed. Specifically, we will illustrate the existence of a threshold velocity separating solutions dominated by velocity shear effects and by density asymmetry effects. Next, the critical velocity separating reconnecting and non-reconnecting solutions is discussed. In section 5, we analyze the motion and properties of the reconnection bulge, which also determines the size of the steady state region, as a function of time and the shear velocity. Finally, in the summary and discussion section, our results will be compared with relevant observations.

3.2 Numerical Method

The numerical simulation in this study uses a two-dimensional compressible MHD code which is discussed in *Otto et al.* [1990]. The time advancement is achieved by the leap frog method with second order accuracy in time and space. The compressible MHD equations used can be written as:

$$\frac{\partial \rho}{\partial t} = -\nabla \cdot (\rho \mathbf{v}) \tag{3.1}$$

$$\frac{\partial (\rho \mathbf{v})}{\partial t} = -\nabla \cdot [\rho \mathbf{v}\mathbf{v} + (p + \frac{B^2}{2\mu_o})\bar{\bar{\mathbf{I}}} - \frac{\mathbf{B}\mathbf{B}}{\mu_o}] \tag{3.2}$$

$$\frac{\partial \mathbf{B}}{\partial t} = \nabla \times [\mathbf{v} \times \mathbf{B} - \eta \mathbf{j}] \tag{3.3}$$

$$\frac{\partial \varepsilon}{\partial t} = -\nabla \cdot \mathbf{S} \tag{3.4}$$

where

$$\varepsilon = \frac{\rho v^2}{2} + \frac{B^2}{2\mu_o} + \frac{p}{\gamma - 1} \quad \text{and} \tag{3.5}$$

$$\mathbf{S} = (\varepsilon + p + \frac{B^2}{2\mu_o})\mathbf{v} - (\mathbf{B} \cdot \mathbf{v})\frac{\mathbf{B}}{\mu_o} + \frac{\eta}{\mu_o}\mathbf{j} \times \mathbf{B} \tag{3.6}$$

and ρ is the mass density, v is the bulk flow velocity, p is the plasma pressure, $\mathbf{B}$ is the magnetic field, $\mathbf{j} = \nabla \times \mathbf{B}/\mu_o$ is the current density and η is the resistivity.

The three basic quantities used for the normalization are the average asymptotic magnetic field (B_0), the average asymptotic density (ρ_0) at $x = \pm\infty$, and the initial current sheet half thickness (a). All the other quantities are normalized in terms of these three. Therefore, the velocity is normalized by the Alfvén velocity $V_{Ao} = B_o/\sqrt{\rho_o \mu_o}$, pressure by the magnetic pressure $B_o^2/2\mu_o$, current by $B_o/\mu_o a$, resistivity by $1/\mu_o a v_{Ao}$, Time is measured in units of Alfvén transit time, $t_A = a/V_{Ao}$. For the dayside, $\rho_o \sim 10cm^{-3}$, $B_o \sim 50nT$, $a \sim 400km$, which leads to an Alfvén velocity of approximately 400 km/s and an Alfvén transit time of 1 second. In the flank region, $\rho_o \sim 2cm^{-3}$, $B_o \sim 25nT$, $a \sim 600km$, which leads to an Alfvén velocity of approximately 400 km/s and an Alfvén transit time of 1.5 seconds. We remark that a typical length scale for the thickness of the field reversal region at the flank is not available from observations. We will discuss time and length scales in section 5.

The initial current sheet is located in the $x = 0$ plane. The initial magnetic field and velocity are specified as

$$\mathbf{B} = \tanh(x)\hat{\mathbf{y}} \tag{3.7}$$

$$\mathbf{v} = v_o \tanh(x)\hat{\mathbf{y}} \tag{3.8}$$

where the magnitude of the shear velocity v_o varies from 0 to 1.2 in this study. A Galilean transformation of the velocity shifts it back into the rest frame of the magnetosphere.

The configuration for the initial conditions is in pressure equilibrium. For a pressure equilibrium, the pressure must be constant throughout, i.e.,

$$p + B^2 = \text{constant} \tag{3.9}$$

In these simulations, the pressure is determined by

$$p_o = p_{msp} + (1 - B_{msh}) \qquad 3.10$$

where the subscripts *msp* and *msh* refer to magnetospheric and magnetosheath, respectively. The density is prescribed in order to have the option of density asymmetry. The initial density profile used is

$$\rho_0 = 1.0 + \Delta\rho \tanh(\frac{x}{a}) \qquad 3.11$$

where $\Delta\rho$ is 0.5 for a majority of the runs presented here. This gives a ratio of 3 to 1 between the plasma densities of the magnetosheath and magnetosphere, respectively. In *Gosling et al.'s* [1986] observations, the density of the magnetosheath is approximately 10 to 50 times that in the magnetosphere. Since our simulation time step is limited by the Courant-Friederichs-Lewy condition, a realistic density ratio would necessitate a very small time step. Therefore, a smaller density ratio of 3 to 1 was used in order to maintain a reasonable time step. We did, however, several runs with a more realistic density ratio of 1 to 9, one of which will be presented.

The simulation domain is a rectangular box in the $x-y$ plane, extending in the x direction from -20 to 20 and in the y direction from -150 to 150. The x direction is perpendicular to the initial current sheet and y is along the unperturbed magnetic field. We identify $x > 0$ with the magnetosheath and the positive y direction as tailward. The two-dimensional approximation is valid close to and tailward of the reconnection region. At larger distances earthward of the reconnection region, the geomagnetic field's increasing strength and curvature become important.

The simulation has 201 grid points in the x direction and 403 grid points in the y direction. The grid is non-uniform, with a higher resolution in the current sheet than at the boundaries. The resolution in the current sheet in the x-direction is 0.05 and in the y direction is 0.5. The derivative of each physical quantity with

respect to the boundary normal direction is set to zero at $y = \pm 150$ and $x = \pm 20$. These are referred to as free boundaries.

The simulation box is designed to be larger than the region of interest in order to decrease the effect of the boundary conditions. In the vicinity of the reconnection region, an approximately steady-state configuration develops. The size of this stationary region increases with time.

All the cases presented in this paper use a localized resistivity applied to a small region in the current sheet. After a short initial period allowing the resistivity to gradually reach its peak value, the position and magnitude of the resistivity do not change with time. The resistivity profile is given by

$$\eta = \eta_o(1.0 - \exp^{-\frac{t}{15}}) \cosh^{-2}\left(\frac{x}{l_x}\right) \cosh^{-2}\left(\frac{y - y_o}{l_y}\right) \qquad 3.12$$

where η_o is 0.05 in the cases presented in this paper. The resistivity profile is centered at $(x, y) = (0, y_o)$ and $l_x = l_y = 3$. The chosen frame of reference implies that the high resistivity region is moving along the y direction with respect to the rest frame of the magnetosphere, in the same direction and half the magnitude of the magnetosheath plasma flow. The presence of resistivity allows the magnetic field lines to violate the frozen-in condition and triggers onset of magnetic reconnection. By keeping it constant and localized, we can examine the dynamics of the reconnection process without the complications invoked with a varying resistivity. For this study, we used a background resistivity of 0.001 in order to dissipate strong gradients on the grid scale, which can develop since the leap frog method used in the simulation has very low numerical dissipation.

Table 2 shows the parameters used in the 9 simulation cases presented in this Chapter. In Table 2, v_o is the initial velocity magnitude on one side of the current layer as in equation 3.10, $\Delta\rho$ is defined by equation 3.11, V_{Amsp} and V_{Amsh} are

Table 2. . Parameters used in the simulation cases

Case	v_o	$\Delta\rho$	V_{Amsp}	V_{Amsh}	$\lvert\Delta V_A\rvert$	$\Delta\lvert V_A\rvert$
1	0.0	0.0	1.0	1.0	2.0	0.0
2	0.6	0.0	1.0	1.0	2.0	0.0
3	0.0	0.5	1.4	0.8	2.2	0.6
4	0.2	0.5	1.4	0.8	2.2	0.6
5	0.3	0.5	1.4	0.8	2.2	0.6
6	0.6	0.5	1.4	0.8	2.2	0.6
7	0.8	0.5	1.4	0.8	2.2	0.6
8	0.9	0.5	1.4	0.8	2.2	0.6
9	0.2	0.8	2.2	0.7	2.9	1.5

the magnitudes of the Alfvén velocity on the magnetospheric ($x < 0$) and magnetosheath ($x > 0$) side of the current layer, respectively; Δ indicates the difference between the asymptotic values across the current layer.

3.3 Shock structure formation in the presence of sheared flow and density asymmetry

In this section, we will confine our study to the structure of the steady-state region. General properties of the reconnection process and the region outside this steady state region will be addressed in the next sections.

In order to provide a reference for the simulation results which follow, we will first illustrate the reconnection geometry obtained with (a) zero initial velocity shear with symmetric density (Case 1), (b) a non-zero velocity shear with symmetric density (Case 2), and (c) zero initial velocity shear with an asymmetric plasma density profile (Case 3). In Figure 3.2, the magnetic field lines and velocity vectors are shown for the cases with (a) $v_o = 0$ and $\Delta\rho = 0$ (Case 1); (b) $v_o = 0.6$ and $\Delta\rho = 0$ (Case 2); and (c) $v_o = 0$ and $\Delta\rho = 0.5$ (Case 3). Figure 3.2 shows only the steady state portion of the simulation box.

The magnetic field lines in Case 1 show a *Petschek*-like reconnection geometry, with symmetry across both the x and the y axes. The four distinct regions associated with magnetic reconnection can be seen in all three cases presented in Figure

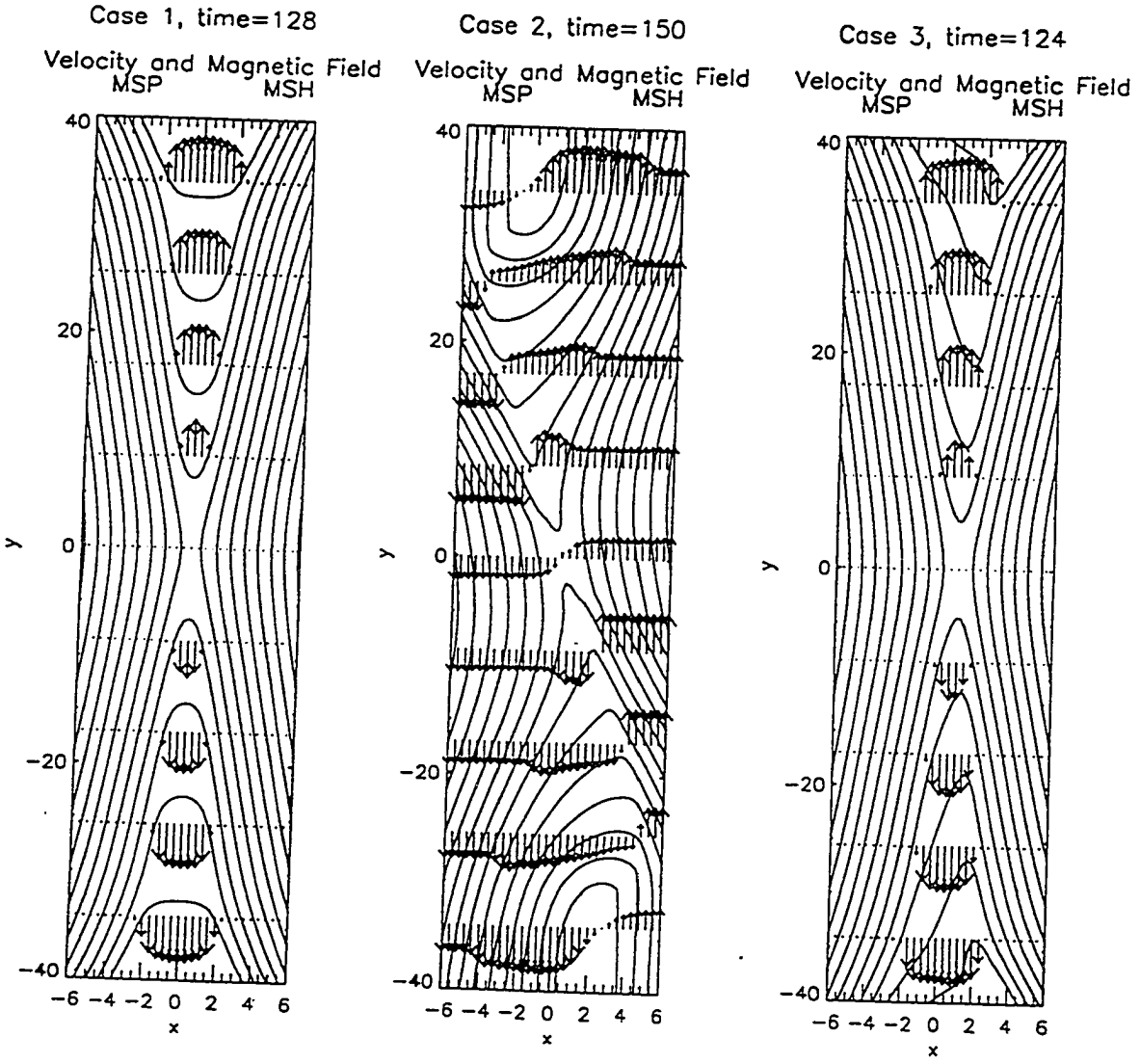

Figure 3.2. The magnetic field lines and velocity vectors are shown for the cases with (a) $v_o = 0$ and $\Delta\rho = 0$ (Case 1); (b) $v_o = 0.6$ and $\Delta\rho = 0$ (Case 2); and (c) $v_o = 0$ and $\Delta\rho = 0.5$ (Case 3).

3.2. Two regions with very low velocity and large magnetic field, are called the inflow regions, and two regions of weak magnetic field and large plasma velocity separating the inflow regions are called the outflow regions, in keeping with convention. The inflow and outflow regions are distinct in the velocity vectors with the accelerated flow confined to the outflow region.

The magnitude of the magnetic field decreases from upstream to downstream across both shocks. The tangential magnetic field, however, does not change sign across either shock. Since the plasma density and plasma pressure (not shown) increase across both shocks, these shocks are identified as slow shocks.

In contrast, the configuration for Case 2 (with an initial velocity shear of magnitude 0.6 and symmetric density) shows a point symmetry about the origin such that $f(x,y) = \pm f(-x,-y)$. In the positive y plane, the magnitude and direction of the magnetic field changes sharply across the shock on the MSP side; on the MSH side of the current sheet, the magnetic field change is considerably less dramatic. Due to the change in plasma flow direction across the shock on the MSP side (in the $x < 0$, $y > 0$ quadrant) enforced by the initial shear, the plasma acceleration across the MSP shock is much greater than the acceleration across the MSH shock and an intermediate shock forms [*La Belle-Hamer et al.*, 1994].

The magnitude of the tangential component of the magnetic field (B_y) decreases across both shock structures. However, across the shock in the $x < 0$, $y > 0$ quadrant, the tangential component of the magnetic field changes sign. The total current which separates the inflow regions is unequally divided between the two shocks. In addition, the plasma pressure and density (not shown) increase from the inflow (upstream) to outflow (downstream) region. The shock on the MSH side (in $x > 0$, $y > 0$ quadrant) is identified as an intermediate shock while the shock on the MSP side is a slow shock [*La Belle-Hamer et al.*, 1994].

The magnetic field line configuration for Case 3 (with no initial velocity shear and an initial density asymmetry across the current sheet) is symmetric only with respect to $y = 0$. The magnetic field changes direction sharply on the MSH side for $x > 0$. Therefore, for zero shear flow in the asymmetric density case, the stronger of the two current layers in the outflow region occurs on the magnetosheath side, which has a higher plasma density. The shocks on the MSH side have been identified as intermediate shocks [*e.g. Scholer*, 1989; *Shi and Lee*, 1990]. Such configurations are especially applicable to the dayside region of the magnetopause.

In the above cases, we have seen that the shock structure of the outflow region can be affected by either a velocity shear across the current layer or an asymmetric density profile. In the flank regions of the magnetosphere both a sheared plasma flow and an asymmetric density profile are present; therefore we examine configurations containing both.

The intermediate shock and stronger current layer always form on the side where a larger plasma acceleration from the inflow to the outflow region is required. This can be due to a larger inertia (higher plasma density), a smaller Alfvén velocity (smaller magnetic field magnitude or higher plasma density), or a larger change of the tangential velocity. Cases 2 and 3 illustrate that for the tailward region ($y > 0$), the effect of the velocity shear and the effect of the plasma density asymmetry are in direct competition with each other. For a given plasma density asymmetry, we expect a threshold velocity v_{thresh} above which the shear flow dominates the reconnection layer structure, forming the intermediate shock on the MSP side. Below the threshold velocity, the shock formation is dominated by the asymmetry in density across the current layer and the intermediate shock forms on the MSH side.

It is important to note that the above discussion applies only to the upper half plane, or tailward of the reconnection site. In the lower half plane, or sunward of

the reconnection site, the picture is considerably different. We see in Cases 2 and 3 that the asymmetric density and the velocity shear in the inflow regions both favor the formation of an intermediate shock on the MSH side. Discussion of the threshold velocity, then, will be confined to the $y > 0$ plane.

From the simulations, the threshold velocity is found to be dependent upon the Alfvén velocities of both inflow regions. Specifically, the threshold velocity is found to be one half the difference between the Alfvén velocities on either side of the current sheet, or the average Alfvén velocity magnitude,

$$v_{thresh} = \frac{|v_{Amsh}| - |v_{Amsp}|}{2} \qquad 3.13$$

In Figure 3.3, the magnetic field and velocity vectors for three cases with velocities below, near, and above the expected threshold are shown. All three cases have a plasma density profile as in 3.12 with $\Delta\rho = 0.5$, i.e., a density ratio of 3 to 1. The magnetic field lines in all three cases shown in Figure 3.3 are indicative of magnetic reconnection. There are distinct inflow and outflow regions with current layers separating the two regions. All three cases have regions with accelerated plasma.

Case 4 (Figure 3.3a) has a velocity shear below the threshold velocity. The density asymmetry dominates the shock structure. The magnetic field contours show that the intermediate shocks forming on the MSH side in both the $y > 0$ and $y < 0$ planes. Thus, the current layers are dominated, although not strongly, by the current on the MSH side for both the upper and lower half planes.

Case 6 (Figure 3.3c) has a velocity above the threshold and asymmetries in the magnetic field contours in both x and y can be seen quite clearly. The velocity vectors, as well, show very different formations for positive and negative y. In addition, any symmetry from left to right for positive y has also been lost with the

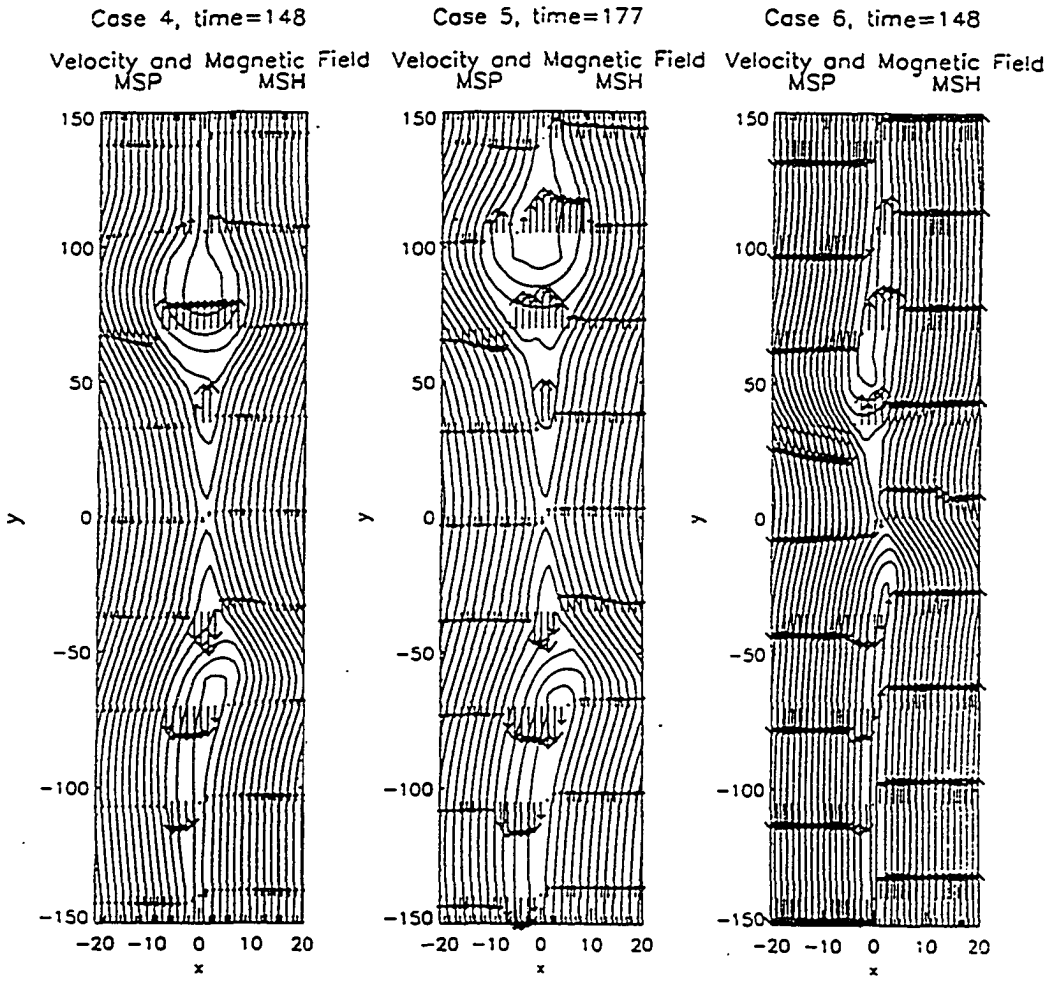

Figure 3.3. Magnetic field lines and velocity vectors for three cases: (a) $v_0 = 0.2$ and $\Delta\rho = 0.5$ (Case 4); (b) $v_0 = 0.3$ and $\Delta\rho = 0.5$ (Case 5); (c) $v_0 = 0.6$ and $\Delta\rho = 0.5$ (Case 6).

increase in velocity shear. The velocity shear, rather than the density gradient, dictates the overall current sheet configuration.

Case 5 (Figure 3.3b), however, is a marginal case with an initial velocity shear approximately at the threshold and is different from the other two runs. The outflow region in the positive y half appears to be symmetric in x. However, in the negative y plane, there is a difference between the magnetosheath (right) side and the magnetosphere (left) side. The shock structures are asymmetric with an intermediate shock forming on the MSH side. This asymmetry shows up in the velocity vectors as well, particularly for $y < -10$ and the current density contours illustrate this asymmetry quite clearly. The positive y half of the plane appears to be more or less symmetric, with two approximately equal current layers. This symmetry is evident in the magnetic field lines, as well as the velocity vectors and the current density contours.

In order to examine these configurations more closely, horizontal slices of the magnetic field (B_y solid line and B_x dotted line), current (J_z), velocity (V_A solid line and V dashed line), pressure (P solid line), and plasma density (ρ dotted line) for Cases 4, 5, and 6 for y positions above and below the reconnection region are shown in Figure 3.4. Again, positive y values are tailward of the reconnection region. Note also that although the magnitude of the current density is approximately the same, the current layer is slightly wider on the MSH side for Case 4 which yields a stronger surface current. In Case 4, the tangential magnetic field tailward of the reconnection site is seen to change sign across the shock on the MSH side, while in Case 6, this occurs on the MSP side. Thus, the magnitude of the velocity shear dictates, all other things being equal, the position of the intermediate shock formation. The upper half plane outflow region is bounded by two slow shocks for Case 5, similar to the zero velocity shear configuration. The two

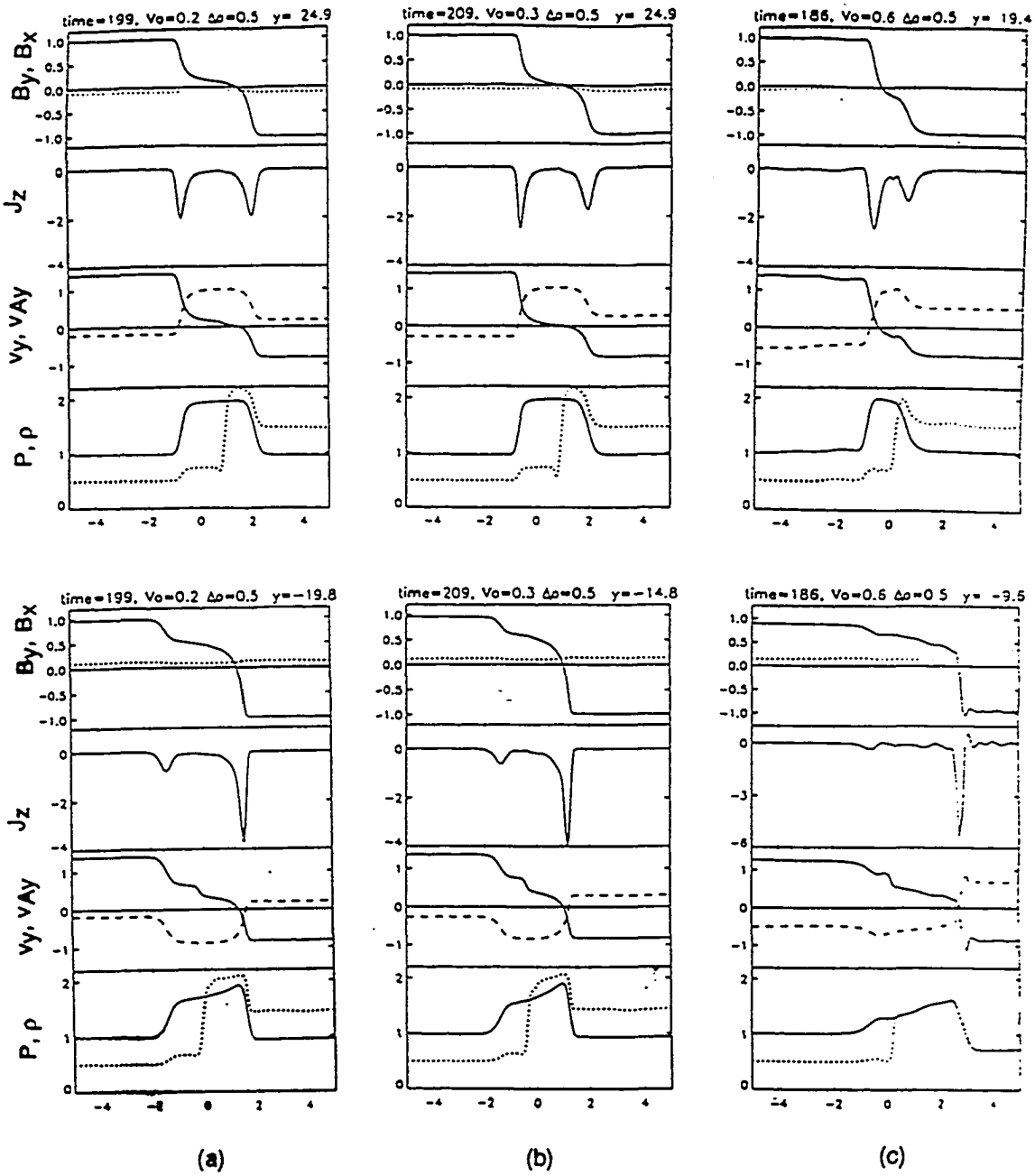

Figure 3.4. Horizontal slices of the magnetic field (B_y solid line and B_x dotted line), current (J_z), velocity (V_A solid line and V dashed line), pressure (P solid line), and plasma density (ρ dotted line) at y positions above and below the reconnection region for three cases: (a) $v_0 = 0.2$ and $\Delta\rho = 0.5$ (Case 4); (b) $v_0 = 0.3$ and $\Delta\rho = 0.5$ (Case 5); (c) $v_0 = 0.6$ and $\Delta\rho = 0.5$ (Case 6).

effects, asymmetric density and velocity shear in the inflow regions, balance each other and the development of an intermediate shock is inhibited.

The current density slices shown in Figure 3.4 clearly illustrates the differences between the four quadrants for these three cases. For negative y, the majority of the current is contained in the shock on the magnetosheath side regardless of the velocity shear. For positive y, the configuration is highly dependent on the velocity shear. In the three cases shown in Figures 3.3 and 3.4, the difference in the Alfvèn velocity magnitudes in the inflow regions is 0.6. For an initial velocity above 0.3, an intermediate shock develops on the magnetosheath side. For an initial velocity below 0.3, an intermediate shock develops on the magnetospheric side. The threshold velocity, then, found through the simulations is 0.3. For the case with the velocity shear equal to the threshold velocity, the two effects balance for $y > 0$.

To estimate the threshold velocity, we consider the small shock angle approximation for the outflow region in the positive y half plane. Using $\Delta v \sim \Delta V_A$ and assuming the plasma density in the outflow region is approximately the same as the adjacent inflow region, then

$$v_{msh} - V_{out} \sim -\frac{B_{msh} - B'_{msh}}{\sqrt{\rho_{msh}}} \tag{3.14}$$

$$v_{msp} - V_{out} \sim \frac{B_{msp} - B'_{msp}}{\sqrt{\rho_{msp}}} \tag{3.15}$$

where the prime denotes downstream of the shock, which is inside the outflow region. Assuming $B'_{msh} = B'_{msp} \equiv B'$, $v_{msh} = -v_{msp} = v_o$, and $\rho_{msh} \neq \rho_{msp}$, where B and v are the y components and carry sign. We obtain the tangential magnetic field in the outflow region:

$$B' = (\alpha - 1)\left[\frac{\rho_{msp} - \rho_{msh}}{\rho_{msp} + \rho_{msh}}\right] \tag{3.16}$$

where α is defined as the ratio of the velocity shear ($2v_o$) to the difference between the Alfvén velocity magnitudes ($\Delta|V_A|$). Since the sheet current across either of the shocks in the outflow region is the change in the magnetic field, $I = \Delta B$, then the current across the MSH current layer is $I_{msh} = 1 - B'$ and the current across the MSP current layer is $I_{msp} = 1 + B'$.

The current in either current sheet depends directly on the magnetic field B'. From equation 3.16, B' is a function of α for any given density asymmetry. If B' is zero, the current sheets are equivalent. It follows that in order to have the density asymmetry effects and the velocity shear effects balance each other, which is manifested by equivalent current sheets, α must equal 1, or

$$\alpha = 1 = \frac{2v_o}{\Delta|V_A|} \qquad 3.17$$

The threshold velocity is then

$$v_o = \frac{\Delta|V_A|}{2} \qquad 3.18$$

For all other values of v_o, the current sheets on the *msp* and the *msh* side are not symmetric.

Figure 3.5 illustrates this asymmetry in current based on the above equations. The current contained in the MSH side (I_{msh}) and the MSP side (I_{msp}) shock structures in the positive y plane are plotted as a function of initial velocity shear. Three density ratios are shown. The solid line has a 3:1 MSH:MSP density ratio, the dotted line has a 9:1 ratio, while the dashed line has a 50:1 ratio. The points on the plot are the values obtained from the simulations. The asteriks are from the simulations with a density ratio of 3:1, while the diamonds are from the simulations with a density ratio of 9:1. For sunward accelerated plasma, the intermediate shock is on the MSH side such that the magnetic field in the accelerated region should have the same orientation as the MSP magnetic field and be close to the same

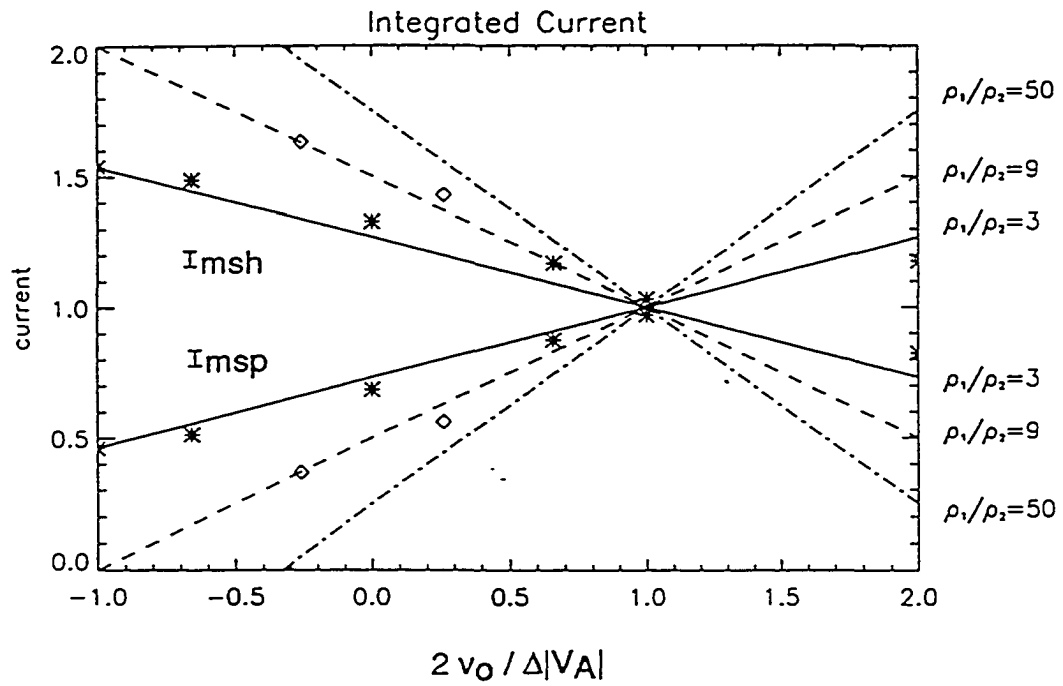

Figure 3.5. The current contained in the MSH and the MSP side shock structures in the $y > 0$ plane. For $2v_o/\Delta|V_A|$ (α) equal to 1, the effects of the velocity shear and the density asymmetry balance and the current sheets are symmetric. Three density ratios are shown. The solid line has a 3:1 MSH:MSP density ratio, the dotted line has a 9:1 ratio, while the dashed line has a 50:1 ratio. The points on the plot are the values obtained from the simulations. The asteriks are from the simulations with a density ratio of 3:1 while the diamonds are from the simulations with a density ratio of 9:1.

magnitude. This result agrees very well with the sunward flow interval in the observations of *Gosling et al.*, [1986].

3.4 Cut off of magnetic reconnection for large flow shears.

It is obvious that reconnection cannot operate for arbitrarily large values of the shear flow. It is expected, therefore, that there exists a critical velocity for the shear flow above which magnetic reconnection is switched off. The value of the critical velocity is important for observations since it determines a velocity range for the tailward motion of the X line with ongoing reconnection.

Mitchell and Kan [1978] predicted a cut-off velocity for the incompressible symmetric case above which magnetic reconnection will not occur. We conducted a parameter search in order to determine the value of the critical velocity in the compressible case and study the physical mechanism for switchoff. For a symmetric compressible plasma configuration, *La Belle-Hamer et al.* [1994] found that this critical value was the Alfvén velocity of the inflow region in agreement with *Mitchell and Kan's* [1978] results.

Figure 3.6 shows the time development of the z component of the electric field E, the z component of the current density J_z, and the y position of the X line for three cases. Case 6 (the solid line) has an initial velocity of $v_o = 0.6$. The initial velocity in Case 7 (dashed line) is $v_o = 0.8$ and in Case 8 (dotted line) is $v_o = 0.9$. The electric field and current density shown in Figure 3.6 are calculated at the X line.

For the smaller initial shear cases (Case 6 is shown in Figure 3.6 as a representative example), J_z increases initially but then maintains a relatively constant value. The nonzero current density and resistivity lead to a nonzero electric field at the X line which is equal to the reconnection rate. Therefore, the presence of a substantial and constant E is equivalent to ongoing reconnection. The y position

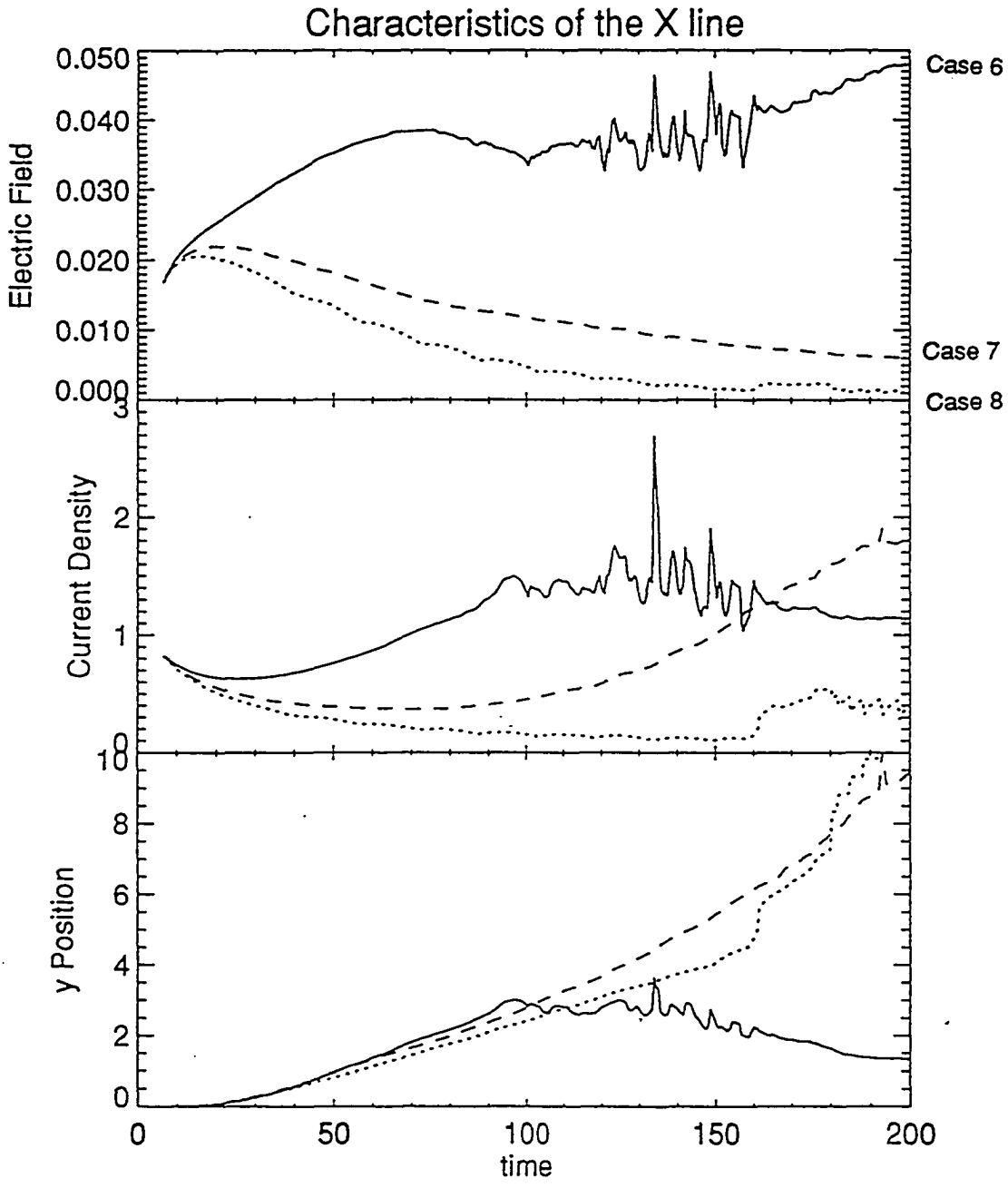

Figure 3.6. Time evolution of the electric field, the z component of the current sheet (j_z) and the y position of the X line for Cases 6 (solid line), 7 (dashed line), and 8 (dotted line) where $\Delta\rho = 0.5$ and $\eta = 0.05$ for all three cases.

for the X line remains approximately constant throughout the interval shown. In this case, and those cases with an initial velocity less than the critical value, a stationary magnetic reconnection region develops.

For Case 7, the electric field is relatively small. Since the electric field at the X line is equal to the reconnection rate, this implies that, although magnetic reconnection continues, the rate is small. After $150t_A$, the electric field goes to nearly zero at the X line even though the current density does not. The X line is slowly convected out of the high resistivity region. Although the velocity shear magnitude is symmetric across the current sheet, the magnetosheath plasma has a larger momentum. The reconnection rate is not quite high enough to maintain the position of the X line. For this case, (see Table 2) the Alfvén velocity of the magnetosheath and the magnetosphere are ~ 0.8 and ~ 1.4, respectively, and the initial velocity is 0.8. Therefore, the initial velocity is approximately equal to the Alfvén velocity of the magnetosheath.

For Case 8, both the electric field and the current density are essentially zero and magnetic reconnection is switched off. This switch off is not the result of convection. The initial velocity in this case is 0.9, slightly above the Alfvén velocity of the magnetosheath. Cases 7 and 8 illustrate that reconnection is switched off if the shear velocity in one of the inflow regions (in the frame of the X line) is larger than the Alfvén velocity in this region.

Figure 3.7 shows the magnetic field lines, velocity vectors, and current density contours for Case 8 (initial velocity shear of $v_o = 0.9$ and $\Delta\rho = 0.5$) at $t = 187t_A$. The magnetic field lines exhibit a very different geometry than seen in the preceding, lower shear flow, cases. Although some reconnected flux is visible, the amount is very small. The basic reconnection geometry with two shocks separating an inflow and outflow region does not appear in this case. The accelerated plasma flow

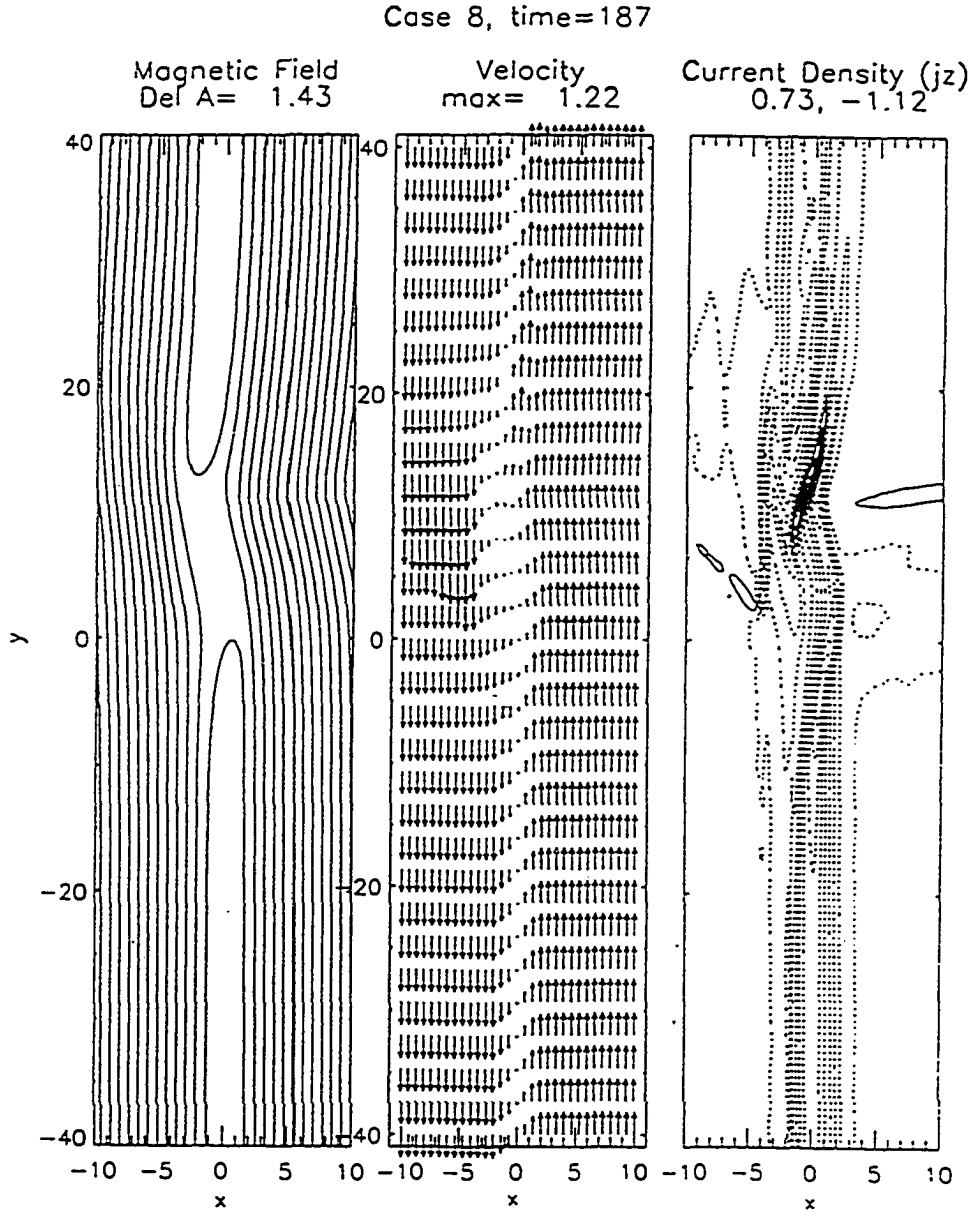

Figure 3.7. The magnetic field lines, velocity contours, and current density contours for the $v_o = 0.9$ case with asymmetric plasma density ($\Delta\rho = 0.5$).

in the outflow regions, a signature of an ongoing magnetic reconnection process, is absent in the super-critical cases.

More significant, perhaps, are the changes in the current density contours. Comparing these to the case seen in Figure 3.5, the striking difference is the splitting of the current sheet in the X line region and the subsequent split in the electric field. The peaks of the current density are labelled 1 and 2 in Figure 3.7. Both the current density and the electric field in the diffusion region tends to zero once the current sheet is split.

The splitting of the current layer and the very low current density in the vicinity of the X line are the local causes for the vanishing reconnection. This also implies a particular magnetic field configuration in the vicinity of the X line. Figure 3.8 shows close up views of the magnetic field lines in the reconnection region for the symmetric density cases with $v_o = 0.6$, 0.8, and 1.2 initial velocity shears are shown. The separatrix angle can be deduced from the magnetic field lines close to the diffusion region. The separatrix angle is found to increase with increasing velocity shear. As this angle approaches 90°, the current in the reconnection region approaches zero and magnetic reconnection ceases.

This effect can be understood as follows. In the vicinity of the magnetic X line, the equation for the vector potential can be written as

$$A_z = \frac{b_1}{2}x^2 - \frac{b_2}{2}y^2 \qquad 3.19$$

which considers the lowest order terms of an expansion of the magnetic field [e.g., *Sonnerup and Priest,* 1975; *Hesse et al.*, 1988]. Here b_1 and b_2 define the magnetic geometry of the X line where the separatrices are locally defined by $x = \pm\sqrt{b_2/b_1}y$ Using $\nabla^2 A_z = -J_z$, the current density is

$$J_z = -b_1 + b_2 \qquad 3.20$$

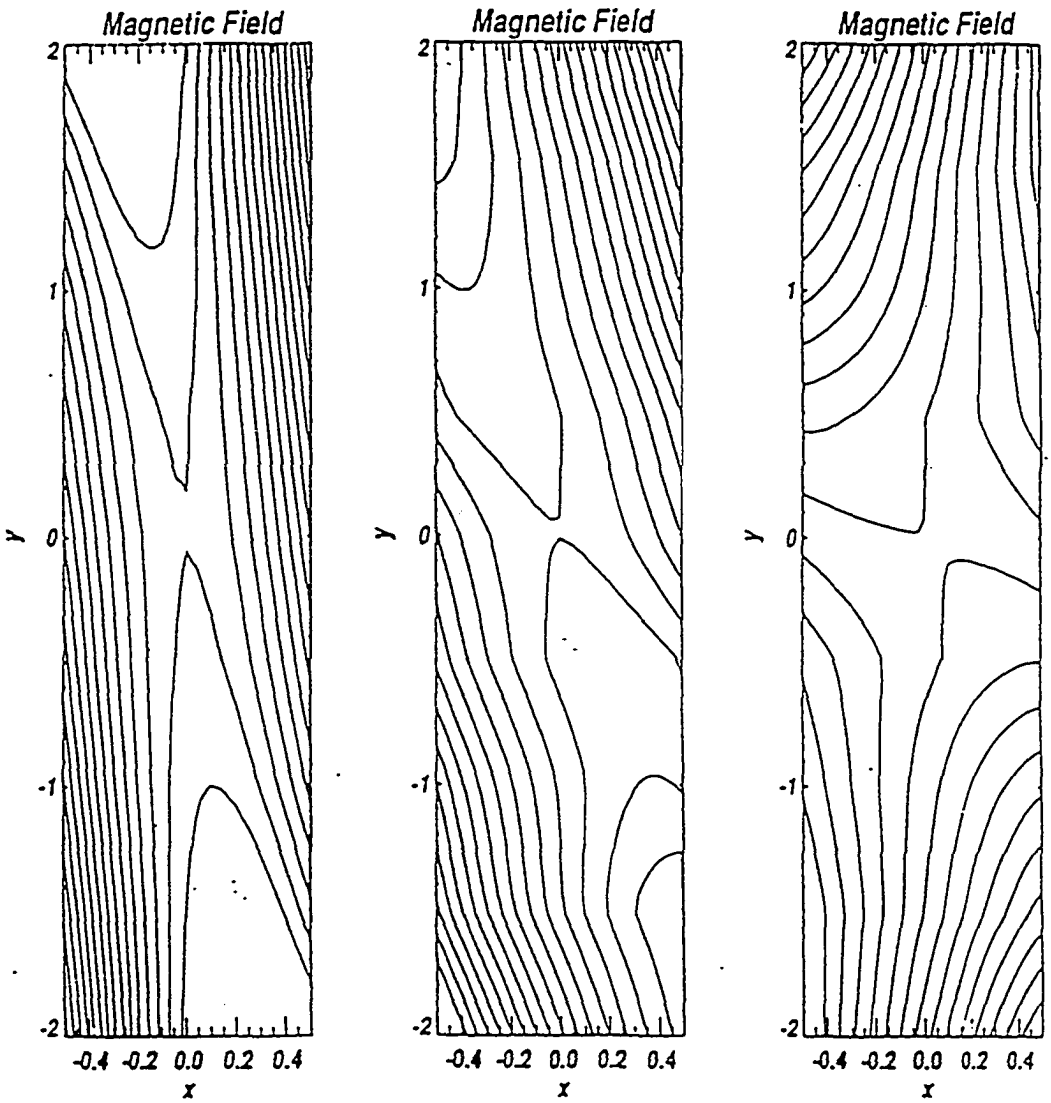

Figure 3.8. Close up viewpoint of separatrix angles for the symmetric cases with initial velocities of (a) 0.6, (b) 0.8, and (c) 1.2.

Therefore, for the case with $b_1 = b_2$, or equivalently, a separatrix angle equal to 90°, J_z will be zero. This can be seen in the simulations. As the separatrix angle approaches 90°, the current at the X line goes to zero and we see a split in the current sheet.

Note that x and y represent a local coordinate system at the X line. In the case of a sheared flow, this local system is rotated with respect to the simulation coordinates. The sense of rotation caused by the shear flow is such that the separatrices at which the outflow velocity is parallel to the initial velocity shear tilt closer to the y axis. Conversely, the separatrices at which the outflow and initial shear velocity are antiparallel tilt away from the y axis. This is consistent with the angular momentum associated with the shear flow in the vicinity of the X line.

In the antiparallel flow frame of reference used in the simulations in this paper, the underlying assumption is that the reconnection region velocity (v_r) is half the solar wind speed and, therefore the simulations are in the rest frame of the reconnection region. In fact, the velocity of the reconnection region is not necessarily half the solar wind speed and is not determined in this paper. However, a range of valid values can be given using the critical velocity. The existence of a critical velocity implies that there is a limited range of magnetosheath plasma velocities expected to be associated with magnetic reconnection events. The critical velocity is the minimum Alfvén velocity so that reconnection only occurs for

$$v_o < \mathrm{Min}[V_{Amsh}, V_{Amsp}]$$

. The reconnection region is assumed to be moving tailward. In the magnetosphere, the tailward velocity of reconnection region (v_r) satisfies

$$-V_{Amsp} < v_r < V_{Amsp} \qquad 3.21$$

for v_{msp} approximately zero. In the magnetosphere, the velocity of the reconnection region satisfies

$$v_{msh} - V_{Amsh} < v_r < v_{msh} + V_{Amsh} \qquad 3.22$$

So that for v_r satisfying

$$\mathrm{Max}[v_{msh} - V_{Amsh}, -V_{Amsp}] < v_r < \mathrm{Min}[v_{msh} + V_{Amsh}, V_{Amsp}] \qquad 3.23$$

magnetic reconnection is not cut off. Since the magnetospheric density is fairly low, the lower limit is $V_{msh} - V_{Amsh}$ such that the reconnection region needs to move tailward if the MSH velocity is super-Alfvénic for reconnection to operate. Further, from equation 3.23 it can be seen that if

$$v_{msh} - V_{Amsh} > V_{Amsp} \qquad 3.24$$

$$v_{msh} > V_{Amsh} + V_{Amsp} \qquad 3.25$$

magnetic reconnection cannot operate at the flanks of the magnetosphere.

3.5 Application to the Magnetosphere

Observations have shown that the properties of accelerated flow regions at the flank of the magnetopause [*Gosling et al.*, 1986] are very different from those observed at the dayside magnetopause [*Sonnerup et al.*, 1981; *Paschmann et al.*, 1986; *Gosling et al.*, 1991]. For the dayside magnetopause, the region of magnetic field turning is quite thin. The magnetopause is identified as a sharp discontinuity in the magnetic field. Accelerated flow is observed on the magnetospheric side of this sharp discontinuity. For the flank magnetopause, the region of magnetic field turning is relatively wide. Contained within this region is accelerated flow. These are the primary differences in the observations and the presence of sheared plasma during magnetic reconnection can explain these differences.

3.5.1 Flank region of the magnetosphere

In the flank region of the magnetosphere, there exists a large velocity shear across the magnetopause as well as a large density asymmetry. For tailward accelerated flow to be observed, the satellite must be located tailward of the reconnection region. Tailward of the reconnection region, the density gradient and the plasma velocity shear across the magnetopause compete (see Figure 3.4). The accelerated flow is confined to the field reversal region which is relatively wide due to the approximately equal current layers. The current layers which bound the accelerated flow regions are similar in strength if the magnetosheath plasma flow is in the range of the threshold velocity. From the simulations, this threshold velocity is the difference between the magnitudes of the Alfvén velocities in the MSH and the MSP. If the magnetosheath flow is larger than the threshold, the majority of the current is contained in the current layer on the MSP side of the steady state reconnection region.

The region earthward of the reconnection region is fundamentally different from the tailward region since the two effects, density gradient and velocity shear, enhance each other. A stronger intermediate shock develops on the MSH side of the outflow region due to combined effects of the density asymmetry and the plasma flow shear. This creates a narrower field reversal region and puts the accelerated flow on the MSP side of this field reversal. The magnetic field in the accelerated flow region is of magnetospheric orientation and magnitude. The plasma in the outflow region is accelerated earthward in the rest frame of the resistivity region. For sunward flow, the magnitude of the outflow velocity must exceed the magnitude of the magnetosheath velocity. However, the most probable observation earthward of the reconnection region is decelerated flow rather than sunward flow which may

be more difficult to identify. During the intermittent periods of sunward flow reported by *Gosling et al.* [1991], the magnetic field orientation is magnetospheric which confirms our prediction.

3.5.2 Dayside region of the Magnetosphere

For the dayside magnetopause, the density asymmetry is very large and the shear flow is negligible. In comparison to the density asymmetry, the asymmetry in the flow speed across the magnetopause is small and the magnetosheath velocity is well below the threshold velocity. With such a strong density asymmetry, the change in the magnetic field from the MSP orientation to the MSH orientation will occur almost completely in only one of the shocks bordering the magnetosheath. Figure 3.5 illustrates that, for parameters consistent with dayside observations (density ratio = 9), about 85% of the current is contained in the current layer on the MSH side of the accelerated plasma region. The prediction for the dayside region, then, is that the MSH shock contain the majority of the current. Simulations show that the MSH shock not only contains the majority of the current, but is also a very thin discontinuity in the magnetic field. The primary turning of the magnetic field takes place in the MSH shock. The accelerated flow region is, then, earthward of the dominant current layer. Observations of the low latitude boundary layer describe a region of accelerated plasma, with densities close to the magnetosheath level, on the magnetospheric side of the major current layer. This strong current layer is commonly addressed as the magnetopause and is very likely the MSH shock identified in the simulations.

3.6 References

Dungey, J. W., Interplanetary magnetic field and the auroral zones, *Phys. Rev. Lett.*, 6, 47, 1961.

Eastman, T. E., B. Popielawska, and L. A. Frank, Three-dimensional plasma observations near the outer magnetospheric boundary, *J. Geophys. Res.*, 90, 9519, 1985.

Fu, Z. F., and L. C. Lee, Simulation of multiple X line reconnection at the dayside magnetopause, *Geophys. Res. Lett., 12*, 291, 1985.

Gosling, J. T., M. F. Thomsen, S. J. Bame, and C. T. Russell, Accelerated plasma flows at the near-tail magnetopause, *J. Geophys. Res.*, 91, 3029, 1986.

Gosling, J. T., M. F. Thomsen, S. J. Bame, T. G. Onsager, and C. T. Russell, The electron edge of the low latitude boundary layer during accelerated flow events, *Geophys. Res. Lett., 17*, 1833, 1990a.

Gosling, J. T., M. F. Thomsen, S. J. Bame, R. C. Elphic, and C. T. Russell, Plasma Flow reversals at the dayside magnetopause and the origin of asymmetric polar cap convection, *J. Geophys. Res.*, 95,8073, 1990b.

Gosling, J. T., M. F. Thomsen, S. J. Bame, R. C. Elphic, and C. T. Russell, Observations of Reconnection of Interplanetary and lobe magnetic field lines at the high-latitude magnetopause, *J. Geophys. Res., 96*, 14097, 1991.

Hesse, M. and K. Schindler, A theoretical foundation of general magnetic reconnection, *J. Geophys. Res.*, 93, 5559, 1988.

La Belle-Hamer, A. L., Z. F. Fu, and L. C. Lee, A mechanism for patchy reconnection at the dayside magnetopause, *Geophys. Res. Lett.*, 15, 152, 1988.

La Belle-Hamer, A. L., The Kelvin-Helmholtz and tearing instabilities in relation to magnetic reconnection at the Earth's dayside magnetopause, *Master's Thesis*, University of Alaska, Fairbanks, 1988.

La Belle-Hamer, A. L., A. Otto, and L. C. Lee, Magnetic reconnection in the presence of sheared plasma flow: Intermediate shock formation, *Phys. Fluids B*, 1, 706, 1994.

Mitchell, H. G., and J. R. Kan, Merging of magnetic fields with field-aligned plasma flow components, *J. Plasma Physics*, 20, 31, 1978.

Otto, A., K. Schindler, and J. Birn, Quantitative study of the nonlinear formation and acceleration of plasmoids in the Earth's magnetotail, *J. Geophys. Res.*, 95, 15,023, 1990.

Paschmann, G., I. Papamasrtorakis, W. Baumjohann, N. Sckopke, C. W. Carlson, B. U. Ö. Sonnerup, and H. Lühr, The magnetopause for larger magnetic shear: AMPTE/IRM observations, *J. Geophys. Res., 91*, 11, 099, 1986.

Scholer, M., Asymmetric time-dependent and stationary magnetic reconnection at the dayside magnetopause, *J. Geophys. Res., 94*, 15, 099, 1989.

Shi, Y. and L. C. Lee, Structure of the reconnection layer at the dayside magnetopause, *Planet. Space. Sci., 38*, 437, 1990.

Shi, Y., C. C. Wu, and L. C. Lee, Magnetic reconnection patterns a the dayside magnetopause, an MHD simulation study, *J. Geophys. Res.*, 96, 17627, 1991.

Sonnerup, B. U. Ö., Magnetic reconnection in a highly conducting incompressible fluid, *J. Plasma Phys., 4*, 161, 1970.

Sonnerup, B. U. O., G. Paschmann, I. Papamastorakis, N. Sckopke, G. Haerendel, S. J. Bame, J. R. Asbridge, J. T. Gosling and C. T. Russell, Evidence for magnetic reconnection at the Earth's magnetopause, *J. Geophys., Res., 86*, 10049, 1981.

Sonnerup, B. U. Ö., and E. R. Priest, Resistive MHD stagnation-point flows in the current sheet, *J. Plasma Phys.*, 14, 283, 1975.

CHAPTER 4
Global Aspects

In Chapter 3, we have addressed the structure of the region with steady state reconnection only. However, as illustrated in Figure 3.3, the region affected by magnetic reconnection is much larger than the region of steady state reconnection. In the outflow region,the accelerated flow pushes plasma in both the positive and negative y directions. This causes a bulge to form, due to the inertia of the plasma, in front of the steady state reconnection region as the plasma is accelerated to the Alfvén velocity. The bulge plasma is essentially a transition region between the developing steady state region and the unperturbed plasma. As reconnection continues, both the steady state and the bulge region expand in the y direction. For asymmetric density and shear flow this expansion velocity is different for the positive and negative y directions as seen in Figure 3.3. In this chapter, we will discuss the properties of the entire reconnection region.

4.1 Size and Evolution of the Reconnection Region

Figure 4.1 shows the magnetic field lines, velocity vectors and contours of constant B_x for a case with more realistic values for the flank region of the density ratio (9:1) and the velocity shear ($v_o = 0.2$). From Figure 4.1, it can be seen that the minimum and the maximum value of the normal magnetic field component ($B_n = B_x$) occurs approximately in the transition region between the steady state region and the bulge. Thus, the total distance between the maximum and minimum normal component is a measure of the size of the steady state reconnection region.

In order to compare our simulation results with satellite observations, estimates of time and length scales are needed. For example, if the reconnection region is moving tailward with respect the magnetosphere with approximately half the solar wind velocity, then in the distance between the position of onset and the satellite

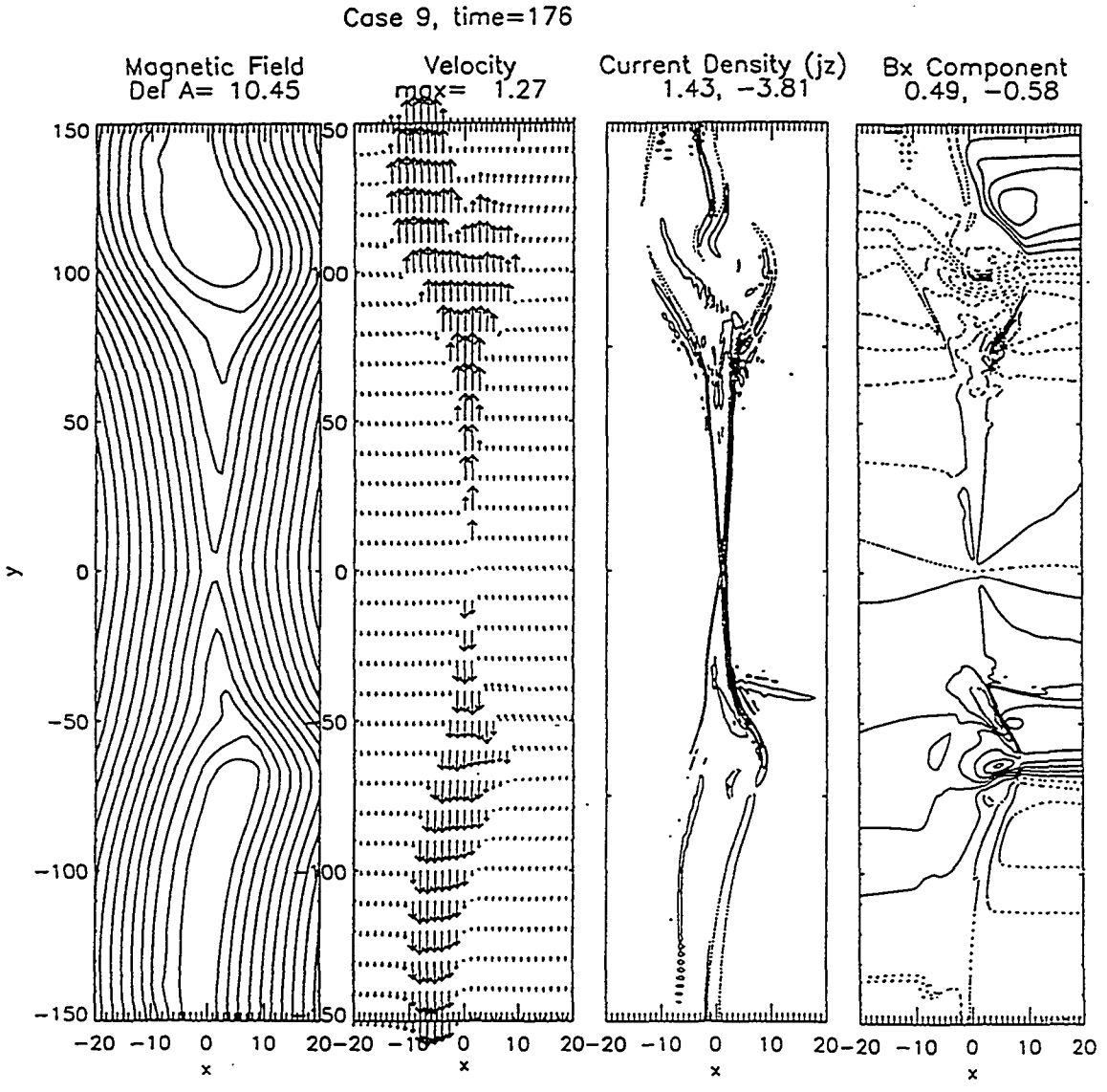

Figure 4.1. The magnetic field lines, velocity vectors, and contours of constant B_x for Case 9.

both the steady state region and the bulge regions grow. The longer the distance travelled, the more likely a substantial steady state region has been established. For this reason, the growth rates of both the steady state region and the bulge are investigated.

The expansion and evolution of the reconnection region is a highly nonlinear and time dependent process to which an exact analytical description is not available. The velocities of the bulges depends on both the Alfvèn wave propagation velocity and the plasma velocity. The velocities of the leading edges of the bulge are $\mathrm{Max}[|V_A| \pm v_o]$, depending upon the the Alfvén velocity direction relative to the plasma shear flow. For the trailing edges, which define the leading edges of the steady state regions, we expect a speed $\lambda \mathrm{Min}[|V_{Amsh}| \pm v_o, |V_{Amsp}| \mp v_o]$, where λ is a constant parameter describing the difference between this estimate and the velocity obtained in Figure 4.1 and is approximately 0.5 from the simulations. The difference between the velocity at the leading edge and the trailing edge of either the earthward ($-y$ direction) or the tailward ($+y$ direction) bulge will define the expansion velocity of that bulge. The sum of the magnitudes of the velocities of the trailing edges of the two bulges will define the expansion velocity of the steady state region.

The velocity of the trailing edge of the bulge earthward of the reconnection region is $\lambda(V_{Amsh} - v_o)$ and the velocity of the tailward bulge is $\lambda \mathrm{Min}[|V_{Amsh}| + v_o, |V_{Amsp}| - v_o]$. The ratio of the earthward and tailward velocities becomes

$$\xi = \frac{|V_{Amsh}| - v_o}{\mathrm{Min}[|V_{Amsh}| + v_o, |V_{Amsp}| - v_o]} \qquad 4.1$$

It can be seen from equation 4.1, both the density asymmetry and the velocity shear affect the expansion velocities of the two bulges. The dashed lines in Figure 4.1 correspond to ξ, which shows fairly good agreement with this crude estimate.

We note that for realistic parameters in the flank region, the large magnetospheric Alfvén velocity always implies that $\xi = (|V_{Amsh}| - v_o)/(|V_{Amsh}| + v_o)$.

Figure 4.2 shows the development in time of the y position of the maximum and minimum normal magnetic field components (B_n) across the current layer. The top panel shows the total distance in the y direction between the maximum B_n and the minimum B_n for four reconnecting cases. The slope of the line indicates the expansion rate of the steady state reconnection in the y direction. Clearly, the higher velocity cases expand at a slower rate than the lower velocity cases. The next four panels in Figure 4.2 show the absolute value of the ratio of y position of the maximum to the y position for the minimum of B_n, which is defined as ξ, for the same four cases. This is approximately the ratio of the size of the steady state regions earthward and tailward of the X line. For ξ equal to 1, the steady state regions earthward and tailward of the reconnection region are equivalent in length. From Figure 4.2 it can be seen that ξ is always less than 1. This means that at a given time, the length in the y direction of the steady state region earthward of the X line is smaller than the length tailward of the X line.

This ratio assumes a relatively constant value after some switch on time. This means that, although the lengths in y are different for the steady state regions earthward and tailward of the X line, the growth rates are the same. The dashed line represents an estimate for this ratio based on the following considerations.

In the rest frame of the magnetosphere, the reconnection region moves tailward with velocity v_o. Assuming the satellite is fixed in space, the tailward motion of the plasma over the satellite will appear as a slice through the simulation along y. Figure 4.3 shows vertical slices of the magnetic field (B_y solid line and B_x dotted line), current density, velocity (V_A solid line and V dashed line), and total pressure at $176t_A$ for two different x values for Case 9. The parameters for Case 9 were

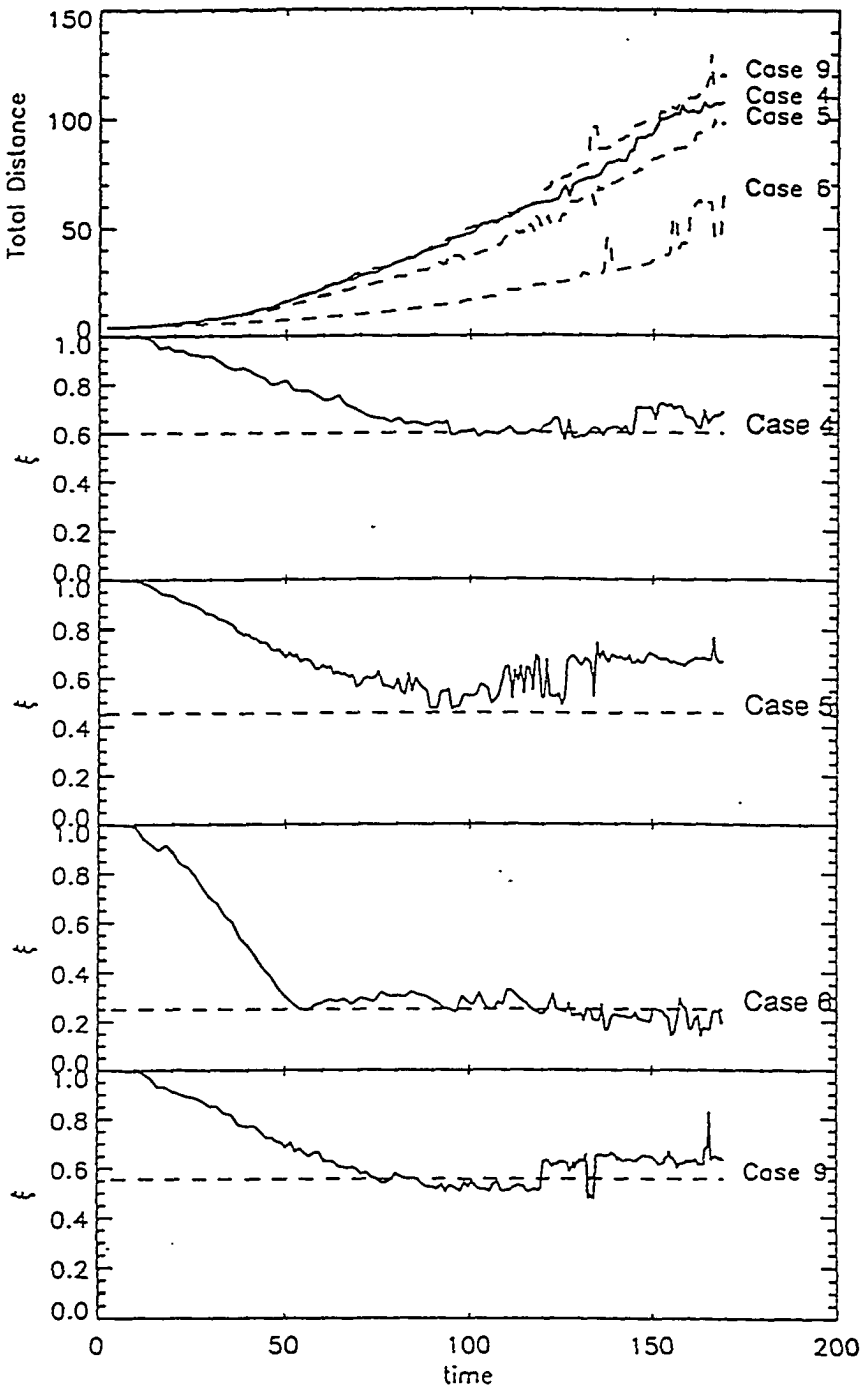

Figure 4.2. The top panel shows the development in time of the total distance between the maximum B_n and the minimum B_n for four cases. The next four panels show the absolute value of the ratio of the y positions of the maximum of B_n to the minimum of B_n (ξ), which gives the relative growth of the steady state regions eathward and the tailward of the X line. Constant ξ implies the growth rates for the regions eathward and the tailward of the X line are equivalent. The dashed lines correspond to the ratio $(V_{Amsh} - v_0)/(V_{Amsh} + v_0)$ for each case.

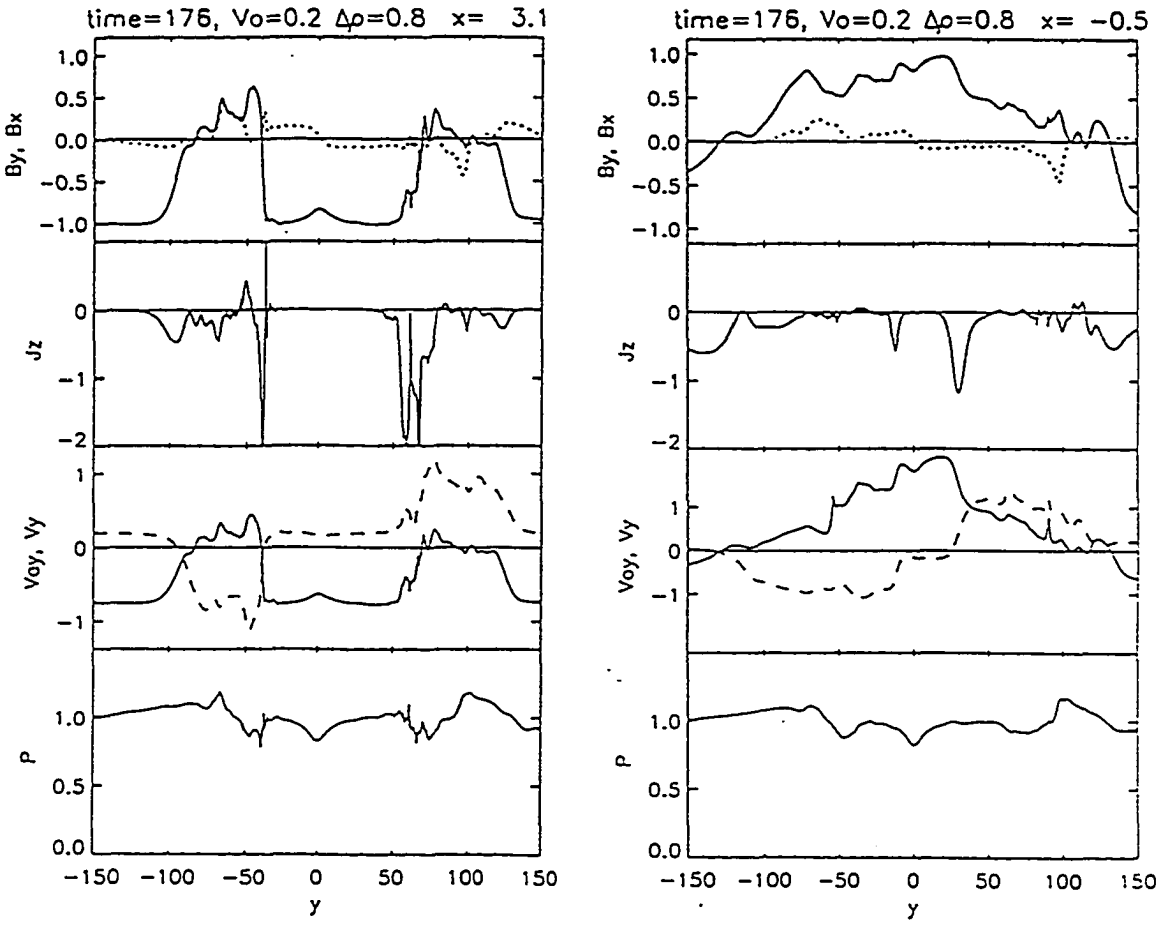

Figure 4.3. Vertical slices for the magnetic field (B_y solid line B_x dotted line), current density, velocity (V_A solid line and V dashed line), and total pressure (solid line) for x=-0.5 and 3.0 for Case 9 at t_A= 176. Scatter plot of v_y versus B_y for Case 9 at t_A=176.

chosen to be more realistic with a large density gradient and an initial velocity shear less than the Alfvén velocity.

In Figure 4.3a, which shows a slice along y for $x = -0.5$ at $176t_A$, there is a tailward accelerated flow region beginning at about $30a$ and extending to about $120a$. The simulation was normalized in such a way that, in the flank region, $a \sim 600km$ and $t_A \sim 1.5s$. For Case 9, then, v_o is approximately $80km/s$. An accelerated region $90a$ long would last approximately 11 minutes. There is also an anti-tailward flowing accelerated region beginning at about $-10a$ and extending to about $-110a$, which corresponds to about 12-13 minutes. Similar accelerated flow regions can be seen in the slice at $x = 3.0$ shown in Figure 4.3b. There the tailward accelerated region is approximately $80a$ long lasting for 10 minutes while the earthward accelerated region is approximately $50a$ long and lasts $\sim$ 7 minutes. This agrees quite well with *Gosling's* observations that accelerated regions last approximately 8-17 minutes. Closer examination of the characteristics of Figure 4.3 reveal other striking similarities with the data.

First, the tailward flowing accelerated region coincides with relatively low magnetic field magnitude in Figure 4.3a and b. The earthward accelerated regions are associated with large magnetic field magnitude while tailward accelerated regions are associated with smaller magnetic field magnitude. This can been seen in Figure 4.3c. The orientation of the magnetic field in the accelerated regions, tailward and anti-tailward, is that of the magnetosphere. In both cases shown, the beginning and ending of the accelerated regions mark the beginning and ending of a magnetic field rotation region. These characteristics of an encounter with the reconnection bulge are consistent with the observations. Due to the large size of the bulge, a satellite encounter with it is more likely than an encounter with the much smaller steady state region.

Table 3. . Plasma Parameters from *Gosling et al.*, [1986]

Event	B_{msh} nT	n_{msh} cm^{-3}	V_{Amsh} km/s	B_{msp} nT	n_{msp} cm^{-3}	V_{Amsp} km/s	$\Delta\lvert V_A\rvert$ km/s	ΔV km/s
1	22.0	5	214	20.0	0.3	800	586	225
2	20.0	3	250	20.0	0.3	800	530	210
3	20.0	4	218	30.0	0.3	1200	982	425
4	20.0	15	112	25.0	0.3	1000	888	200

4.2 Application to the Magnetosphere

Table 3 contains values taken from the observations from the flank region reported in *Gosling et al.* [1986] in order to quantitatively compare the magnetospheric and magnetosheath plasma parameters with our simulation results. Applying these values from the four cases in *Gosling et al.* to Figure 3.5 shows that our model predicts a 20-40% reduction in the magnetic field magnitude while the magnetospheric orientation is maintained in the accelerated flow region. The data agrees qualitatively with this prediction. However the field in the accelerated plasma region varies considerably more than implied by the steady state region in our simulations. The encounter with the reconnection bulge, as discussed in the previous section, could explain some of this variation. Qualitatively, the reconnection bulge has many of the same properties as the steady state region, i.e. the accelerated flow is confined to the region where the field is rotating from the MSH to the MSP orientation. However, it varies considerably more in the bulge region than in the steady state region, as seen in Figure 4.3. A simple test of this hypothesis is the total pressure. The total pressure is approximately constant in the steady state region, but enhanced in the bulge region. We remark that the significant increase seen in the total magnetic field magnitude [see Figure 3 in *Gosling et al.*, 1986] may indicate an increase in the total pressure. Since the size of the

bulge perpendicular to the magnetopause is much larger than that of the steady state region, an encounter, or partial encounter, of the bulge is more likely and may explain the multiple encounters of the accelerated flow seen in the observations. We remark that the altering flow direction of the accelerated plasma in *Gosling et al.* [1991] at high latitude observations may indicated multiple passages of an X line at the satellite location.

A final point is the difference between the magnetic shear observed in association with accelerated flow in the flank regions and flux transfer events. While at the dayside, reconnection is found to operate down to 60° rotation from MSH to MSP orientation, the flank cases show largely antiparallel fields, i.e. all but one are 135° or greater. Our simulations show that shear flow has a stabilizing effect on magnetic reconnection. Increasing the shear flow decreases the reconnection rate. In fact, we identified a critical velocity above which reconnection ceases altogether. This critical velocity is based on the Alfvén velocity for the antiparallel components of the magnetic field in the MSP and the MSH. Smaller antiparallel components lead to smaller Alfvén velocities and a smaller critical velocity. Although reconnection is possible for smaller magnetic shears, the rate will be rather low.

4.3 References

Gosling, J. T., M. F. Thomsen, S. J. Bame, and C. T. Russell, Accelerated plasma flows at the near-tail magnetopause, *J. Geophys. Res.*, 91, 3029, 1986.

Gosling, J. T., M. F. Thomsen, S. J. Bame, T. G. Onsager, and C. T. Russell, The electron edge of the low latitude boundary layer during accelerated flow events, *Geophys. Res. Lett.*, *17*, 1833, 1990a.

Gosling, J. T., M. F. Thomsen, S. J. Bame, R. C. Elphic, and C. T. Russell, Plasma flow reversals at the dayside magnetopause and the origin of asymmetric polar cap convection, *J. Geophys. Res.*, *95*, 8073, 1990.

Gosling, J. T., M. F. Thomsen, S. J. Bame, R. C. Elphic, and C. T. Russell, Observations of Reconnection of Interplanetary and lobe magnetic field lines at the high-latitude magnetopause, *J. Geophys. Res.*, *96*, 14097, 1991.

CHAPTER 5

Magnetic Reconnection, Sheared flow and Field Aligned Currents

Birkeland [1908] first suggested a current system with vertical currents which follow the Earth's magnetic field lines and horizontal currents parallel to the Earth's surface at an altitude of about 120 km. Although Birkeland was not aware of the conducting ionosphere, he concluded that field-aligned currents ($j_{||}$) could produce and maintain localized magnetic activity; thereby explaining the localized aurora. *Zmuda, Martin and Heuring* [1966] were the first to report satellite observations that were later interpreted as field-aligned currents by *Cummings and Dessler* [1967] (and named Birkeland currents).

The average flow distribution of the observed field-aligned currents in the high latitude region can be divided into two parts: Region 1, or the poleward part, and Region 2, or equatorward part, [*Iijima and Potemra*, 1976]. The intensity of Region 1 is about twice that of Region 2. Since both Region 1 and Region 2 currents increase with increasing magnetic actitivity, we are primarily interested in the upward field-aligned current which imply downward streaming electrons. The field aligned currents are upward in the evening sector of Region 1 and the morning sector of Region 2.

It is now an accepted fact that field-aligned currents are a manifestation of magnetosphere-ionosphere coupling The Region 1 and 2 current system appears to be a permanent feature of the auroral zone [*Bythrow et al.*, 1983]. For southward IMF, the current density over the whole auroral zone increases and the equatorward motion of all boundaries expands the entire pattern [*Bythrow et al.*, 1983]. This indicates that for IMF southward the source for the field-aligned currents is primarily the solar wind/IMF dynamo. For a northward IMF, Region 1 and 2 currents maintain a residual level. In addition, there exist intense field-aligned

currents poleward of, and with reversed polarity to, the Region 1 currents [*Iijima*, 1983]. This indicates that, while the solar wind/IMF dynamo dominates during active times, there is another source for the Birkeland currents. A pair of field-aligned currents are observed near the dayside cusp region. The poleward part is called the mantle field-aligned current while the equatorward part is called the region 1 field-aligned current at noon [e.g., *Iijima and Potemra*, 1976; *Erlandson et al.*, 1988; *Saunders*, 1989]

The Birkeland current density does not appear directly in the momentum equation. Its derivative along a field line can be obtained from the current continuity equation ($\nabla \cdot \mathbf{J} = 0$) and the perpendicular current density. The height integrated perpendicular current for steady state consists of three terms: the pressure gradient term, the inertia term, and the viscous term. These three terms are often examined independently, although the important aspect is the total current, summed over all drift effects [*Vasyliunas*, 1983]. The current density can be defined in terms of either the particle velocity distribution functions or the magnetic and electric fields using Maxwell's equations.

Driving, or generating, mechanisms which have been proposed for these currents in the past are closely related to plasma flows, namely solar wind near the magnetopause and the convection within the magnetosphere. Some mechanisms are associated with magnetic reconnection [*Lee et al.*, 1985; *Saunders*, 1989;*Lin and Lee*, 1993]. In this section we will explore a simple mechanism for generating field aligned currents. In our two-dimensional model, there are three components of both the magnetic field and the velocity. From the induction equation and momentum equation, it can be seen that if B_z and v_z are initially set to zero they will always remain zero. However, we will show that when a non-zero v_z component is present, a non-zero B_z component can develop. Thus, the presence of even a

small v_z component can generate large field-aligned currents, since the current is initially in the y direction.

5.1 Generation of B_z

For the preceding chapters in this thesis, the simulation is carried out in the x-y plane with all three components of the magnetic field and velocity. Figure 5.1 shows the locations on the magnetopause where the mechanism discussed in this chapter is relevant. The simulation coordinates apply differently, with respect to the GSM coordinates, for the flank and the dayside regions.

The induction equation (Equation 2.3) advances the magnetic field in time. Recall that in this two-dimensional simulation, the derivative with respect to z is zero. From Ampére's law, then, the current in the x and y direction depends only on the z component of the magnetic field. The time advancement of the z component of the magnetic field, namely,

$$\frac{\partial B_z}{\partial t} = \frac{\partial(v_x B_z - v_z B_x)}{\partial x} + \frac{\partial(-v_y B_z + v_z B_y)}{\partial y} - -\eta \nabla_\perp^2 B_z \qquad 5.1$$

shows that if both v_z and B_z are initially zero, a z component of the magnetic field can never develop. This is a property of the MHD equations. A non-zero v_z, even with an initially zero B_z, can lead to a non-zero B_z. This is seen clearly from the above equation. A physical mechanism will be described later in this chapter.

The initial velocity is described by

$$\mathrm{v} = v_{yo} \tanh\left(\frac{x}{a}\right)\hat{\mathrm{y}} + v_{zo} \tanh\left(\frac{x}{a}\right)\hat{\mathrm{z}} \qquad 5.2$$

where v_{yo} and v_{zo} are the initial magnetitudes of the y and z components, respectively. The density is symmetric across the current sheet in all cases in this Chapter in order to identify the effects of non-zero v_z for a simple case.

Figure 5.2 shows the contour plots of the vector potential showing the magnetic field lines in the x-y plane, velocity vectors in the x-y plane, contours of constant

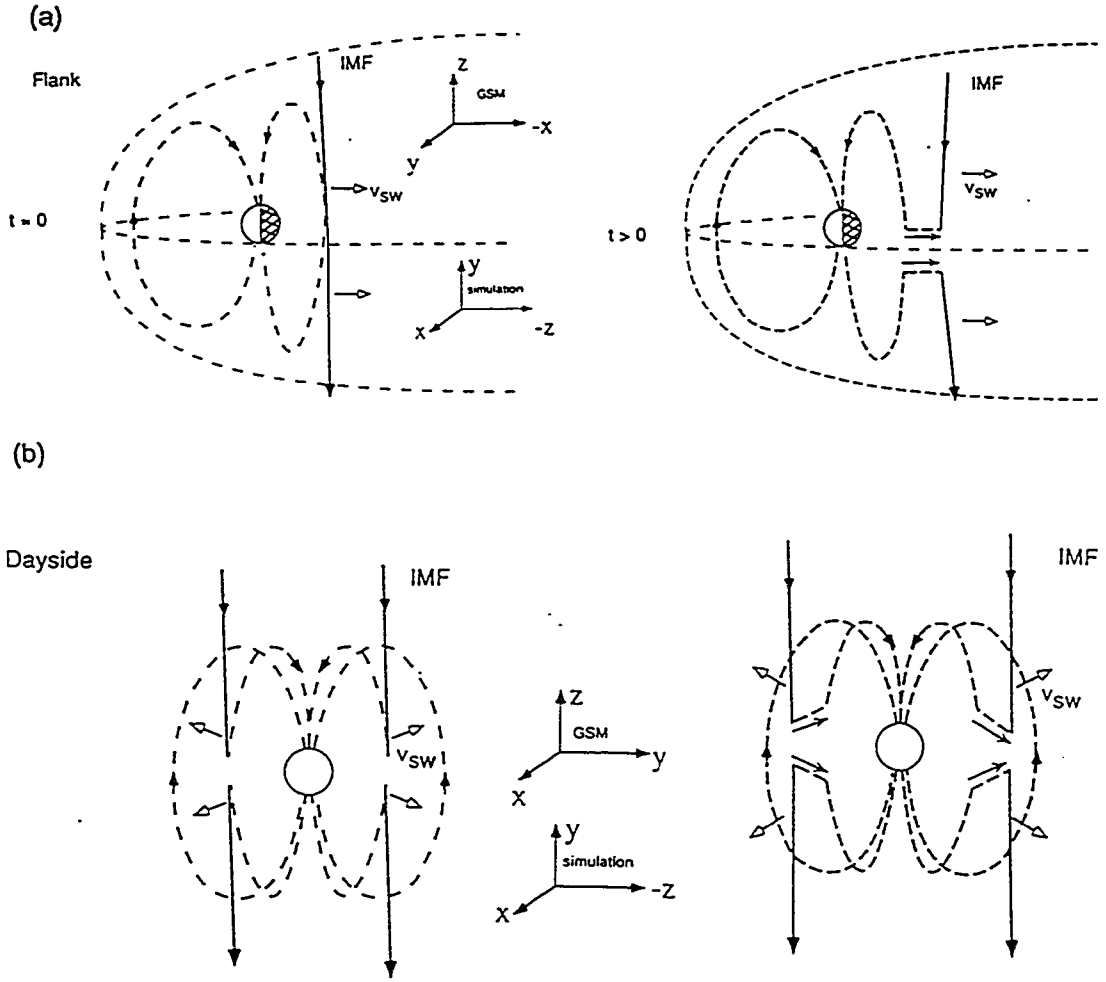

Figure 5.1. Schematic of field aligned current generation applied to the Earth's magnetosphere for (a) the flank region and (b) the dayside region.

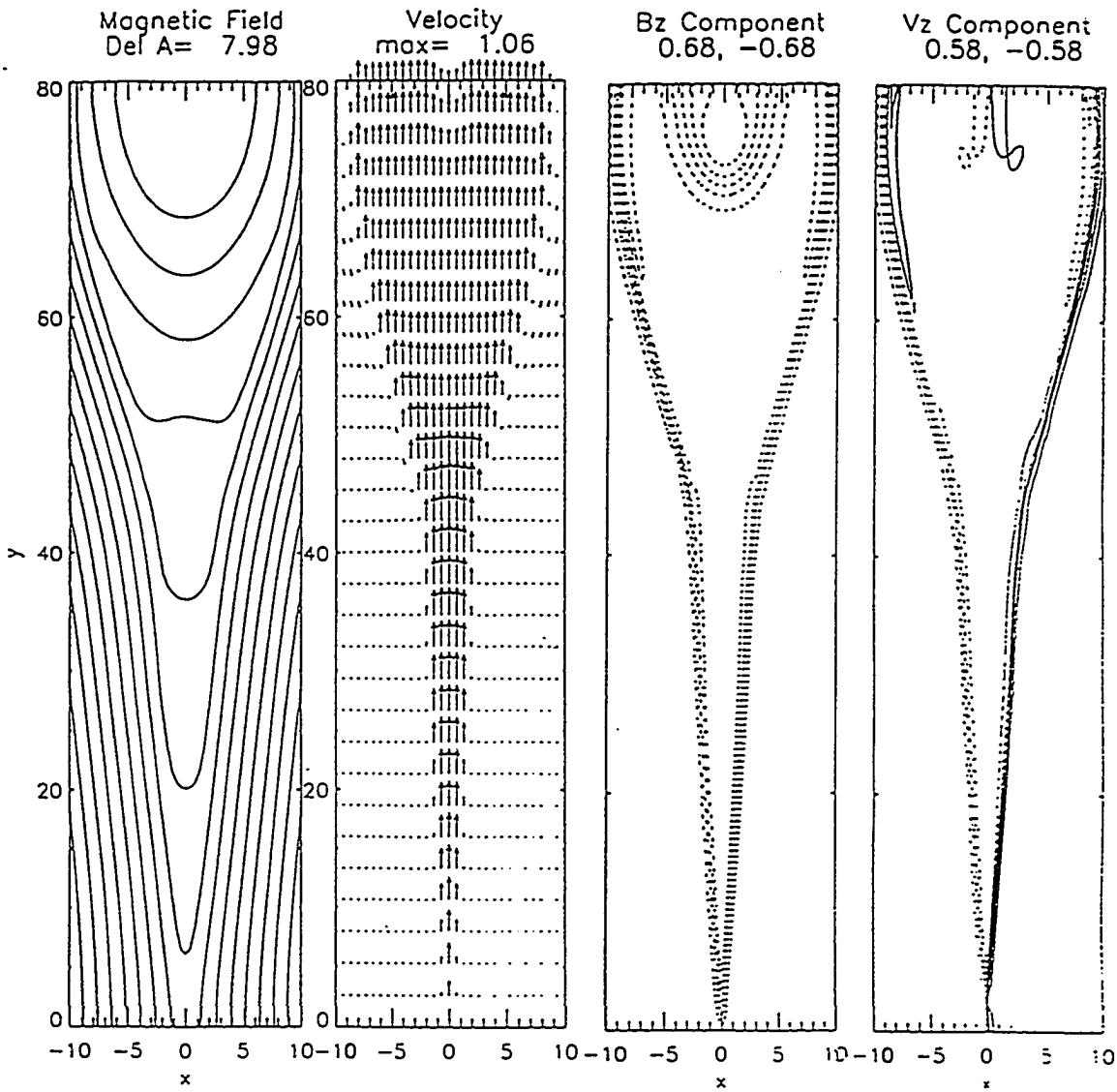

Figure 5.2. Contours of the vector potential showing the magnetic field lines in the x-y plane, velocity vectors in the x-y plane, contours of constant B_z and contours of constant v_z for the case with zero initial B_z and v_{yo} and v_{zo}=0.4 at $t = 149$. The density in this case is symmetric across the current sheet.

B_z and contours of constant v_z for the case with zero initial B_z and v_{yo} and v_{zo}=0.4 at $t = 149$.

The magnetic field lines and the velocity vectors in the x-y plane are the same as the case with symmetric density and no shear flow in the y direction (shown in Figures 2.1 and 3.2). The primary difference between the previous cases and the one shown in Figure 5.2 is the assumption of a non-zero v_z and the generation of a non-zero B_z. In the contour plots in Figure 5.2, the dashed lines indicate negative values while the solid lines indicate positive values.

In order to examine the configuration with respect to x, a horizontal slice through the steady state region is shown in Figure 5.3. The first panel contains the magnetic field, where B_x is the dotted line, B_y is the solid line, and B_z is the dashed line. The second panel contains the current, where the j_x is the dotted line, j_y is the dashed line, and j_z is the solid line. Also shown in this panel is the current parallel to the magnetic field. The third panel contains the velocity, where v_x is the dotted line, v_y is the solid line, and v_z is the dashed line. The fourth panel contains the plasma pressure and the density. Although the magnetic field and velocity in the x-y plane remain the same for this case as the cases with zero initial v_z, there are some striking differences.

A substantial z component of the magnetic field has developed in the outflow region, while the magnetic field in the inflow regions has no z component. As a direct consequence of the non-zero B_z, currents in both the x and y directions have developed. The field-aligned current that is evident in the second panel in Figure 5.3 will be addressed more fully in the next section. The velocity has a non-zero z component only in the inflow regions, v_z is zero in the outflow region. The pressure and density profiles are unchanged from the zero v_z case.

The Rankine-Hugoniot jump condition,

$$\Delta V = \pm \Delta V_A \qquad 5.3$$

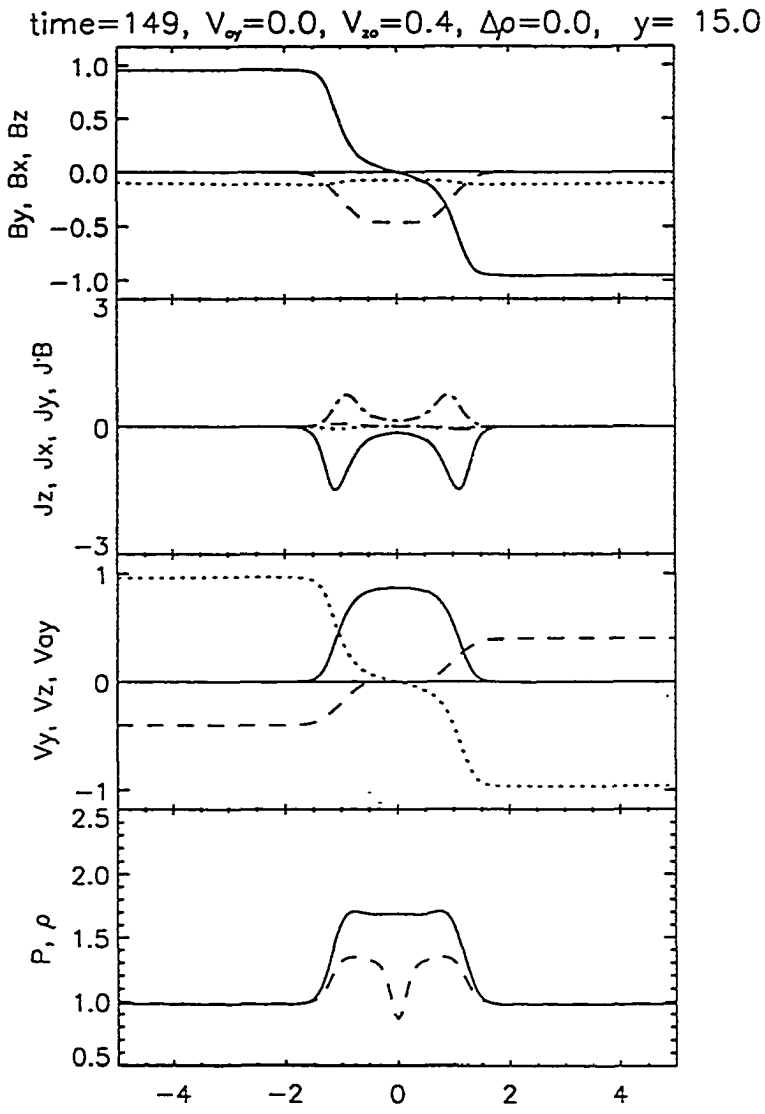

Figure 5.3. Horizontal slice through the steady state reigon for the case with v_zo=0.4, v_o=0.0, and symmetric density at $t = 149$. The first panel contains the magnetic field where B_x is the dotted line, B_y is the solid line, and B_z is the dashed line. The second panel contains the current, where j_x is the dotted line, j_y is the dashed line, and j_z is the solid line. Also shown in this panel is the current parallel to the magnetic field. The third panel contains the velocity, where v_x is the dotted line, v_y is the solid line, and v_z is the dashed line. The fourth panel contains the plasma pressure and the density.

can be applied approximately to the shocks in the steady state region of the simulation box. Since B_z is zero in the inflow regions and v_z is zero in the outlfow regions, the z component of equation 5.3 is simply

$$B_z(outflow) \sim -v_{zo} \qquad 5.4$$

This can be seen in Figure 5.3, where the B_z generated in the outflow region in the steady state portion is equivalent to v_{zo}.

Figure 5.3 is a slice through the steady state region only. In Figure 5.4, the maximum B_z, $\mathbf{j} \cdot \mathbf{B}$, and their y and x locations are shown as a function of time for the case with v_{zo}=0.4, v_o=0.0, and symmetric density. The maximum values are determined using the entire simulation box at each time. In the y and x plots, the solid line represents the maximum of $\mathbf{j} \cdot \mathbf{B}$ and the dashed line the maximum of B_z. The maximum of $\mathbf{j} \cdot \mathbf{B}$ is smoothly varying in time until about $90t_A$. From the y position, it can be seen that the maximum leaves the steady state region at about the same time as the sporadic values begin. The largely varying values of $\mathbf{j} \cdot \mathbf{B}$ are most likely values in the bulge, or non-steady region. The maximum of B_z plateaus at just above the v_{zo} value. Again, the maximum B_z increases after about $90t_A$, although considerably smoother than the $\mathbf{j} \cdot \mathbf{B}$.

The maximum magnitude of the z component of the velocity has grown from the initial value of ± 0.4 to $\sim \pm 0.6$ at $t = 127$, where the entire simulation box was used to calculate the maximum. The z component of the magnetic field has grown from an initial value of zero to a magnitude of $\sim \pm 0.5$ in the steady state regions and a maximum of $\sim \pm 0.7$ for the whole plane at $t = 149$. The structure is symmetric with positive B_z in the $y < 0$ half plane.

Figure 5.5 shows the maximum B_z generated due to the non-zero v_z as a function of the magnitude of the v_z component. The solid line connects the points taken from the simulations, which are indicated by asterisks. The dashed line is

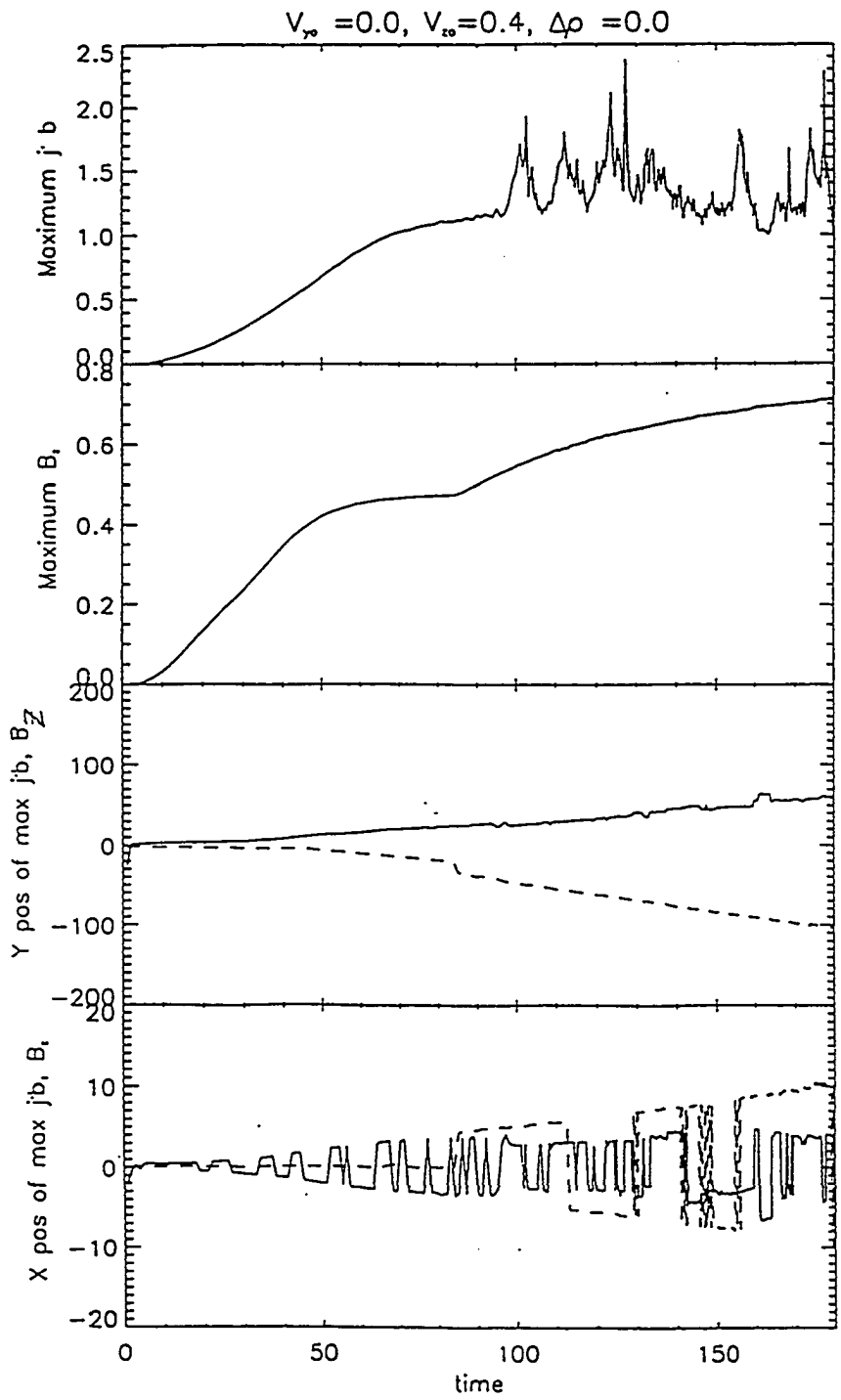

Figure 5.4. The maximum B_z, $\mathbf{j} \cdot \mathbf{B}$, and their y and x locations as a function of time for the case with v_{zo}=0.4, v_{yo}=0.0, and symmetric density. The maximum values are determined using the entire simulation box at each time.

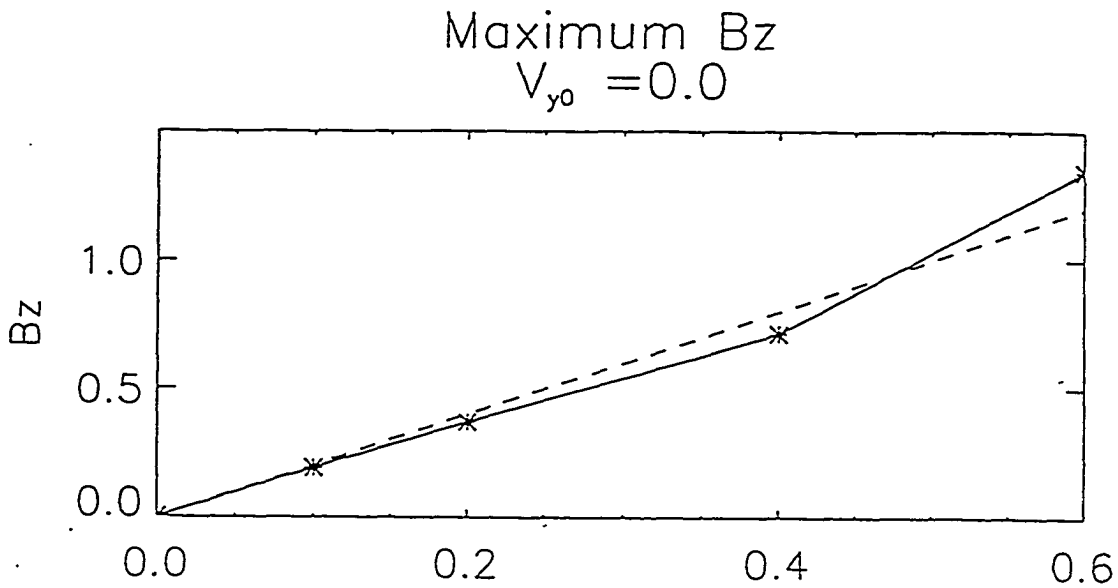

Figure 5.5. The maximum B_z generated due to the non-zero v_z as a function of the magnitude of v_z. The solid line connects the points taken from the simulations, which are indicated by asterisks. The dashed line is $B_z = 2v_{z0}$ and added as an approximate fit to the data.

$B_z = 2v_{zo}$ and added as an approximate fit to the data. The magnitude of the B_z generated depends directly on the initial v_z. The greater the initial v_z, the greater the resultant B_z. Notice that, although the relationship between B_z and v_z is still linear, the slope is greater than one. The reason for this can be seen in Figure 5.4. The location of the maximum B_z migrates in time toward the positive y and the location of the corresponding minimum migrates toward negative y. At later times, the maximum B_z is located outside of the steady state region, at the trailing edge of the bulge. This can be seen in Figure 5.3, where the maximum B_z is located at the trailing edge of the bulge region.

5.2 Generation of field-aligned currents

From Ampére's law, the currents in the x and y direction depend on the magnetic field in the z direction. In a two-dimensional system, such as the one I am using, j_x and j_y depend solely on B_z. Therefore, for B_z zero, there are no field-aligned currents since

$$j_{\|} = \frac{\mathrm{j} \cdot \mathrm{B}}{B} = \frac{j_x B_x + j_y B_y + j_z B_z}{B} \qquad 5.5$$

If, however, B_z is non-zero, all three terms in equation 5.5 become non-zero as well. In the cases discussed in the previous section, a finite B_z was generated from an initially zero B_z by the presence of a non-zero v_z. It can be seen immediately that this v_z also generates non-zero field-aligned currents.

Figure 5.6 shows the current vectors (j_x and j_y) in the x-y plane, contours of constant j_z, and contours of constant current parallel with the magnetic field for the case with symmetric density, $v_o = 0.0$, and $v_{zo} = 0.4$ at $t = 149$. The current in the x-y plane is strongly confined to the shock layers separating the inflow and outflow regions where the magnetic field changes dramatically. The x component of the current is negative and the smallest in magnitude of the three components.

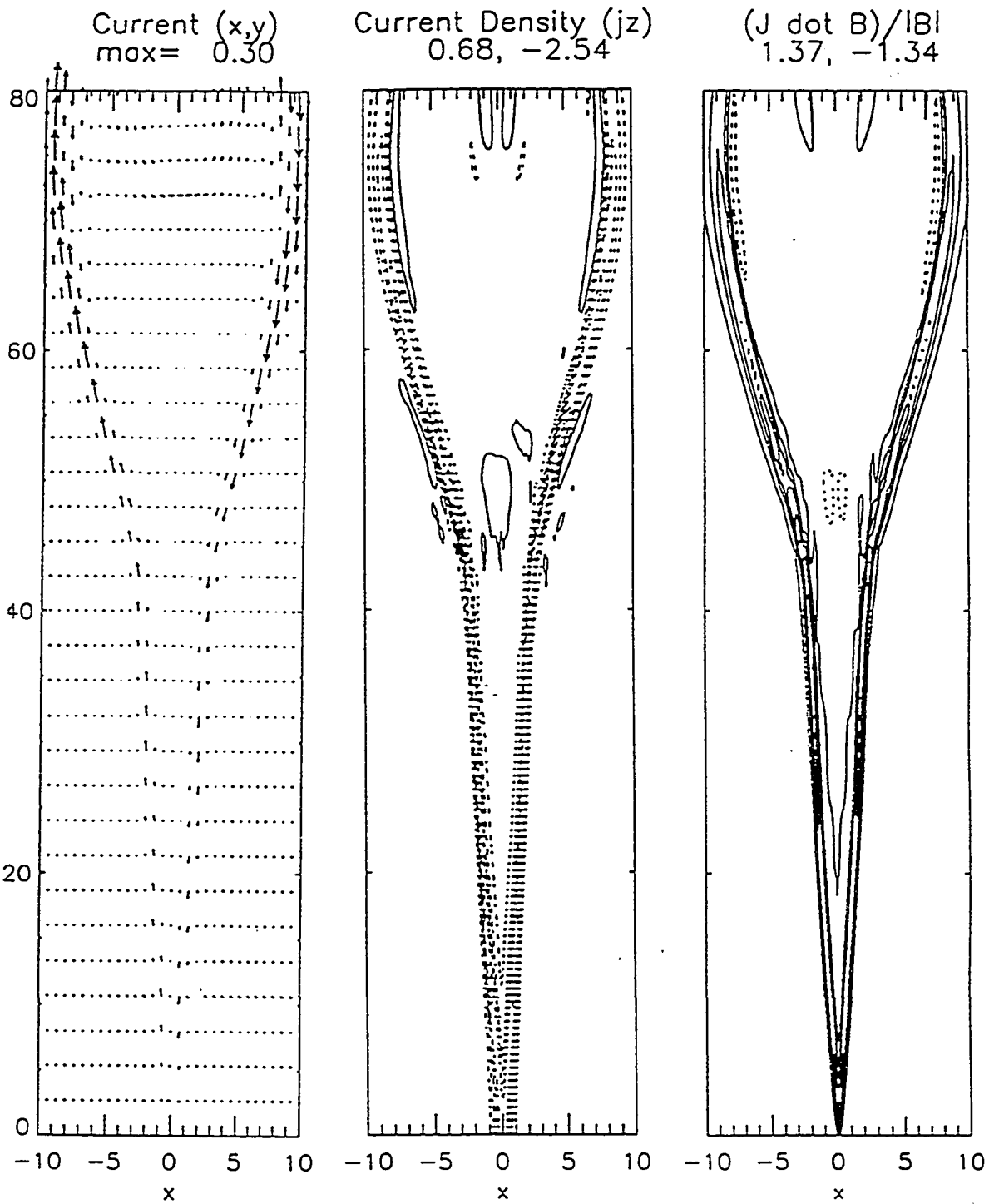

Figure 5.6. Current vectors in the x-y plane, contours of constant j_z, and contours of constant current parallel to the magnetic field for the case with symmetric density, $v_{yo} = 0.0$, and $v_{zo} = 0.4$ at $t = 149$.

The y component of the current, although larger than j_x, is also smaller than the z component. Since the B_z generated by the presence of v_z is substantial, the z component of the current dominates the field-aligned current (see equation 5.5).

The current parallel to the magnetic field is substantial, even for the relatively small v_z. Figure 5.7 shows the maximum $\mathbf{j} \cdot \mathbf{B}$ generated due to the non-zero v_z as a function of v_z. Notice that this is not the field-aligned current but the value of $\mathbf{j} \cdot \mathbf{B}$. The magnitude of $\mathbf{j} \cdot \mathbf{B}$ increases with increasing v_z. The dominate term in $\mathbf{j} \cdot \mathbf{B}$ is the z component. Notice that the maximum of $\mathbf{j} \cdot \mathbf{B}$ and the minimum of B_z may not coincide.

So far, I have shown that the presence of a non-zero v_z will generate a non-zero B_z when B_z is initially set to zero. This finite z component of the magnetic field leads to the presence of field-aligned currents in the shock regions separating the outflow from the inflow regions. The next question that needs to be addressed is the effect, or effects, that these field-aligned currents might have on the magnetic reconnection rate. Figure 5.8 shows the characteristics of the X line for the cases with $v_z = 0.1$, 0.2, 0.4, and 0.6. The different cases are represented with different line styles, but to list them is not necessary. It is evident that there is no effect on the electric field, current density, and position of the X line by the presence of the non-zero v_z. The presence, then, of B_z, v_z, and field aligned currents does not hinder nor enhance the magnetic reconnection.

This can be understood by separating the induction equation into the components z direction and those in the x-y plane. Expressing the magnetic field in the x-y plane in terms of the vector potential ($\nabla \times \mathbf{A} = \mathbf{B}$),

$$\mathbf{B} = \nabla A_z \times \hat{\mathbf{z}} + B_z \hat{\mathbf{z}} \qquad 5.6$$

where $\frac{\partial}{\partial z} = 0$ is assumed and $\mathbf{A}(x, y) = A_z(x, y)\hat{\mathbf{z}}$. For my purposes, it is sufficient to write $\mathbf{B}$ as

$$\mathbf{B} = \mathbf{B}_\perp + \mathbf{B}_z \qquad 5.7$$

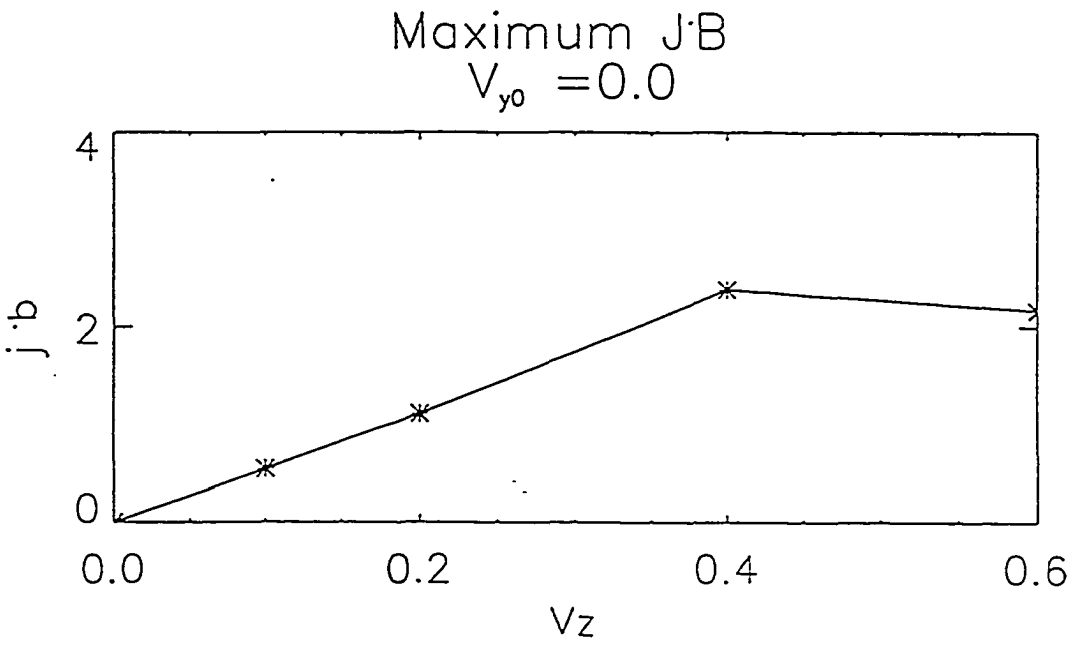

Figure 5.7. The maximum $\mathbf{j} \cdot \mathbf{B}$ generated due to the non-zero v_z as a function of v_z. The solid line connects the data from the simulations, shown as asterisks.

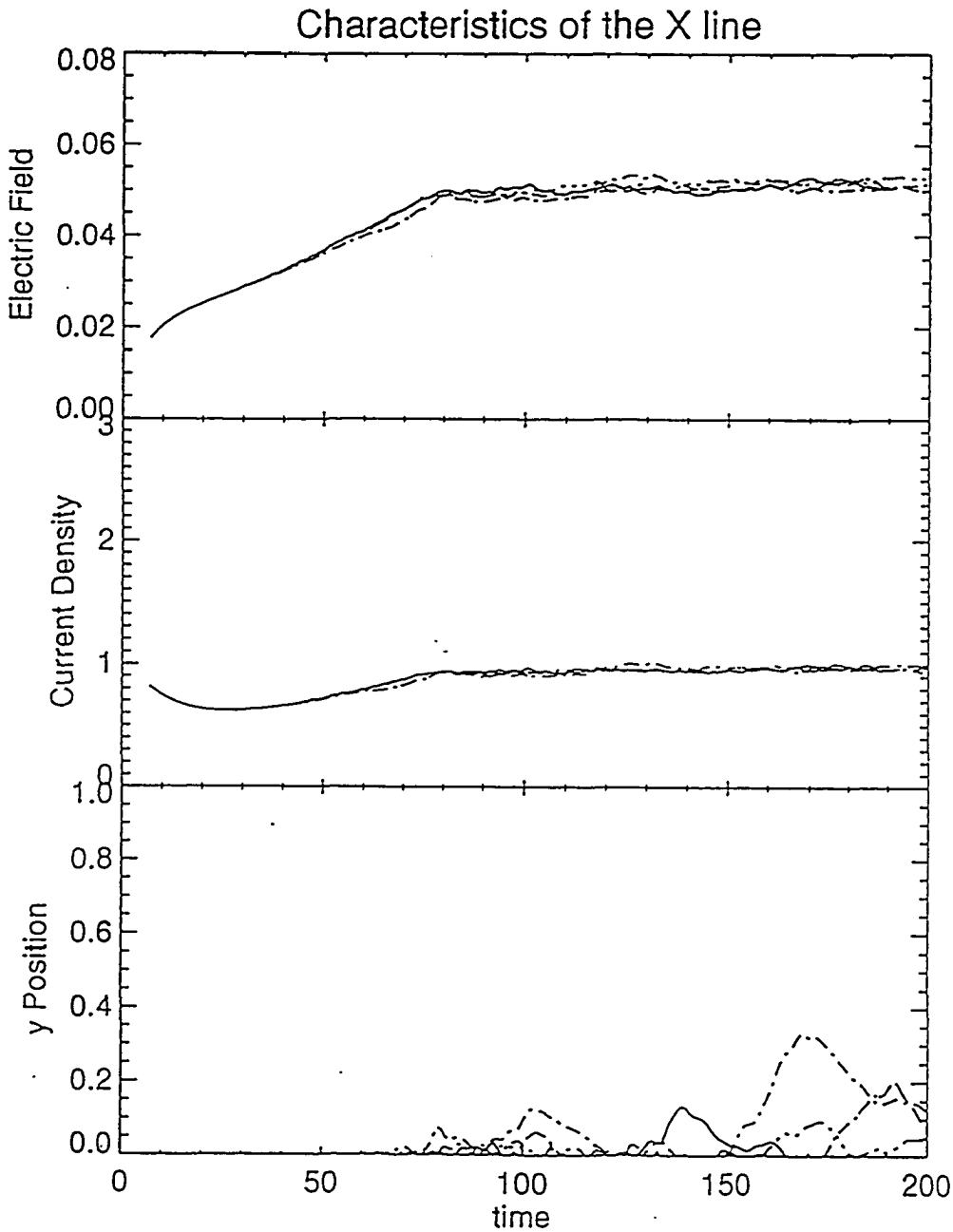

Figure 5.8. The electric field, current density, and y position at the X line for the cases with $v_z = 0.1, 0.2, 0.4$, and 0.6 as a function of time. The different cases are represented with different line styles, but to list them is not necessary. It is evident that there is no effect on the electric field, current density, and position of the X line by the presence of the non-zero v_z.

where $\mathbf{B_z}$ is $B_z\hat{z}$. In addition, the velocity in the incompressible limit can be expressed as

$$\mathbf{v} = \mathbf{v}_\perp + \mathbf{v_z} \tag{5.8}$$

where $\mathbf{v_z}$ is $v_z\hat{z}$. The induction equation can be written in two parts, one for the z component and one for the x-y (poloidal) plane, denoted by the "$\perp$" subscript. In two dimensions, the operator $\nabla_\perp \equiv \nabla$ and will be denoted ∇ in the following equations.

$$\frac{\partial \mathbf{B}_\perp}{\partial t} = \nabla \times (\mathbf{v}_\perp \times \mathbf{B}_\perp) + \eta \nabla^2 \mathbf{B}_\perp \tag{5.9}$$

$$\frac{\partial \mathbf{B_z}}{\partial t} = \nabla \times (\mathbf{v}_\perp \times \mathbf{B}_z) + \nabla \times (\mathbf{v_z} \times \mathbf{B}_\perp) + \eta \nabla^2 \mathbf{B_z} \tag{5.10}$$

These two equations are decoupled in such a way that the dynamics of $B_\perp$ are not effected by the dynamics of B_z. Examination of the momentum equations reveals that the momentum equation can be separated into z and x-y components as follows.

$$\left[\frac{\partial \rho \mathbf{v}_\perp}{\partial t} + \mathbf{v}_\perp \cdot \nabla(\rho \mathbf{v}_\perp)\right] = \nabla P + \frac{1}{\mu_o}\left[(\nabla \times \mathbf{B}_\perp) \times \mathbf{B}_\perp + \frac{1}{2}\nabla B_z^2\right] \tag{5.11}$$

$$\left[\frac{\partial \rho \mathbf{v_z}}{\partial t} + \mathbf{v}_\perp \cdot \nabla(\rho \mathbf{v_z})\right] = \frac{1}{\mu_o}\left[(\nabla \times \mathbf{B_z}) \times \mathbf{B}_\perp\right] \tag{5.12}$$

Notice that the ∇B_z^2 term in equation 5.11 acts as a pressure term. For B_z constant in space, these equations decouple similarly to the magnetic field equations. That is, for $\nabla B_z^2 = 0$, the dynamics of v_z does not affect $v_\perp$. In the incompressible limit with B_z uniform, the magnetic reconnection morphology in the x-y plane is unchanged by the generation of B_z.

In our case, there is some coupling due to the non-uniformity of B_z, but it is localized. Near the X line and in the outflow region in general, however, B_z is constant. In the inflow regions, B_z is zero. Across the shocks, B_z transitions from zero in the inflow to a constant value in the outflow.

5.3 Mechanism

The mechanism for the generation of B_z and field-aligned currents due to the presence of non-zero v_z is best described with the aid of a sketch. Figure 5.9 shows one reconnected field line that was originally in the x-y plane. The velocity in the z direction effectively drags the magnetic field in the z direction. This dragging creates a small component of the magnetic field in the z direction. It is important to note that the field line must be a reconnected field line for the B_z component to be generated. If the magnetic field is not connected across the current sheet, the velocity shear in the z direction would not generate B_z. The frozen-in condition dictates that the magnetic field moves with the plasma. Along a non-reconnected field line, the plasma is moving uniformly in the z direction. For a reconnected field line, the plasma is moving in opposite directions for different sides of the current layer. The magnetic field is sheared and B_z is generated.

In this way, the reconnection process in the x-y plane acts as a catalyst for efficient generation of magnetic flux along the z direction. This is a classical example of the dynamo process. In general, twisting a magnetic flux rope is a dynamo effect [*Song and Lysak*, [1990]; *Wright and Berger*, [1989]]. The dynamo mechanism described here for the generation of B_z uses kinetic energy to generate magnetic energy. The process of magnetic reconnection converts magnetic energy into kinetic energy. The magnetic field is generated by the currents induced by its motion across lines of force. We have, then, two opposing processes. Figure 5.10 shows the variation in the kinetic energy and the magnetic energy. The solid line represents the case with zero v_{yo}, zero v_{zo}, and symmetric density. The evolution is as expected for magnetic reconnection, i.e., conversion of magnetic energy into kinetic energy. Not shown is the thermal energy, which also increases.

The next four lines represent the non-zero v_{zo} cases. Notice that the growth of the kinetic energy and the decay of the magnetic energy is highly dependent on

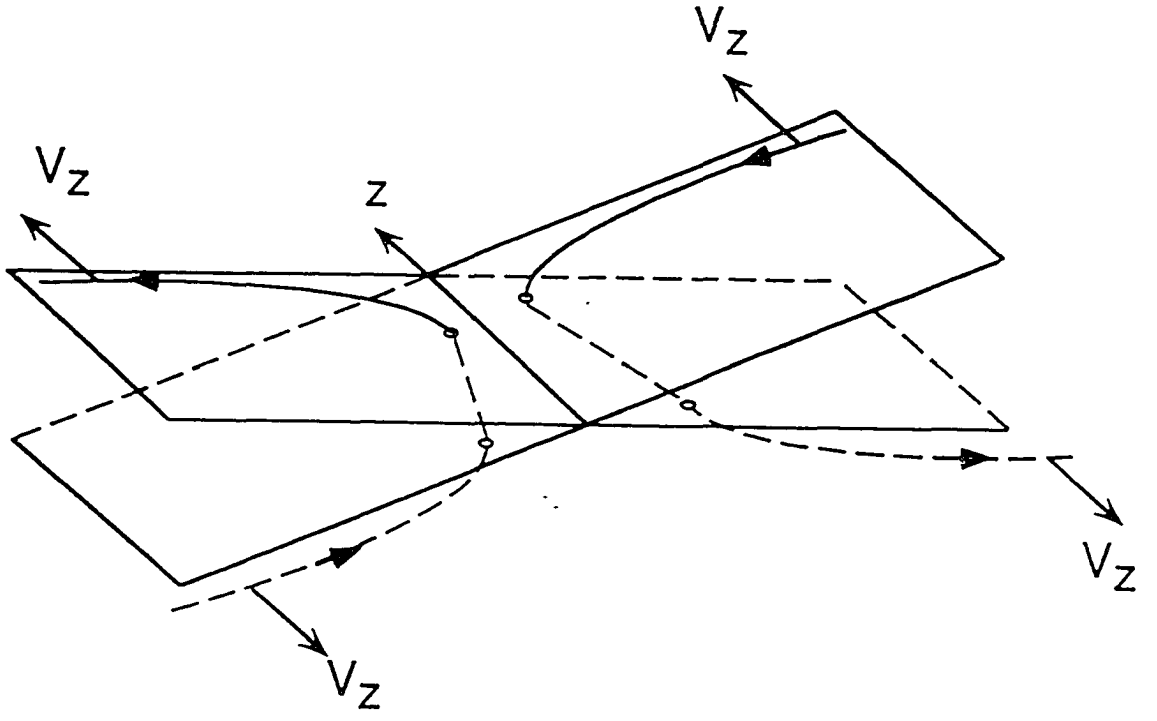

Figure 5.9. A sketch of the mechanism for the generation of B_z due to the presence of non-zero v_z.

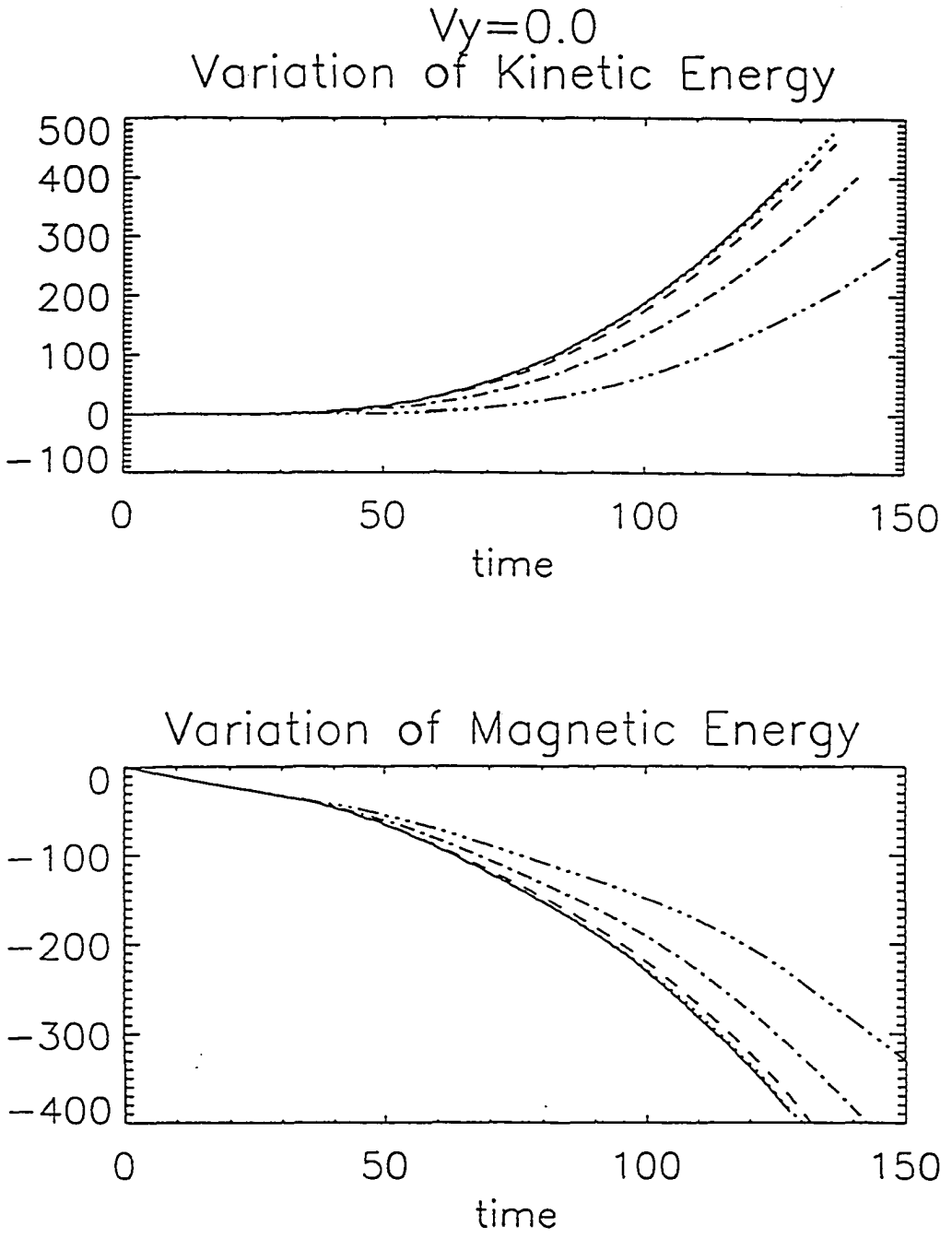

Figure 5.10. The variation of kinetic and magnetic energy as a function of time for various v_{z0} cases with $v_{y0} = 0$. The solid line indicates the $v_{z0} = 0$ case; the dotted line, $v_{z0} = 0.1$ the dashed line, $v_{z0} = 0.2$; the dot-dash line, $v_{z0} = 0.4$; the dot-dot-dot-dash line, $v_{z0} = 0.6$.

the initial v_z. Notice, also, that Figure 5.10 shows only the change from initial energies and not the actual value. For large v_z the initial kinetic energy is larger than for small v_z, however, the change is smaller. The generation of B_z by the presence of v_z increases the magnetic energy. The increase in magnetic energy is at the expense of the kinetic energy. We know from Figure 1.7 that the magnetic reconnection rate is not affected and that the dynamics in the x-y plane are not affected by the presence of v_z. Thus, the decrease of kinetic energy and the increase of magnetic energy for the increasing v_z are due to the dynamo process.

5.4 Effect of V_y

In the preceding sections of this chapter, the effects of a non-zero v_z were examined in the simplest case. That is, there was no shear plasma flow in the y direction and no density asymmetry to change the shock structures we know and love from Petschek's model. In this section, I will examine the effects of an additional component of the velocity in the y direction, namely, a velocity flow shear like the one examined in Chapters 2, 3, and 4.

Figure 5.11 shows the contours of constant vector potential (magnetic field lines in the x-y plane), velocity vectors in the x-y plane, contours of constant B_z and v_z for the case with v_o=0.6, v_{zo}, and symmetric density at $t = 166$. Comparing the magnetic field lines and the velocity vectors with a similar case without a v_z component shows little, if any difference. The dynamics in the x-y plane are decoupled from the dynamics in the z direction, via equations 5.8– 5.12. Case 2 in Chapter 2 of this thesis has symmetric density and a velocity shear flow with v_o=0.6. The intermediate shock which develops on the MSP side of the outflow region in Case 2 is clearly seen in Figure 5.11. The flow in the x-y plane is still accelerated from the negative y direction in the inflow region on the MSP side to

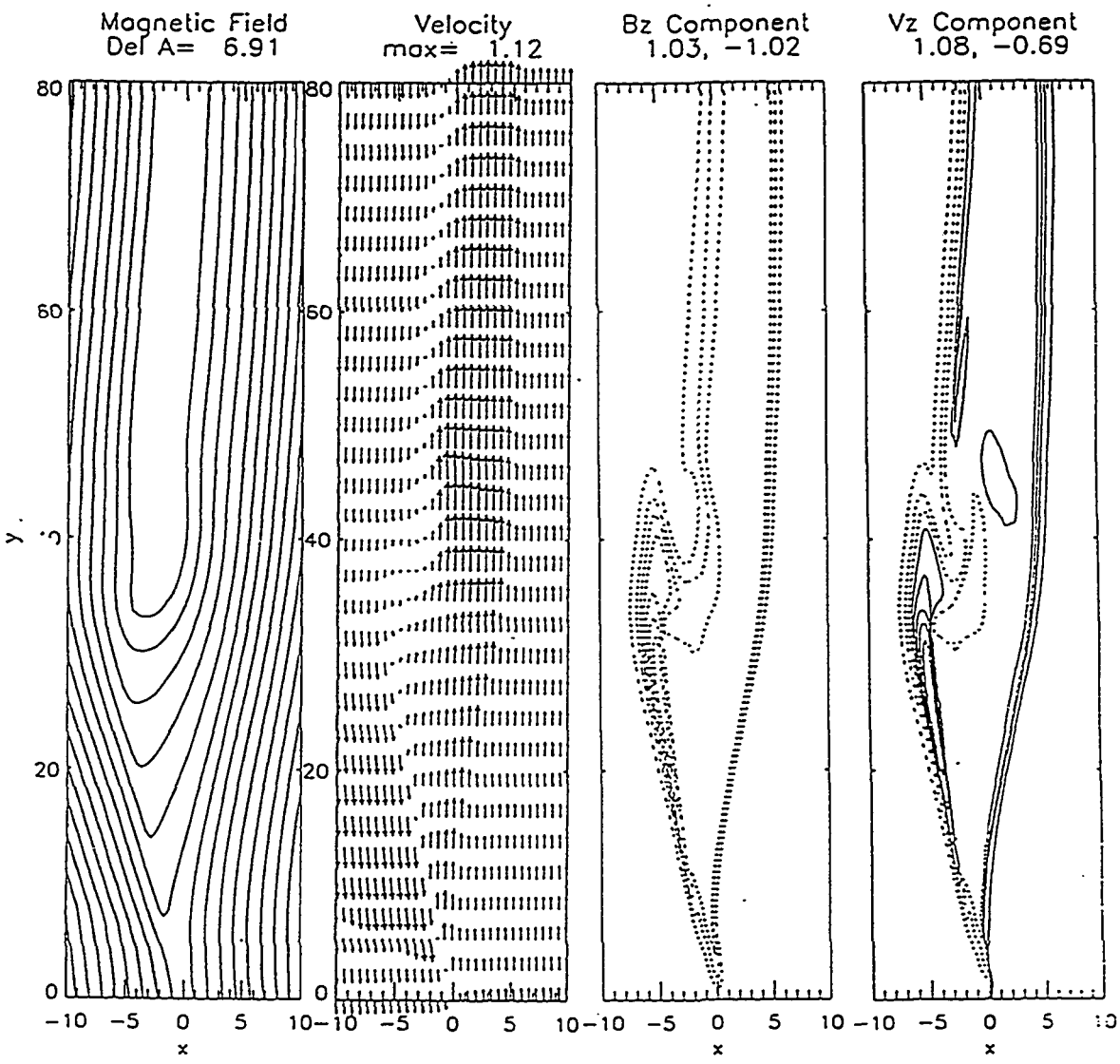

Figure 5.11. The contours of constant vector potential (magnetic field lines in the x-y plane), velocity vectors in the x-y plane, contours of constant B_z and v_z for the case with v_{yo}=0.6, v_{zo}=0.4, and symmetric density at $t = 166$.

the positive y direction in the outflow region. The intermediate shock develops to facilitate this acceleration.

As in the case with no sheared plasma flow, the B_z generated by the presence of v_z is confined to the shock structures separating the inflow and outflow regions. Since the shock structure is no longer symmetric due to the sheared plasma flow, the distribution of B_z is also not symmetric. The maximum B_z is located in the steady state region, specifically at the intermediate shock. This can be seen in Figure 5.11. Note that the change in direction of the v_z component of the velocity is now located with the intermediate shock structure. In the case with no initial shear flow, v_z remains zero within the outflow region.

For a closer examination of the steady state region, Figure 5.12 shows a horizontal slice through the steady state region for the case with v_{yo}=0.6, $v_{zo} = 0.4$, and symmetric density. The panels contain the following: magnetic field (B_y solid, B_x dotted, and B_z dashed), the current density (J_z solid, J_x dotted, and J_y dashed), the velocity (v_y solid, v_z dashed, and V_{Ay} dotted), and the field-aligned current (FAC). The asymmetry is seen immediately. Note the y component of the magnetic field still dominates the structure and changes sign across the shock on the MSP side. (I am retaining the MSP and MSH notation used in earlier chapters for consistency, even though the symmetric density makes such distinctions moot.) There are several notable differences in this cut compared to the zero v_z case. First, the x component of the magnetic field is significantly larger in the case with $v_{yo} \neq 0$ than with zero shear in the y direction. This is consistent with the sheared (v_{yo}) case with zero shear in the z direction. The shear in z, again, does not affect the topology of the x-y components of the magnetic field. In fact, the x and z components of the magnetic field are equivalent in the outflow region between S1 and S2. At S1, the z component magnitude is at its maximum. The peak of B_z is contained in the region where the magnetic field rotates from the inflow region

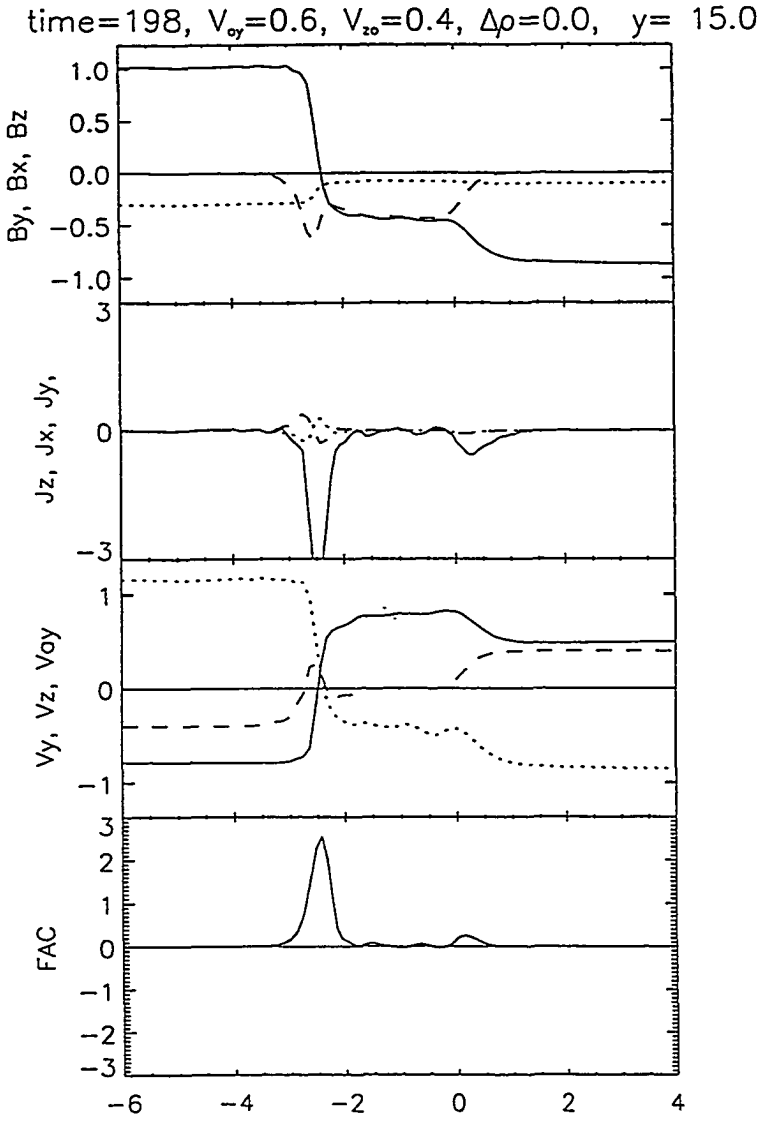

Figure 5.12. Horizontal slice through the steady state region for the case with v_{yo}=0.6, v_{zo} = 0.4, and symmetric density. The panels contain the following: magnetic field (B_y solid, B_x dotted, and B_z dashed), the current density (J_z solid, J_x dotted, and J_y dashed), the velocity (v_y solid, v_z dashed, and V_{Ay} dotted), and the field-aligned current (FAC).

configuration to the outflow region confiuration. At S2, the z component of the magnetic field decreases to zero. Again, the change in B_z is confined to the region of strongly changing B_y. Similar to the cases discussed in the previous section, however, B_z is zero in the inflow regions.

The current, still dominated by the $j_z B_z$ term, follows B_z. The peak appears in the MSP intermediate shock with a smaller peak in the MSH shock. Notice that the peak value is ~ 2. This is larger than the non-sheared case. We will discuss the field aligned current generated in the next section.

The velocity panel shows some striking differences between this case and the case with no shear in the y direction. The z component has a large positive peak within the region of large change in B_y, or the intermediate shock region. There is a smaller negative peak just inside the outflow region.

The maximum field-aligned current is located in the shock region of the steady state region. Due to the formation of an intermediate shock in the sheared v_y case, the field-aligned current becomes highly localized. Figure 5.13 shows the current vectors in the x-y plane, contours of constant j_z, and contours of constant current parallel to the magnetic field for the case with symmetric density, $v_{yo} = 0.6$, $v_{zo} = 0.4$, and symmetric density at $t = 166$. The field-aligned current contours show the strong localization effect of the intermediate shock. Without the shear in the v_y component, the field-aligned current was evenly distributed between the two shocks separating the inflow from the outflow regions. The asymmetry associated with the intermediate shock is translated to the field-aligned current through the presence of B_z. This follows since the z component term of $\mathbf{j} \cdot \mathbf{B}$ dominates the field-aligned current.

Figure 5.14 shows the maximum B_z and the maximum $\mathbf{j} \cdot \mathbf{B}$ generated by the presence of a non-zero v_z as a function of v_z. Unlike the case with no sheared flow, the maximum B_z generated is not a linear function of v_z. The B_z generated is

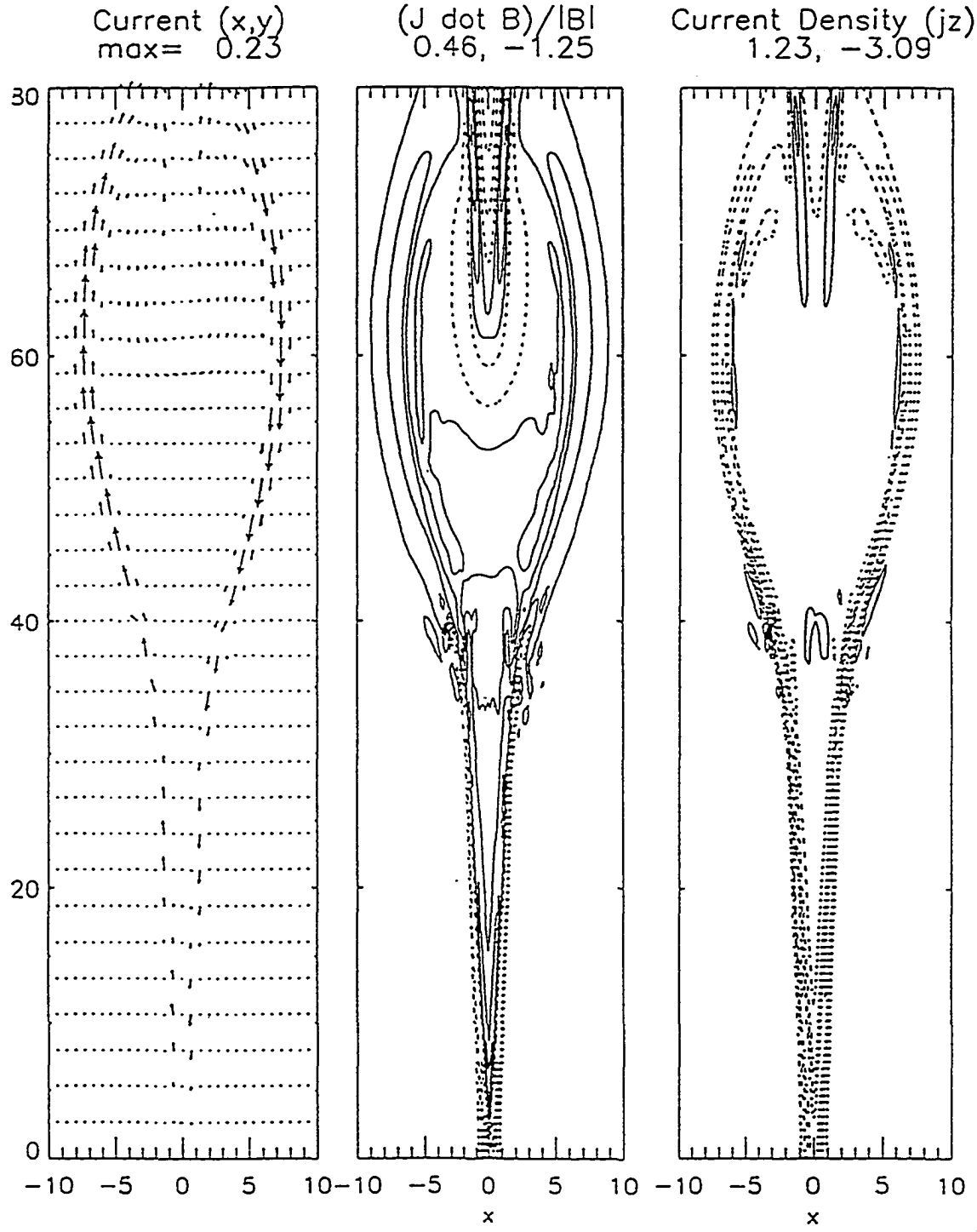

Figure 5.13. Current vectors in the x-y plane, contours of constant j_z, and contours of constant current parallel to the magnetic field for the case with symmetric density. $v_{y0} = 0.6$, $v_{z0} = 0.4$, and symmetric density at $t = 166$.

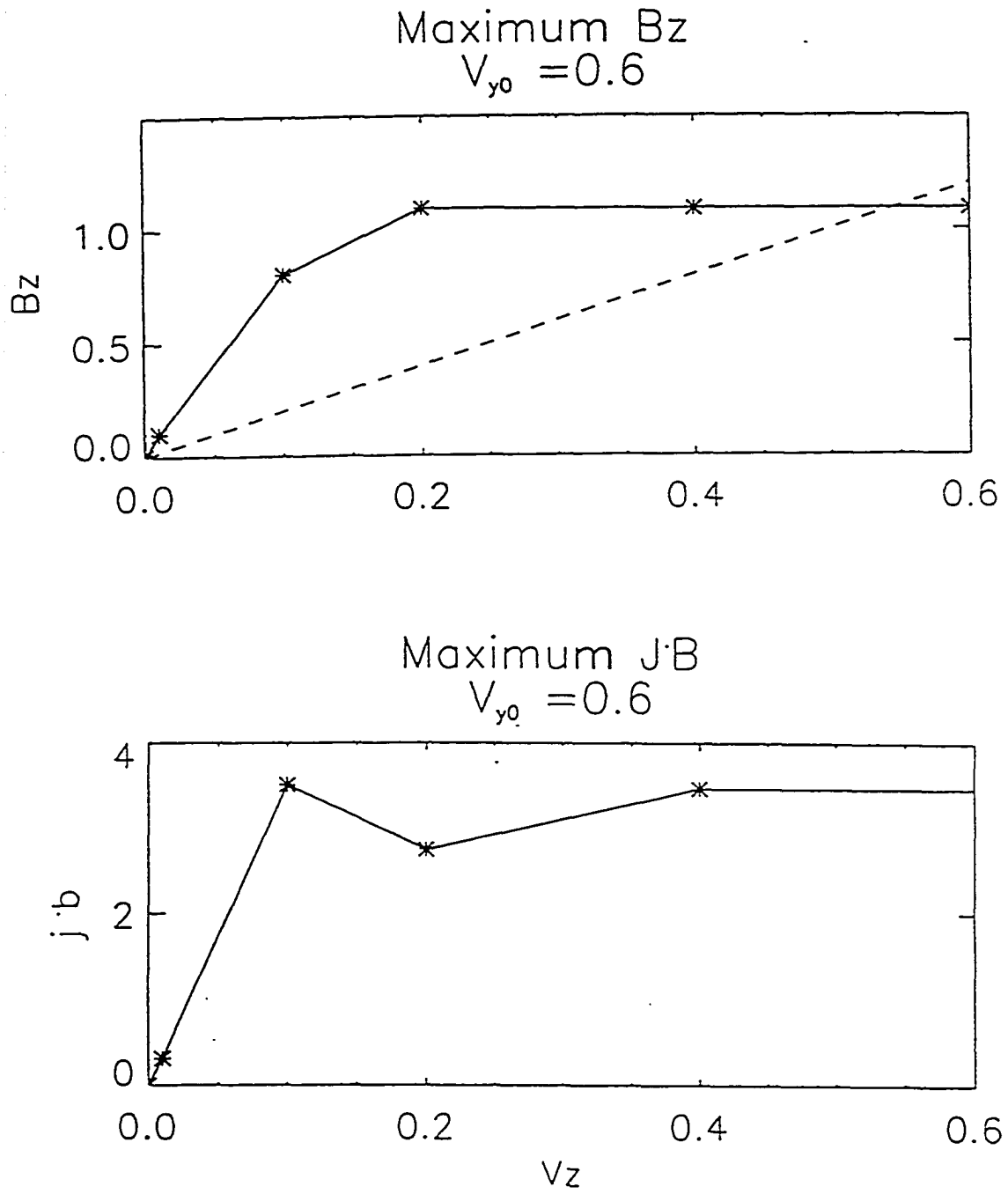

Figure 5.14. (a) The maximum B_z generated by the presence of a non-zero v_z as a function of v_z and (b) the maximum $\mathbf{j} \cdot \mathbf{B}$ as a function of v_z.

larger for each v_z than the case without sheared flow in the v_y component. The maximum B_z is coincident with the intermediate shock. The current density in the intermediate shock is significantly larger than in the slow shock of the non-sheared cases. Since the dynamo process generates and maintains magnetic field via the stretching of the magnetic field lines, a higher B_z for a stronger current layer is consistent with the dynamo theory. The $\mathbf{j} \cdot \mathbf{B}$ maximum, again, follows B_z.

5.5 Combined Effects of B_z and v_z

The mechanism for the generation of field-aligned currents and B_z dicussed so far leads to currents that are either parallel or antiparallel in a given region. However, ionospheric observations indicate that the presence of adjacent layers of parallel and antiparallel (downward and upward) currents [e.g., *Lanchester and Rees,* 1987 and the references therein]. Another process which generates field-aligned currents is the presence of B_z in a reconnection geometry [*Lee and Fu* , 1985; *Sonnerup,* 1987; *Otto,* 1990]. The direction of the field-aligned currents in these cases is given by the sign of the initial j_z and B_z components. A possible scenario for the observed bi-directional currents is the combination of these two mechanisms, i.e. the one suggested in this chapter and a pre-existing B_z.

All the examples seen so far in this chapter have zero initial B_z. In this section, I will examine the effects of having both an initial B_z and a generated B_z due to the presence of v_z. Figure 5.15 shows the contours of constant field-aligned current for the case with v_o=0.0, v_{zo}=0.4, and B_{zo}=0.3 at $t = 127$, where the initial B_z profile is constant in both x and y. The field-aligned current is significantly different in the case with no initial B_z. In the steady state region, the field-aligned current is bi-directional, whereas with no initial B_z it was strictly positive. The peak has diminshed from the zero B_z case as well.

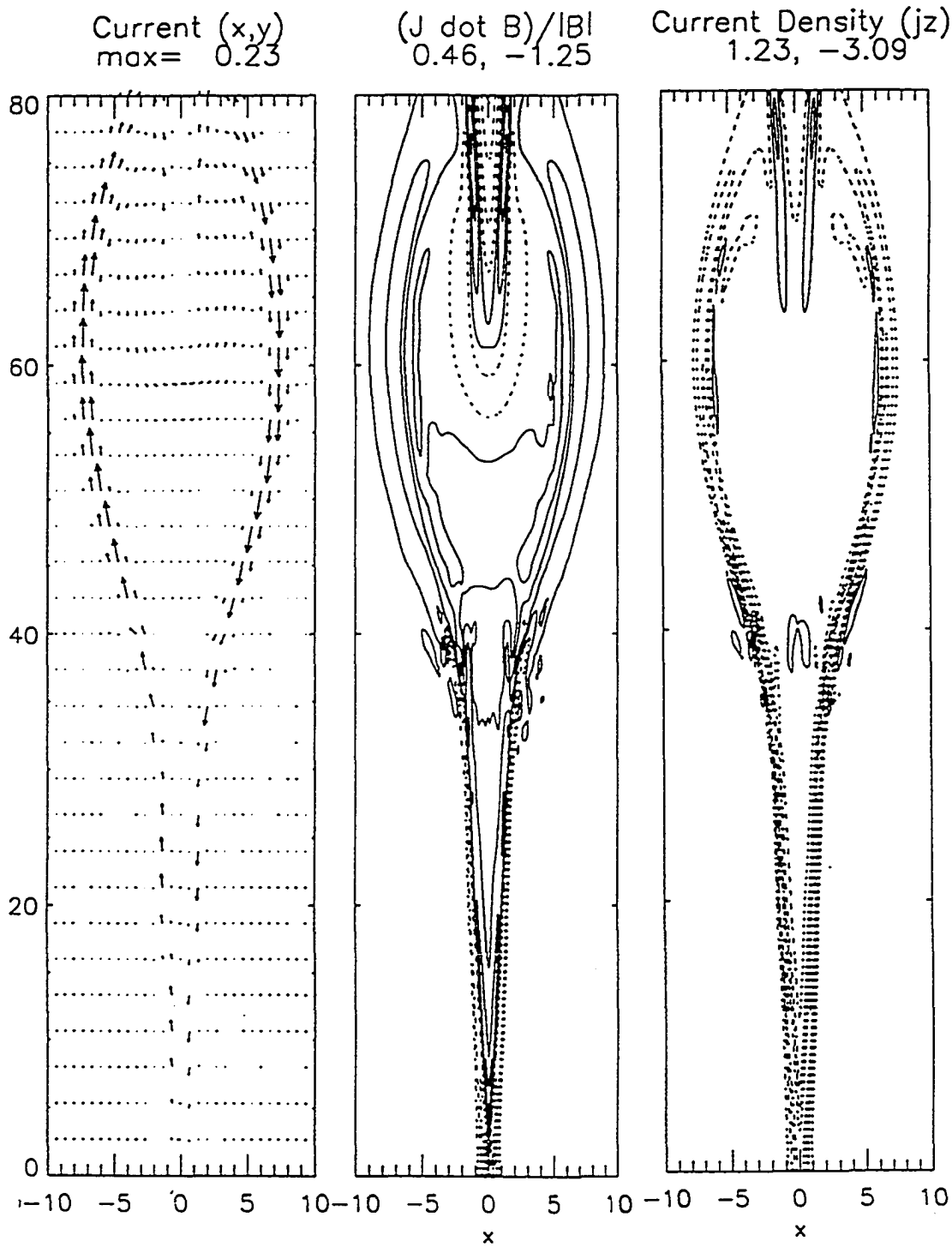

Figure 5.15. The contours of constant field-aligned current for the case with v_o=0.0, v_{zo}=0.4, and B_{zo}=0.3 at t = 127.

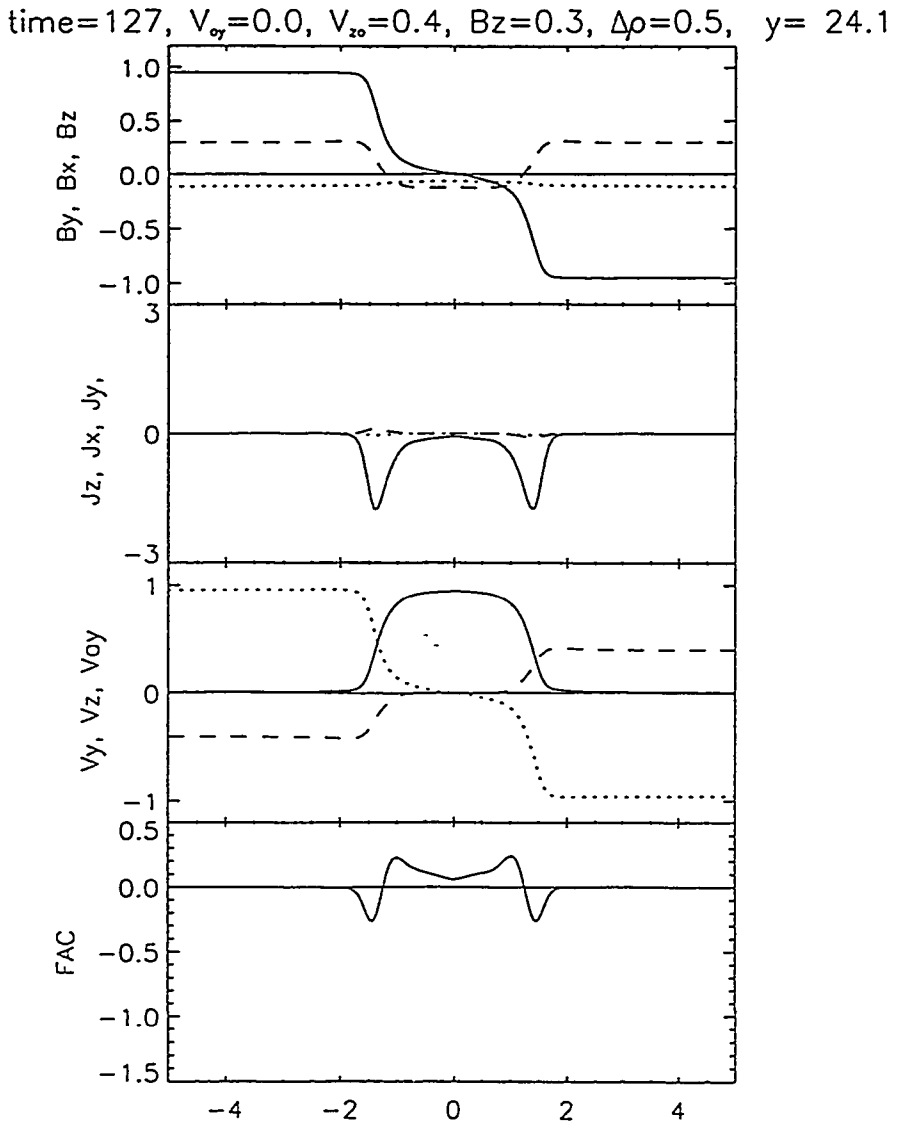

Figure 5.16. A horizontal slice through the steady state region of the case with v_o=0.0, v_{zo}=0.4, and B_{zo}=0.3 at t = 127. The panels are defined the same as in Figure 5.12.

Figure 5.16 shows a horizontal slice through the steady state region of the case with v_o=0.0, v_{zo}=0.4, and B_{zo}=0.3 at t = 127. The B_z profile shows the initial positive constant value with the generated B_z in the outflow region. The B_z generated is negative and just slightly larger than the initial B_z in magnitude. This profile reduces the effective B_z in the current layer compared to the zero initial B_z case. The z component dominates $\mathbf{j} \cdot \mathbf{B}$. The addition of a positive B_z changes the sign of the dominate component for part of the current layer and the field-aligned current becomes bi-directional.

5.6 References

Birkeland, K., The Norwegian aurora polaris expedition 1902-1903, Volume 1, First section, H. Aschehoug and Co., Christiania, pp. 319-801, 1908.

Bythrow, P. F., T. A. Potemra, and L. J. Zanetti, Variation of the auroral Birkeland current pattern associated with interplanetary and geomagnetic conditions, *Magnetosspheric currents*, AGU Monograph #28, edited by T. Potemra, 1983.

Cummings, W. D. and A. J. Dessler, Field-aligned currents in the magnetosphere, *J. Geophys. Res.*, 72, 1007, 1967.

Egeland, A., Kristian Birkeland: The man and the scientist, *Magnetosspheric currents*, AGU Monograph #28, edited by T. Potemra, 1983.

Erlandson, R. E., L. J. Zanetti, T. A. Potemra, P. F. Bythrow, and R. Lundin. IMF B_y dependence of region 1 Birkland currents near noon, *J. Geophys. Res.*, 93, 9804, 1988.

Iijima, T. and T.A. Potemra, The amplitude distribution of field-aligned currents at northern high latitudes observed by TRIAD, *J. Geophys. Res.*, 81, 2165, 1976.

Iijima, T. and T. A. Potemra, Large-scale characteristics of field-aligned currents associated with substorms, *J. Geophys. Res.*, 83, 599, 1978.

Iijima, T., Field-aligned currents during northward IMF, *Magnetosspheric currents*, AGU Monograph #28, edited by T. Potemra, 1983.

Lanchester, R. S. and Rees, M. H., Field-aligned current reversals and fine structure in a dayside auroral arc, *Planet. Space Sci.*, 35, 759, 1987.

Lee, L. C., and J. R. Kan, Field-Aligned currents in the magnetospheric boundary layer, *J. Geophys. Res.*, 85, 37, 1980.

Lee, L. C., J. R. Kan, and S.-I. Akasofu,'On the origin of the cusp field-aligned currents, *J. Geophys. Res.*, 57, 217, 1985.

Lin, Y. and L. C. Lee, A Mechanism for the Generation of Cusp Field-Aligned Currents, to appear in *AGU monograph on Solar Wind Sources of Magnetospheric ULF Waves*, M. J. Engebretson and K. Takahashi, eds. AGU, Washington DC, 1993

Otto, A., K. Schindler, and J. Birn, Quantitative study of the nonlinear formation and acceleration of plasmoids in the Earth's magnetotail, *J. Geophys. Res.*, 95, 15,023, 1990.

Saunders, M.A., Origin of the cusp Birkeland currents, *Geophys. Res. Lett.*, 16, 151, 1989.

Song, Y. and R. L. Lysak, The current dynamo effect and its statistical description during 3-D time-dependent reconnection, Geophysical Monograph 58, *Physics of Magentic Flux Ropes*, edited by C. T. Russell, E. R. Priest, and L. C. Lee, 1990.

Sonnerup, B. U. Ö., On the stress balance in flux transfer events, *J. Geophys. Res.*, 92, 8613, 1987.

Vasyliunas, V. M., Fundamentals of current description, *Magnetosspheric currents*, AGU Monograph #28, edited by T. Potemra, 1983.

Wright, A. N. and M. A. Berger, The effect of reconnection upon the linkage and interior structure of magnetic flux tubes, *J. Geophys. Res.*, 94 1295, 1989.

Zmuda, A. J., J. H. Martin, and F. T. Heuring, Transverse magnetic disturbances at 1100 km in the auroral region, *J. Geophys. Res.*, 5033, 1966.

CHAPTER 6
Discussion and Summary

Many interesting problems in interplanetary space, magnetospheric physics, and solar physics research involve magnetic reconnection. For this reason, the magnetic reconnection process is a central issue in space physics. The possible effects of sheared plasma flow on magnetic reconnection have been largely ignored.

One of the first reconnection models developed, the *Sweet-Parker* [1958] model, uses only diffusion to account for the plasma acceleration in magnetic reconnection process. The reconnection rate achieved by this mechanism was not sufficient to explain the fast release of kinetic energy observed in solar flares. *Petschek* [1964] proposed a model in which the diffusion process dominates only in a small compared to the system. MHD shocks accounted for the acceleration and heating of plasma. Specifically, two slow shocks separate the inflow regions from the outflow regions. This model accomplishes two things: first, the diffusion time depends on the size of the diffusion region such that a smaller region yields a smaller diffusion time and second, the MHD shocks accelerate the plasma in the outflow region.

Petschek's [1964] model stimulated much work examining the nature of the MHD shocks and possible extensions of the model to fit more realistic scenarios. In the context of magnetospheric physics, the application of magnetic reconnection involve two plasmas with different magnetic field magnitudes, plasma densities, temperatures, and velocities, characteristics of the solar wind and the magnetospheric plasma. The model of the magnetic reconnection process, then, needs to contain these differences if they significantly alter the physical process.

As mentioned earlier, it has long been postulated that violation of any of the three basic assumptions in Petschek's model will lead to the formation of intermediate waves in the outflow region. Namely, the assumptions in the compressible

model used by Petschek are: (i) all plasma parameters are symmetric across the neutral sheet; (ii) the magnetic fields on the two sides of the neutral sheet are strictly anti-parallel (iii) the magnitude of the external magnetic field is independent of distance from the neutral line. Various violations of the above assumptions, in an attempt to approach a more realistic scenario, have been studied by many authors [e.g., *Levy et al.*, 1964; *Petschek and Thorne*, 1967; *Mitchell and Kan*, 1978; *Scholer*, 1989; *Shi and Lee*, 1990; *Lin and Lee*, 1993] and, indeed, the shock structure is affected by asymmetries in the inflow plasma characteristics. The plasma flow velocity is an important inflow plasma characteristic which often displays asymmetry in observations of space plasmas. This thesis is the first examination of the effects of sheared plasma flow on the magnetic reconnection process using compressible MHD simulations.

In this thesis, I have systematically examined many aspects of magnetic reconnection in the presence of sheared plasma flow. I began with the simplest model, completely symmetric, to examine effects that the plasma flow would have on the reconnection layer, symmetry conditions, and reconnection rate. As the complexity of the model grows, so does its applicability to space physics. The effects of flow shear on the magnetic reconnection process can be described both quantitatively and qualitatively.

Quantitatively, the reconnection layer structure, morphology, and time scales achieved with the presence of shear flow are consistent with the observations. For the small shear flow and high density asymmetry at the dayside magnetopause, the model predicts a strong, thin intermediate shock forming on the magnetosheath side of the outflow region. For the shear flow and density asymmetry typical of the flank region of the magnetosphere, the model predicts a wide magnetic field transition region with the accelerated flow contained within this region. Further, the model can predict testable characteristics of the flank region. Namely, the total

pressure is increased in the non-steady state bulge region; and the earthward flow regions, or deccelerated flow regions, contain plasma with magnetospheric magnetic field orientation. These results indicate that the alterations of the magnetic reconnection process due to the presence of a velocity shear can explain some of the differences between the dayside and flank magnetopause observations.

Qualitatively, the magnetic field topology, reconnection layer structure, and energy conversion are all affected by the sheared flow. That is, the very essence of the magnetic reconnection model is altered by the presence of sheared plasma flow. For the cases with a shear in the y direction only, the reconnection rate is affected by the presence of the plasma flow shear. The conditions under which reconnection occurs, then, is afffected. For a large flow shear, reconnection is cut off. In addition, for a moderate flow shear the development of the steady state region is slower than for a smaller flow. More significantly, the morphology of the outflow region is greatly altered by the shear flow.

For cases with a sheared flow in the z direction, the magnetic reconnection process acts as a catalyst to the dynamo process. The connection of magnetic field lines across the current sheet allows the v_z to generate a magnetic field in the z direction. The energy in the system is changed by the presence of the dynamo. In addition, once B_z is non zero, field-aligned currents can develop. Field-aligned currents are an intricate part of the magnetosphere-ionosphere (M-I) coupling. Thus, the mechanism presented here to generate B_z with sheared flow has immediate ramifications for application to magnetospheric physics. However, the application is not limited to M-I coupling models. Solar physics, for example, has many scenarios in which the magnetic reconnection process co-exists with sheared plasma flows. Interplanetary space, as well, has plasmas with sheared flow where magnetic reconnection may be possible.

Thus, the results indicate that a plasma flow shear in the inflow region of the reconnection morphology has a significant impact on the magnetic reconnection process. While many aspects of the effects of sheared flow on the reconnection process are addressed in this thesis, the work on this topic is far from complete. Like most science, every answer produces many more questions.

The following is a summary of the major findings in this thesis.

• This is the first report of the formation of intermediate shocks due to the presence of sheared plasma flow. Although the plasma properties and magnetic field strength are symmetric across the neutral sheet, the presence of a velocity shear introduces an asymmetry in the structure of the outflow layer. By violating the symmetric conditions of Petschek's model, the reconnection layer structure in the neutral sheet changes. The plasma requires greater acceleration across one shock in order to reverse the flow direction. This acceleration is accomplished via an intermediate shock. My results show that the slow shock pair of Petschek's model is replaced by an intermediate shock and weaker slow shock pair.

• For asymmetric inflow conditions, I identified a threshold velocity separating the two solutions for the configuration of the region tailward of the reconnection region. A density asymmetry across the magnetopause favors the formation of an intermediate shock on the MSH side of the reconnection layer. In contrast, a velocity shear favors the formation of an intermediate shock on the MSP side for the region tailward of the resistivity region. The development of the shock structure in the steady state region depends upon the relative strengths of the density asymmetry and the velocity shear. For initial shears exceeding $v_{thresh} = \Delta|V_A|/2$, the reconnection structure is dominated by the shear flow effects. For initial shears less than v_{thresh}, the density gradient effects dominate.

• I have also identified a critical velocity in the asymmetric case above which magnetic reconnection does not occur. For symmetric conditions and a sheared

plasma flow, the magnetic reconnection process is cut off when the shear flow velocity exceeds the Alfvén velocity. For asymmetric density profiles such that $\rho_{msp} < \rho_{msh}$ and velocities below $V_c = V_{Amsh}$, stationary reconnection takes place in the rest frame of the resistivity region. The reconnection rate decreases with increasing shear flow since the separatrix angle increases with increasing flow shear. If the separatrix angle approaches 90°, the current in the resistivity region goes to zero. With no current in the resistivity region, the electric field in that region is also zero. Since the electric field is a measure of the reconnection rate, the magnetic reconnection rate is zero at a separatrix angle of 90°.

• In addition to the steady state region, the structure and evolution of the entire reconnection configuration is examined. The main characteristics of magnetic reconnection under the influence of sheared plasma flow are evident in the bulge region as well as the steady state region. In particular, the accelerated flow region is contained within the broad magnetic field transition region. For a tailward propagating reconnection region, a satellite located in the flank region of the magnetosphere is likely to see the bulge pass over. The time scales and main characteristics of the bulge are consistent with the observations. In addition, the model provides predictions that can be tested by observations. First, the total pressure in the bulge should increase while in the steady state region the total pressure is constant. Second, the magnetic field orientation for an earthward flow should be magnetospheric due to the position of the intermediate shock.

• I have demonstrated that a substantial component of the magnetic field in the invariant direction (z in the simulations) can be generated by the presence of a non-zero v_z, even with an initially zero B_z. In turn, the non-zero B_z leads to field aligned currents, which has application to magnetosphere-ionosphere coupling. The growth rate of both the generated B_z and, consequently, the field aligned currents

can be increased significantly by the addition of a non-zero v_y. The reconnection dynamics are not altered by the developments in the z direction.

• If a non-zero B_z component is initially present, the B_z generated by v_z can lead to bi-directional currents within the strong current layer of the steady state region. Thus, both upward and downward field-aligned currents occur within the same current layer.

6.1 References

Levy, R. H., H. E. Petschek and G. L. Siscoe, Aerodynamic aspects of the magnetospheric flow, *AIAA J., 2,* 2065, 1964.

Lin, Y. and L. C. Lee, Structure of reconnection layers in the magnetosphere, *Space Science Reviews*, 00:1-120, 1993.

Mitchell, H. G., and J. R. Kan, Merging of magnetic fields with field-aligned plasma flow components, *J. Plasma Physics*, 20, 31, 1978.

Petschek, H. E., Magnetic field annihilation, in AAS-NANA Symposium on the Physics of Solar Flares, *NASA Spec. Publ., SP-50*, 425, 1964.

Petschek, H. E., and R. M. Thorne, The existence of intermediate waves in neutral sheets, *Astrophys. J.*, 147, 1157, 1967.

Scholer, M., Asymmetric time-dependent and stationary magnetic reconnection at the dayside magnetopause, *J. Geophys. Res., 94*, 15, 099, 1989.

Shi, Y. and L. C. Lee, Structure of the reconnection layer at the dayside magnetopause, *Planet. Space. Sci., 38*, 437, 1990.

Sweet, P. A., The neutral point theory of solar flares, in *Elcctromagnetic Phenomena in Cosmical Physics*, ed. by B. Lehnert, p. 123, Cambridge University Press, London, 1958.